Cell-based Screening of Natural Chemicals in Search of Compounds to Treat Stress, Cancer, and Old Age-related Pathologies

June 2018

Sukant GARG

Abstract

Stress is a state that triggers change in normal physiology and recognized by human body and brain as an unfavorable event causing concern, worry or anxiety. It may vary from physical, metabolic, physiological or emotional often culminating into wide range of ailments that may range from common cold, decline in functional efficacy of body systems or even cancer. A variety of natural compounds have been used for anti-stress and disease preventive potentials in worldwide traditional home medicine systems. They have recently attracted attention in research laboratories to dissect their mode of action to promote safe and economic drug development. Cancer is one of the most important healthcare matters in question, with the worst prognosis but the best possibilities for scientific development. It is uncontrolled proliferation of abnormal cells, resulting from a host of mutations developing into functional disabilities. Environmental insults from the daily life like heavy metal, smoke, anger, hypoxia, oxidizers and radiations play vital role in worsening the prognosis of cancer and causes metastasis. Its likeliness to increase in the future to cause global havoc designates it as an epidemic. Cancer development requires urgent intervention. Past few decades have witnessed extensive research to challenge carcinogenesis. Treatment involving synthetic discipline is often associated with severe adverse effects, or even worsened prognosis. Cancer chemotherapy is toxic and complicated by undesirable secondary effects. Metastasis, cancer cell's ability to move from the primary site and invade distant tissues in the body, accompanied by emergence of drug resistant variants, is another major hurdle in cancer treatment. Accordingly, newer economic and patient friendly anti-metastasis molecules are deemed useful in intervention of cancer cell aggressiveness and drug resistant properties. Many natural substances have proved their potential so far. *Helicteres angustifolia* L. is a shrub that forms a common ingredient of several cancer treatment recipes in traditional medicine system both in China and

Laos. In order to investigate molecular mechanisms of its anticancer activity, we prepared aqueous extract of *Helicteres angustifolia* L. Roots (AQHAR) and performed several *in vitro* assays using human normal fibroblasts (TIG-3) and osteosarcoma (U2OS). We found that AQHAR caused growth arrest/apoptosis of U2OS cells in a dose-dependent manner. It showed no cytotoxicity to TIG-3 cells at doses up to 50 μg/ml. Biochemical, imaging and cell cycle analyses revealed that it induces ROS signaling and DNA damage response selectively in cancer cells. The latter showed upregulation of p53, p21 and downregulation of Cyclin B1 and phospho-RB. Furthermore, AQHAR-induced apoptosis was mediated by increase in pro-apoptotic proteins including cleaved PARP, caspases and BAX. Anti-apoptotic protein BCL-2 showed decrease in AQHAR-treated U2OS cells. *In vivo* xenograft tumor assays in nude mice revealed dose-dependent suppression of tumor growth and lung metastasis with no toxicity to the animals suggesting that AQHAR could be a potent and safe natural drug for cancer treatment. One of the important known bioactives from *Helicteres angustifolia* is Cucurbitacin B. We found that whereas AQHAR was relatively safe to the normal cells, Cucurbitacin B was toxic and unsuitable for application in the living tissue for medicinal purposes. Here, we have developed a 1:500 molar ratio combination of Cucurbitacin B and Withanone (=CucWi-N), and analyzed its anticancer potential using non-small-cell lung cancer cells. CucWi-N at this ratio dose was found to be safer to the normal cells than the cancer cells. In our initial *in silico* model, Cucurbitacin B showed prospect to abrogate mortalin-p53 interaction (necessary for cancer cell proliferation) and in combination with Withanone had synergistic affinity to engage hnRNP-K protein (necessary for cancer cell migration). In *in vitro* analysis, we found that the combination significantly and dose-dependently caused changes at cellular and protein level indicating (i) sensitization of cancer cells to environmental stressors (ii) inhibition of stemness

and aggressiveness of the cancer cells, and (iii) induction of replicative senescence. We believe that CucWi-N is a potential anticancer drug that warrants further mechanistic and clinical studies.

Contents

List of figures

(top right); quantified colony number (bottom left); quantified absolute cell count by dissolving crystal violet in de-staining solution and using slope equation for C6 cells (bottom right).

Fig. 51. Troubleshooting guide for QCV assay.

Abbreviations and nomenclature

4EBP1, 4E-binding protein 1; 5-mC, 5-methyl cytosine; ACLY, ATP citrate lyase; AKT/PKB, Protein kinase B; ALI, Acute lung injury; aP2, Adipocyte protein 2; APAF1, Apoptotic protease activating factor 1; APC, Adenomatous polyposis coli; AQHAR, Aqueous extract of *Helicteres angustifolia* root; ATG, Autophagy related gene; ATP, Adenosine triphosphate; BAK, Bcl2 antagonist/killer; BAX, Bcl2 associated X apoptosis regulator; BCL-XL, B-cell lymphoma-extra large; BCL2, B-cell lymphoma 2; BDNF , Brain-derived neurotropic factor; BRCA1, Breast cancer 1; BSO, Butithione sulfoxime; C/EBPα, CCAAT-enhancer binding protein α; cAMP, Cyclic AMP; CBP, CREB-binding protein; CCL20, Chemokine (C-C motif) ligand 20; CD36, Cluster of differentiation 36; CDC2, Cell division cycle 2; CDK, Cyclin-dependent kinase; CIP2A, Cancerous inhibitor of protein phosphatase 2A; COX, Cyclo-oxygenase; CSK1α, Casein kinase 1α; CUB-PLC-BER; Cucurbitacin B poly(ε-caprolactone) berberine hydrochloride; DABCO, 1,4-Diazabicyclo(2,2,2)octane; DACE, 2-deoxy-2-amine-cucurbitacin E; DEPMPO, 5-Diethoxyphosphoryl-5-methyl-1-pyrroline N-oxide; DNA, Deoxyribonucleic acid; DNMT, de novo methyl transferase; Dyrk1B, Dual-specificity tyrosine phosphorylation regulated kinase 1B; EGFR, Epidermal growth factor receptor; EIF2AK2, Eukaryotic translation initiation factor 20alpha kinase 2; ELISA, Enzyme-linked immune-sorbescent assay; ELK1, ETS-like gene 1, tyrosine kinase 1 oncogene; EMT, Epithelial-to-mesenchymal transformation; ER, Estrogen receptor; ERK, Extracellular signal regulated kinase; FAK, Focal adhesion kinase; FOS, Finkel-Biskis-Jinkins murine osteogenic sarcoma; FOXO, Forkhead box O; FTICR, Fourier transform ion cyclotron resonance; FZD7, Frizzled receptor 7; GDP, Guanosine 5'-diphosphate; GFAP, Glial fibrillary acidic protein; GnRH, Gonadotropin-releasing hormone; GSK3, Glycogen synthase kinase 3; GTP, Guanosine 5'-triphosphate; H_2O_2, Hydrogen peroxide; HCC, Hepatocellular

carcinoma; HDAC, Histone deacetylase; HER2, Human epidermal growth factor receptor 2; HIF, Hypoxia inducible factor; HIV-AIDS, Human immunodeficiency virus-acquired immune deficiency syndrome; hnRNP, Heterogeneous ribonucleoprotein; HO1, Heme oxygenase 1; HPLC, High-performance liquid chromatography; hTERT, Human telomerase reverse transcriptase; HUVECs, Human umbilical vein endothelial cells; IL, Interleukin; iNOS, Inducible nitric oxide synthase; INF, Interferon; JAK, Janus activated kinase; JNK, Jun N-terminus kinase; KLF5, Kruppel like factor 5; kRAS, Kirsten rat sarcoma viral oncogene; LC-ES-MS, Liquid chromatography-electrospray mass spectrometry; LDH, Lactate dehydrogenase; LIMK, LIM domain kinase; LPS, Lipopolysaccharide; LTB, Leukotriene B; MAP2, Microtubule associated protein 2; MAPK, Mitogen activated protein kinase; MCP, Monocyte chemotactic protein; MEK, MAPK/ERK kinase; MEP, 2-C-methyl-d-erythritol 4-phosphate; MHC, Major histocompatibility protein; MMP, Matrix metalloproteinase; mTOR, Mammalian target of rapamycin; mTORC 1 and 2, Mammalian target of rapamycin complex 1 and 2; MVA, Mevalonate; cMYC, Chicken myelocytomatosis viral oncogene; NAC, n-acetyl-ι-cysteine; NCAM, Neural cell adhesion molecule; NFκB, Nuclear factor-κ beta; NMDA, N-methyl-D-aspartate; NMR, Nuclear magnetic resonance; NNK, Nicotine-derived nitrosamine ketone; NQO1, NADPH dehydrogenase quinone 1; Nrf2/ARE, Nuclear erythroid 2-related factor 2/antioxidant responsive element; NSAIDs, Non-steroidal anti-inflammatory drugs; NSCLC, Non-small cell lung cancer; PARP, Poly-adenosine diphosphate-ribose polymerase; PCAF, p300/CBP-associated factor; PCNA, Proliferating cell nuclear antigen; PDK1, Phosphoinositide-dependent kinase-1; PEO-b-PBCL, Poly(ethylene oxide)-block-poly(α-benzyl carboxylate ε-caprolactone); PEO-b-PCL, Poly(ethylene oxide)-block-poly(ε-caprolactone); PI3K, Phosphatidylinositol-3-kinase; PIP2, Phosphatidylinositol 4,5-bisphosphate; PIP3, Phosphatidylinositol 3,4,5-trisphosphate; PKA, Protein kinase A; PP2A,

Protein phosphatase 2A; PPARγ, Peroxisome proliferator-activated receptor γ; PTEN, Phosphatase and tensin homolog; RB, Retinoblastoma; RCC, Renal cell carcinoma; Rheb, RAS-homolog enriched in brain; RhoA, RAS homolog gene family, member A; RNS, Reactive nitrogen species; ROCK, Rho-associated protein kinase; ROS, Reactive oxygen species; S6K, Serine 6 kinase; STAT, Signal transducer and activator of transcription; TEMP, 2,2,6,6-tetramethyl-4-piperidone hydrochloride; TGF, Transforming Growth Factor; Th1, T-helper cell type 1; TLR2/4, Toll-like receptor 2/4; TNFα, Tumor necrosis factor α ; TPX2, Targeting protein for Xenopus kinesin-like protein; TSC1/2, Tuberous sclerosis complex gene ½; ULK1, Unc-51 Like Autophagy Activating Kinase 1; UV, Ultraviolet; VASP, Vasodilator-stimulated phosphoprotein; VEGF, Vascular endothelial growth factor; VEGFR2, VEGF-receptor 2; WHO, World Health Organization

Chapter 1

Cancer

1.1 Introduction

Cancer is a syndrome of diseases wherein the cells upon aberrant mutations/environmental stresses witness either the activation of proto-oncogenes or the suppression of tumor suppressor proteins. Resultantly, they undergo uncontrolled infinite replication, lose their functional characteristics, and exploit their physiological neighbors for nutrients and space. The process is often accompanied with malignant transformation and metastatic spread - EMT [1], especially when the availability of resources at a particular cancer niche shortens. Various mechanisms like autocrine and endocrine regulation of growth factors, platelet adhesion, quiescence, cytoskeleton rearrangements, cancer cell differentiation, micro metastasis, EMT, angiogenesis and niche formation determine the outcome. WHO data states that the global cancer burden is likely to rise to 22 million by 2030 [2], due to a variety of homeostatic insults. Cancer cells operate via various molecular mechanisms, popularly categorized as the cell signaling pathways. I here provide an outline of the major tumor suppressor and oncogenic pathways, which regulate the process of human carcinogenesis.

Tumor suppressor p53 protein (Fig. 1) is known as the guardian of the genome [3-6]. External or internal cellular injury to a normal cell activates the p53 tumor suppressor pathway. It directs the cell into growth arrest and apoptotic state via activation of several downstream effectors including growth arrest ($p21^{WAF1}$ and others) and apoptosis (BAX, PUMA and others) inducing proteins. Retinoblastoma (RB) protein (Fig. 1) coded by RB1 tumor suppressor gene [7-9]. At the G_1-S checkpoint, escalated Cyclin D binds with CDK4 leading to pRB phosphorylation, abrogation of pRB-E2F complexes and free E2F, which translocate to nucleus and activates genetic transcription via polymerase secretion, which is crucial for proliferation.

Wnt protein interacts with frizzled receptor extracellularly and deactivates β-catenin-destruction complex, which is made up of GSK3, Axin, CSK1α, PP2A and APC, coded by their respective genes [10]. The complex binds to β-catenin present in the cytoplasm and degrades it via phosphorylation-ubiquitination-proteasomal degradation. Mutations in any of them (ultimately resulting into cancer), most frequently in APC, result in faulty complex structure, which fails to bind to and degrade β-catenin. Excess β-catenin translocates to the nucleus, binds with galectin-3, interacts with T-cell transcription, lymphoid enhancing transcription factors, and promotes genes, which code for cyclin D protein essential for G_1/S cell cycle transition. STAT3 is a latent transcriptional factor in the cytoplasm, which is regulated by JAK phosphorylation (Fig. 1) [11-18]. It directly or indirectly upregulates genes associated with tumor proliferation and survival, and constitutes an important intracellular signal transduction pathway in cancer, which regulates cancer cell growth and differentiation. Inactivation or de-phosphorylation of the protein forces cells to undergo growth arrest and apoptosis.

Cancer tissue is fast growing and evading, central mass of which often suffers hypoxia. Emergency mechanisms such as HIF signaling get activated, which trigger angiogenesis, metastatic spread of disease, and resistance to chemotherapy. HIF-1 monomer is continuously transcribed and translated, and degraded via ubiquitin mediated proteasomal degradation under normoxic conditions. In hypoxic condition, this degradation is downregulated, resulting into accumulation of monomer. Accumulated monomers translocate to the nucleus and dimerize with HIF-1β to form a complex, which modulates transcription and translation of the target genes. NFκB proteins function as dimeric transcription factors and regulate the expression of genes influencing immunological, stress, and inflammatory response [19]. NFκB pathway proteins are normally bound to IκB and remain in an inactive state. Pro-inflammatory cytokines and other mitogens

activate IKK complex (IKKβ-IKKα-NEMO), which phosphorylates IκB proteins for its ubiquitination and proteasomal degradation. Free and active NFκB upon further phosphorylation, acetylation and glycosylation, translocate to nucleus to induce target gene expression.

Activated dimer of GFR phosphorylates RAS-GDP complex to RAF-GTP, which via series of downstream phosphorylation activates RAF kinase, MEK, MAP kinase and cMYC in cytosol and ELK1 in the nucleus (Fig. 1) [20]. ELK1 further activates cFOS transcription, which dimerize with cJUN. Activated cMYC and cJUN-cFOS complex trigger subsequent transcription, which are essential for DNA replication, such as cyclin D. Receptor tyrosine kinase activates PI3K, a complex of p85 and p110 proteins [21]. Activated PI3K phosphorylates PIP2 into PIP3, which via PDK1 activation phosphorylates AKT. After downstream signaling involving TSC1/2, Rheb and mTORC1 activates p70S6K and 4EBP1, which via estrogen receptor further translate to cell survival, growth, proliferation, differentiation, migratory potential and metabolism. Telomeres are specialized chromosome ends in the cells consisting of tightly held specialized and repetitive (10-15 kb) TTAGGG sequence, and protein caps, which protect chromosomes from terminal fusion [22, 23]. Every time a normal cell divides a small portion of the telomeric end gets eroded of about 50-200 base pairs until the bare chromosomal ends are left. At this stage, cell enters an irreversible and non-proliferative phase called replicative senescence. Most cancer cells acquire the ability to synthesize enzyme telomerase, which helps to regenerate telomeric ends. Autophagy is a conservation-indicated destructive process, wherein the non-functional or stressed cytoplasmic organelles and other constituents are delivered to lysosomes [24]. Lysosome engulfs and digests the material, and release energy and other important elements, which may be utilized in cellular metabolism. It is frequently found to take place as a response to cellular stress, but skeptical as it may be either protective or discretely destructive. It is characterized by the appearance of large

cytoplasmic vacuoles or vesicles with up regulation of ATG family proteins viz., LC3II/I, ULK1/2, and Beclin1, etc. Stress stimuli, nutritional imbalance, hypoxia and other chemical mediators like ROS and insults to intracellular homeostasis may lead to induction of autophagy response.

Prevention of production of ROS or catabolic destruction of ROS is explicitly defined as the antioxidant mechanism. ROS are charged super-ions, continually generated and released in the cells, presenting with vacuolization in cytosol and reaction with biomolecules like cell organelles and genetic material to generate peroxides and malondialdehyde. These alter membrane potential and signal transduction, and may induce cell offing mechanisms like necrosis, apoptosis and autophagy. ROS generation increases as a result of environment insults like pollution, radiations, infestation, etc. Prevention and control of cancer is one of the most expensive and least prolific healthcare investments, on top of which it is also burdened with toxic adverse effects associated with chemotherapy and radiotherapy. Use of natural medicines could not only lower the expenditure in the disease extensively, but may also bring down the adverse effect rate in clinical patients. Holistic approach (consumption of the natural molecules and relatives in the ratio prepared by the nature) for the treatment of cancer, as it is naturally prepared by the nature, could be adopted. Kaefer and Milner enumerated a list of benefits if the treatment of the disease is mainly herbal, and their probable role in the cancer [25]. Many biologically active molecules from the herbal sources have been identified in the last few decades, which in experiment have potential to prevent the disease, control its growth, and possibly eradicated it completely. Cucurbitacin B is one of the most extensively studied natural bioactives.

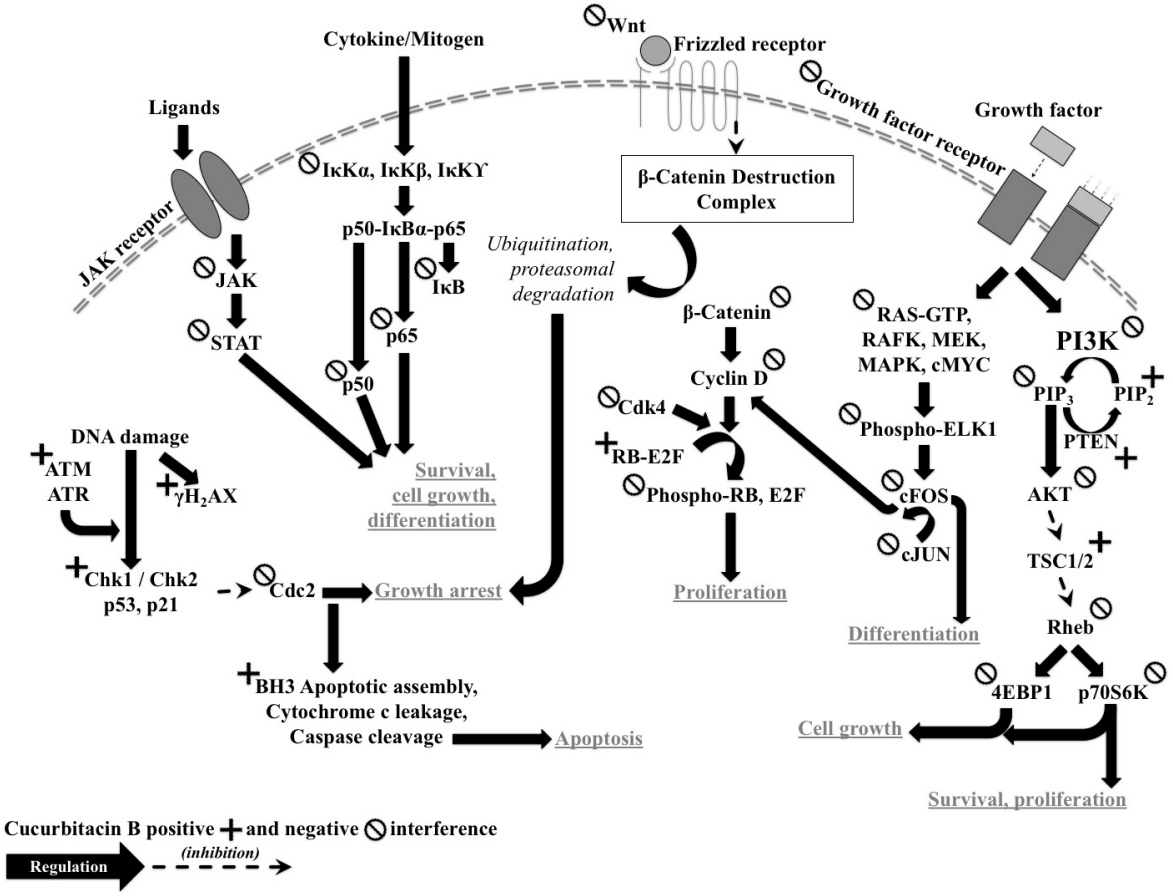

Fig. 1. Major cell signaling pathways contributing to cancer, and modulation by Cucurbitacin B.

Upregulation (✚) and downregulation (-) of protein expression.

Garg et al. 2018 International Journal of Oncology 52(1): 19-37

Chapter 2

Helicteres angustifolia

2.1 Introduction

Helicteres angustifolia L. (*H. angustifolia*) is a small shrub widely distributed in slopping grassland such as the Southeast China, Laos, Japan, Australia and many Southeast Asian countries. The dry root of *H. angustifolia*, known as "Shan Zhi Ma" in Chinese, has been popularly consumed as a medicinal liquor or tea to promote general wellness, and widely used to treat a variety of ailments ranging from flu to cancer [26-30]. Although popularly used for health and medicinal benefits, the scientific evidence behind their mechanism of action is limited. Previous investigations on active phytochemicals in the roots of *H. angustifolia* have identified various chemicals including Cucurbitacins and their derivatives [31, 32] in its extracts that exhibited inhibition of growth in a variety of human cancer cells [32-34]. Considering that the water extract is more favorable for human consumption, we investigated anticancer potential of aqueous extract of *H. angustifolia* roots (AQHAR) and found, for the first time, that it possesses potent anti-cancer activity [29]. In the present study, we demonstrate the mechanism of such anti-cancer activity using *in vitro* cell-based assays, with further validation in the immune-compromised animal model. Oxidative stress is characterized by excessive production of reactive oxygen species, which oxidizes intra-cellular structures and extinguish their functions. AQHAR induced DNA damage and oxidative stress signaling causing death of cancer cells [29].

Previously, some studies have reported anti-cancer activity of Cucurbitacin B in different types of cancers including liver [35], breast [36], laryngeal [37], brain [38], bone [39] and lung [40]. It has been shown to possess anticancer activity either as independent agent, or in synergism with other natural or synthetic molecules. Cucurbitacin B has been one of the extensively studied small molecules not only for cancer, but also for other ailments. While the therapeutic dose required as anti-inflammatory and other complementary conditions is relatively low, cancer essentially

requires a high dose as the mainstay of the treatment is to kill the cells. However, the toxicity profile of the molecule in the normal human cells has not been significantly explored.

Cancer cells pose threat to human organ systemic functions because they invade space and nutrients, which should ideally be used by the normal cells for growth and positive contribution to the health. Cancer cells are often described as the threat that at first sit quietly, learn from the surroundings and survive, so that when the time comes they may grow to gluttonous proportion, which the normal defense mechanism fails to comprehend, thereby contentedly invading the rights from the normal cells. Since the cancer cells are concurrently present with the normal cells in the diseased state of the body, it is important to eliminate them without causing much harm to the normal tissue.

Cucurbitacin B is one of the documented primary bioactives found in the roots of *H. angustifolia* [31]. For this reason, we first determined the toxicity profile of Cucurbitacin B for human normal lung cells and for a variety of cancer derived cells. We found that Cucurbitacin B was toxic to the most of cancer cells and showed moderate toxicity to normal cells as well. It caused cellular disruption and forced both the normal and cancer cells into death via series of significant and irreversible molecular signaling. Hence, the use of Cucurbitacin B at the cancer-killing dose as cancer therapeutics could not be precisely applauded.

2.2 Materials and Methods

2.2.1 Aqueous extract of H. angustifolia roots (AQHAR), cells and reagents

The roots of *H. angustifolia* used in the present study were collected from Vientianei, Laos as described earlier [29]. AQHAR (8.4%) was prepared by extraction of dried root powder with

distilled water at room temperature [29]. Human cancer and normal cells were obtained from the Japanese Collection of Research Bioresources (JCRB, Japan).

2.2.2 In-vitro cell-based assays

Short and long term cytotoxic effect of AQHAR was determined by MTT {3-(4, 5-dimethylthiazol-2-yl)-2,5-diphenyltetrazolium bromide (Life Technologies) and colony formation assay, respectively. The ROS (Reactive Oxygen Species) and DNA damage were detected using fluorescent staining using the Image-iTTM LIVE Green Reactive Oxygen Species Detection Kit (Molecular Probes Inc., USA) as per manufacturer's instructions and described earlier [29]. The expression levels of proteins in control and AQHAR treated cells were determined by immunoblotting and immunofluorescence assays [29]. Quantitation was performed using the Image J software (National Institute of Health).

2.2.3 In vivo assay

Tumor growth assays were performed using female BALB/c nude mice. Subcutaneous xenograft and tail vein- lung metastasis models were used to examine the effect of AQHAR on tumor growth and metastasis potential of A549 cells.

2.2.4 Statistical analysis

All experiments were carried out in triplicates, and data were expressed as mean ± standard deviation (SD). Statistical analysis was performed using the SPSS 13.0 software (SPSS Inc., Chicago, USA). Differences among samples were evaluated by using analysis of variance

(ANOVA) and Duncan's multiple comparison method. Significant difference was assumed at $p<0.05$.

2.3 Results and Discussion

2.3.1 AQHAR selectively inhibited the growth of cancer cells and caused apoptosis at higher doses

Human normal and cancer cells were treated with AQHAR (25 μg/ml) for 48 h. As shown in Fig. 2, we found that AQHAR caused toxicity to cancer. Of note, normal cells treated in parallel did not show toxicity at equivalent doses. AQHAR inhibited cancer cell multiplication in a dose-dependent manner, while normal cells remained unaffected. Apoptotic population of cancer cells increased significantly with increasing doses of AQHAR compared with the untreated control group. The data was evident by examining both cell count and cell morphology observed under the microscope, suggesting that AQHAR is selectively toxic to human cancer cells. Cancer cells treated with AQHAR also showed inhibition of their long-term multiplication and colony-forming efficacy. The data suggested that AQHAR causes death of cancer cells selectively and hence may be very useful for cancer therapy [41-44]. In light of this, we set out to determine the mechanism of action of AQHAR-cytotoxicity. Molecular analyses on detection of DNA damage and oxidative stress revealed that cancer cells treated with AQHAR suffered DNA as well as oxidative damage and stresses (Fig. 3). DNA damage was detected by Comet assay wherein the presence of DNA tail indicated the DNA damage. Whereas cancer cells showed comet assay-tail, normal cells showed no DNA tail after AQHAR treatment. Reactive oxygen species are chemically reactive molecules that have interruptive role normal cell structures and functions. Excessive amount of reactive oxygen species may cause irreversible damage to internal cell organelles, proteins and lipids

leading to cell death. We elucidated protein expression and found that key cell growth proteins were reduced selectively in the cancer cells upon the treatment with AQHAR. Our findings are consistent with the other studies wherein these proteins have been identified as anti-cancer targets [45-47].

2.3.2 AQHAR caused tumor-suppression and inhibited lung cancer metastasis in animal model

Since the anticancer activity in aqueous extract could be extremely beneficial for human consumption, we examined its anti-cancer effect in mice model (Fig. 4). We found that the tumor growth of untreated mice gradually increased, but AQHAR-treated mice showed 75% suppression of tumor growth, with no notable side effects. There was also a marked decrease in blood vessel formation and other factors necessary for the tumor growth in the AQHAR-treated mice with a large area of tissue degradation in cancer mass. We also investigated the anti-metastasis activity of AQHAR in mice lungs. Untreated mice showed big tumors in the lung, whereas AQHAR-treated mice showed significant reduction in the number (more than 50%) and volume of lung tumors, suggesting that AQHAR possessed a strong anti-metastasis potential. Taken together, we propose that AQHAR could be useful as a potent and safe natural anti-cancer medicine.

2.3.3 Comparison of AQHAR and Cucurbitacin B activity

We next used Cucurbitacin B, a major constituent of AQHAR. We found that Cucurbitacin caused comparable cell death in both the cancer and the normal cells. Although the pattern of death in the cancer cells was identical to that was caused by AQHAR extract, toxicity in the normal cells raised serious questions to conclude the presence of alternate chemicals in the constituency of extract that offered protection to the physiological. We tested various types of cancer cells.

Osteogenic sarcoma is a highly aggressive and malignant cancer of bone, characterized by production of malignant osteoid and rapid metastasis to the rest of the body. Non-small cell lung carcinomas are cancer of lung, of various types, varying in aggressiveness and origin. Cervical cancer arises in cervix and is characterized by severe and abnormal vaginal bleeding and pelvic pain along with the tumor formation and failure of fertility. Breast cancer is characterized by lump development, severe pain, aggressiveness, and varying molecular rapport. Colorectal carcinoma is the cancer of colon and rectal wall, characterized by extensive swelling, secretions, loose and bloody stools, and indigestion. Malignant melanoma is one of the most aggressive forms of skin cancer, with a very high recurrence rate. It is characterized by patchy nodule formation, which often bleed and pain and spread to internal organs to eventually shut the body completely.

We tested the potential of Cucurbitacin B against a variety of cancer derived cells and found that the toxicity was highly variable and hence optimization of the dose would be required for different cancers. In parallel assays, using human normal cells we found that contrary to AQHAR, Cucurbitacin B caused toxicity in normal cells as well (Fig. 5). Cytotoxicity of Cucurbitacin B to the human living cells has been earlier attributed to disruption internal structures crucial for cell division [48, 49]. Direct observation of cells under the microscope and cell cycle analysis supported these data.

2.4 Conclusion

The present study demonstrated anti-cancer activity in the aqueous extract of *H. angustifolia* roots (AQHAR), both at cellular level and animal model. Mechanism of AQHAR as evidenced is summarized in Fig. 6.

Herbal medicines have been known to enhance the immune function and speed up recovery, alleviate radiochemotherapy-related toxicities, improve quality of life, and extend survival, hence are popular as complementary treatments [29]. However, the exact mechanism of their activities has not been resolved and limits their usage in clinic. We, hereby, report that the aqueous extract of AQHAR causes selective toxicity to cancer cells (Fig. 7). The mechanism is through an induction of reactive oxygen species and DNA damage, ultimately leading to the cell growth arrest and cell death. Of note, normal cells remained unaffected at the equivalent doses. Cucurbitacin B was toxic to both cancer and normal cells. The selective cancer cell toxicity was translated in animal model by tumor growth suppression and anti-metastasis in mice, without any apparent toxic effect (Fig. 7).

AQHAR is proposed as a promising natural and safe anti-cancer reagent for cancer treatment, and warrant further studies, to dissect the molecular mechanisms of such multiple activities of AQHAR and its chief components such as Cucurbitacin B followed by its possible recruitment for effective cancer treatment.

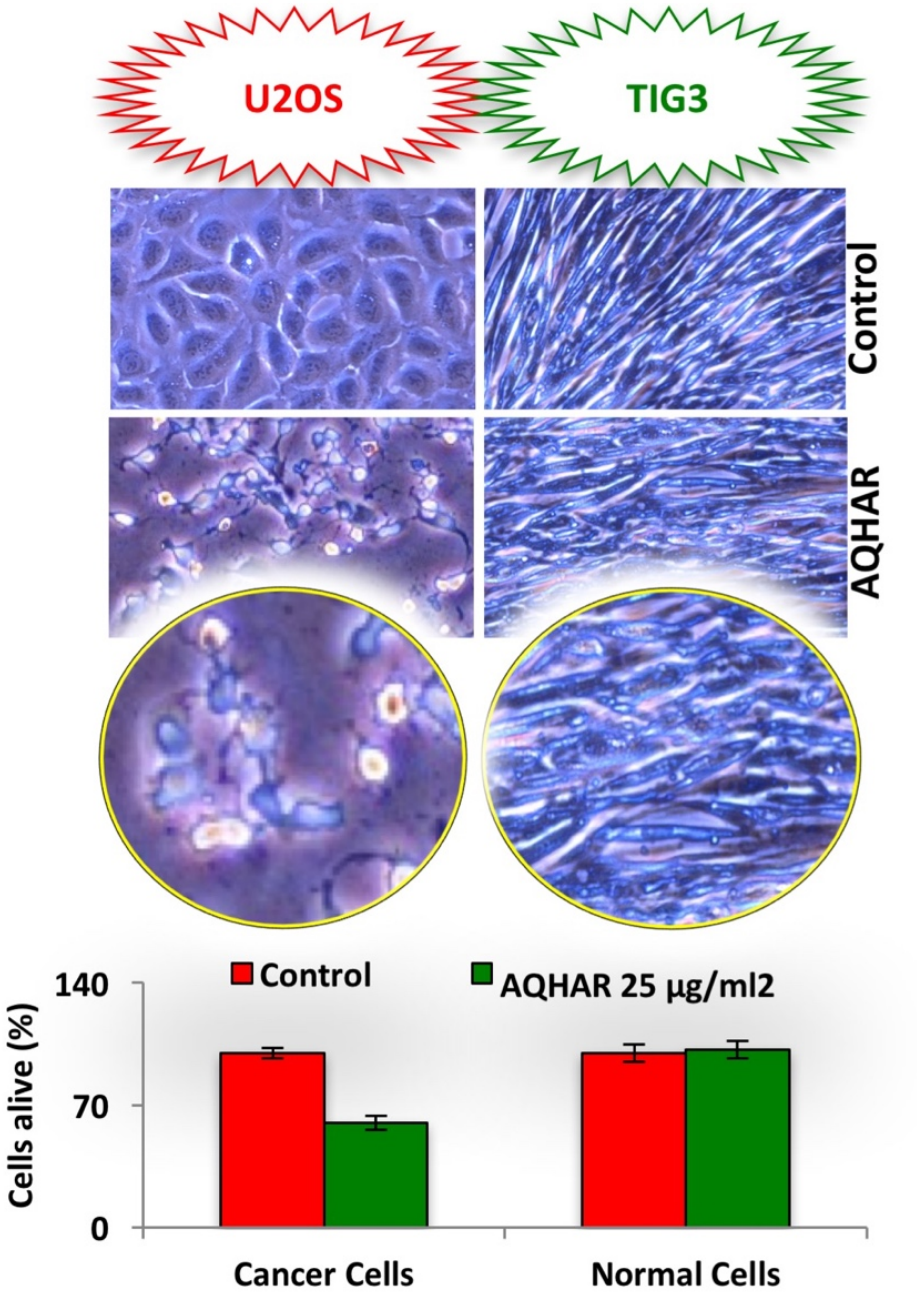

Fig. 2. AQHAR was selectively toxic to the U2OS cancer cells at 25 mg/ml dose at standard *in vitro* conditions.

Li and Garg et al. 2016 PLoS One 11(3): e0152017

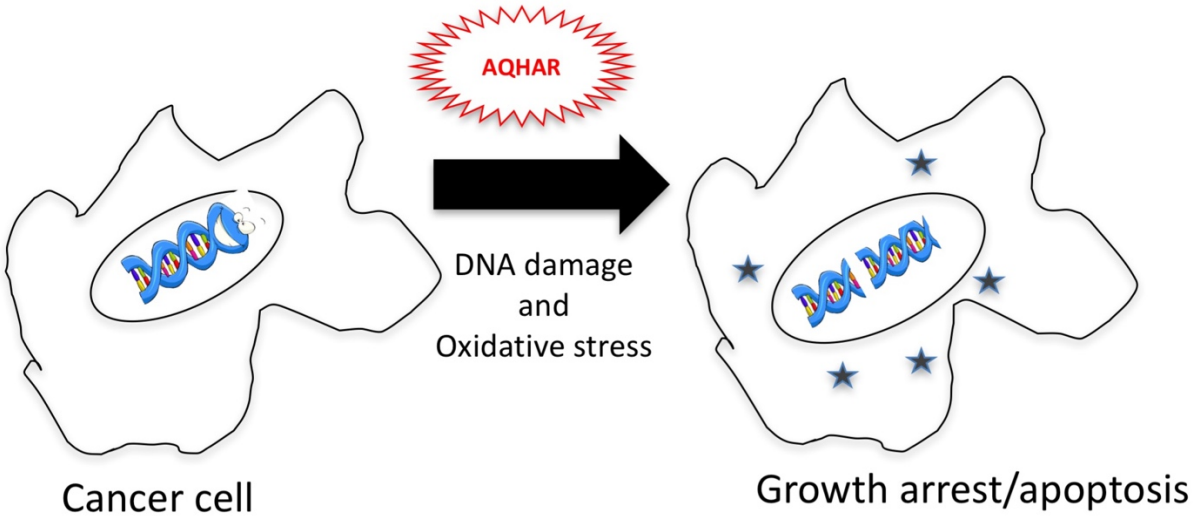

Fig. 3. AQHAR caused DNA damage and oxidative stress in the cancer cells, which resulted into growth arrest and apoptosis via the induction of reactive oxygen species

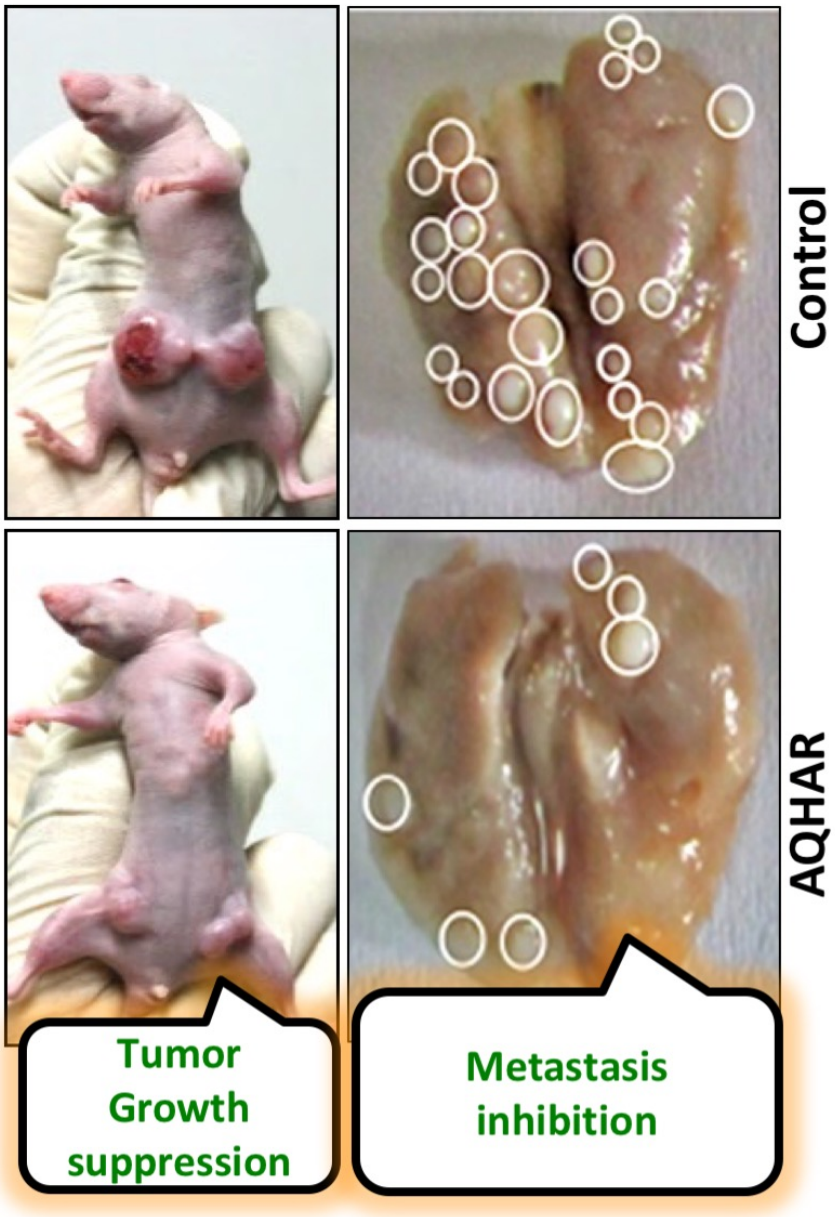

Fig. 4. AQHAR continual treatment in the *in vivo* balb/c nude mice model caused suppression of the growth of subcutaneously placed cancer cell xenograft, and caused inhibition of lung metastases.

Li and Garg et al. 2016 PLoS One 11(3): e0152017

No.	CELL LINE	TISSUE	DISEASE
1	TIG-3	Lung	-
2	U2OS	Bone	Osteosarcoma
3	HT1080	Connective Tissue	Fibrosarcoma
4	NCI-H1299	Lung	Carcinoma (NSCLC)
5	HeLa	Cervix	Adenocarcinoma
6	MDA-MB-231	Breast	Adenocarcinoma
7	MCF7	Breast	Adenocarcinoma
8	A549	Lung	Carcinoma
9	DLD-1	Colon	Colorectal adenocarcinoma
10	A427	Lung	Carcinoma
11	G361	Skin	Malignant Melanoma

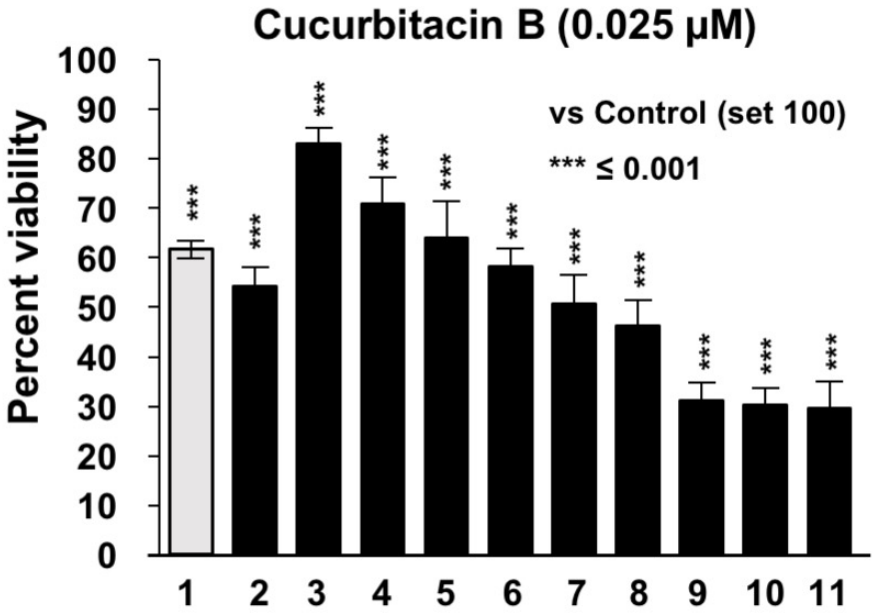

Fig. 5. Cytotoxicity of Cucurbitacin B on cancer and normal human cells. Effect of Cucurbitacin B on a variety of human cancer and normal cells, $^{***}p<0.001$ denotes statistically significant difference between the control and treated groups.

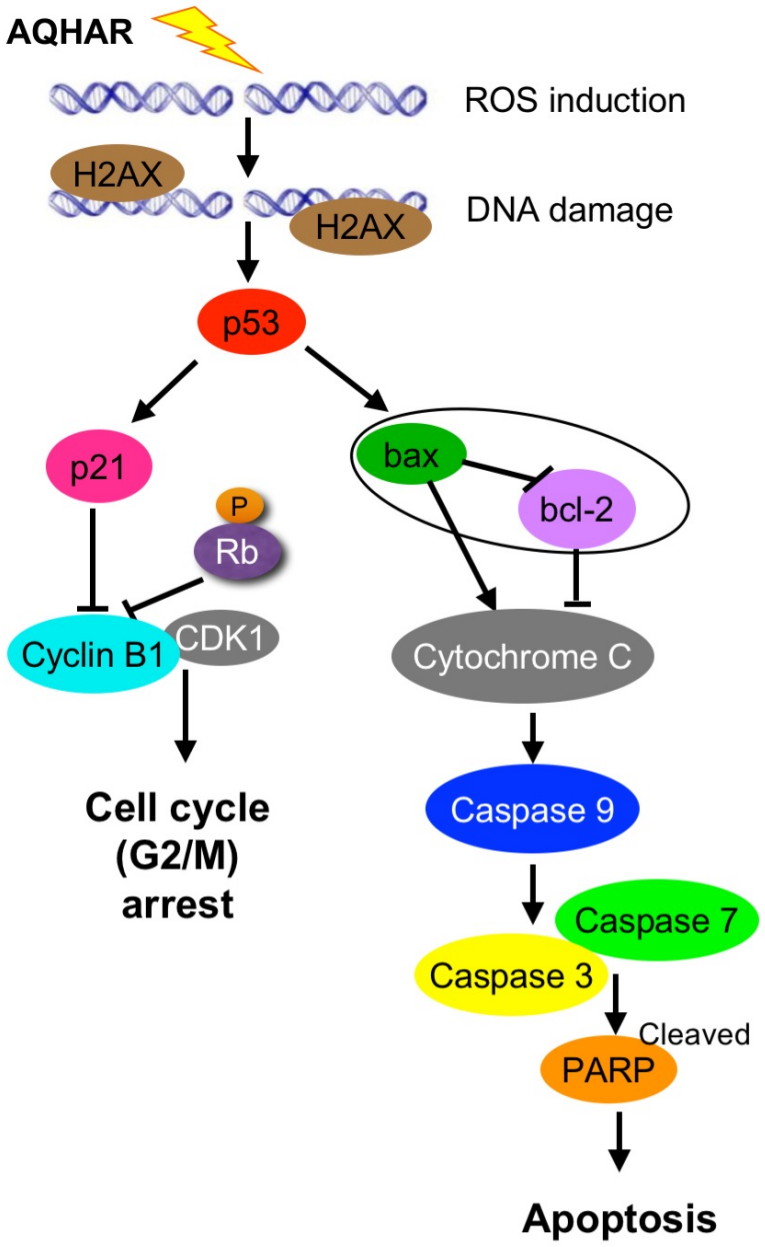

Fig. 6. Schematic representation showing the effect of AQHAR on cancer cells by induction of oxidative stress (ROS) and DNA-damage leading to activation of growth arrest and apoptosis signaling.

Li and Garg et al. 2016 PLoS One 11(3): e0152017

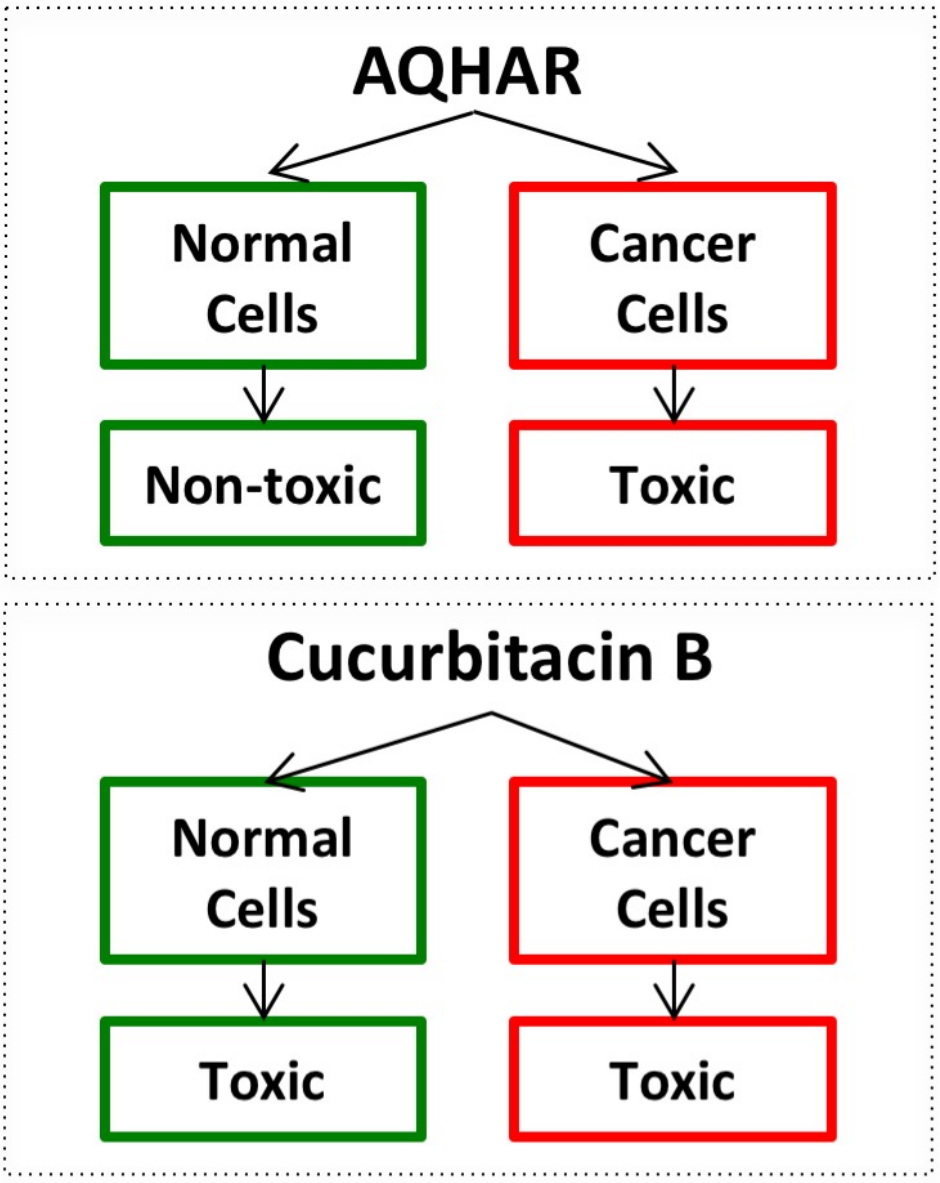

Fig. 7. Summary of selectivity in toxicity caused by AQHAR treatment, but not Cucurbitacin B in the cancer cells and normal cells.

Chapter 3

Cucurbitacin B

3.1 Introduction

Cucurbitacins are chemically characterized by tetracyclic cucurbitane (triterpene hydrocarbon) nucleus skeleton 19-(10→9β)-abeo-5α-lanostane base, varied by the positional substitution of an oxygen atom (Fig. 8) [50, 51]. There are mainly 40 known species of Cucurbitacins and their derivatives, divided into 12 groups namely A, B, C, D, E, I, H, Q, R, dihydrocucurbitacin B, etc. [52]. These are usually crystalline in nature, purgative, hydrophobic and easily soluble in organic solvents with absorption maxima for ultraviolet light ranging from 228 to 234 nm, having exceptions such as Cucurbitacin H, which is usually an amorphous solid. Various studies have been conducted to the effects of these compounds in various cell lines *in vitro* and *in vivo* against different cancer subtypes (A/B/E/D/I/Q - lung; B/E/D/I/dihydrocucurbitacin B - breast, neurological, colon and hepatocellular; E/I - prostate; E - ovarian; D/dihydrocucurbitacin B - leukemia; D - lymphoma; Q - murine). Cucurbitacin B has been one of the most explored for its role in biological systems. Cucurbitacin B ($C_{32}H_{46}O_8$, molecular weight 558.712 g/mol, 19-(10→9β)-abeo-10-lanost-5-ene triterpene), found in the plants of Cucurbitaceae and other plant families like Brassicaceae, is classified as a steroid with peculiar bitter taste and cytotoxic properties. Its bitterness could offer it protection against predators and parasites [53]. It has previously been known to be effective against various illnesses notably generalized inflammation and algesia, carbon chloride-induced hepatotoxicity and profound cholestasis, CD18-mediated disorders, infestation of insects, cell adhesion and leukemic disorders, immune mediated and angiogenic disorders, etc. [54-56]. Dantas et al. analyzed few derivatives of Cucurbitacin obtained from the seeds of *Cayaponia racemosa* for cytotoxic potential [57]. Nearly all were lethal to brine shrimp and inhibited cancer cell proliferation. However, their toxicity did not reach the order to inhibit the biological development of sea urchin or mouse erythrocytic lysis. The authors credited

this to the chemical structure of Cucurbitacins, and postulated that such differences in toxicity profile could be attributed to the position of carbonyl group at carbon-11 and absence of a double bond between carbon-23 and carbon-24. In another study, authors isolated a chemical substitute of Cucurbitacin B from the fruiting bodies of mushroom *Leucopaxillus gentianeus*, which differed from Cucurbitacin B in lacking an oxygen substituent from at carbon-16, and screened for anti-tumor toxicity with respect to chemical structure variation [55]. This minute substitution might be responsible for its significant (about 6-fold) anti-tumor profile. It has high affinity for glycosides and - not rare to find Cucurbitacin B in a naturally bound form. Hatam et al. isolated and performed NMR studies on Cucurbitacin glycosides derived from the fruit of *Citrullus colocynthis* L. Schrad [58]. Cucurbitacin B showed strong affinity to human serum albumin via hydrophobic and electrostatic forces, and increased the binding of ibuprofen to albumin [59]. This indicated the catalytic role of Cucurbitacin B in NSAIDs-pharmacokinetics.

3.2 Cucurbitacin B - sources

Cucurbitacin B has been extracted from plants of various families and genera around the world for research purpose. We examined the effect of Cucurbitacin B, derived from *Helicteres angustifolia* [29], on a variety of cancer and normal cells and discovered its cytotoxic potential in bone osteosarcoma cells at nanomolar doses. Cucurbitacin B fractionated from the methanolic extract of *Licaniaintra petiolaris* was analyzed for toxicity via kenacid acid cytotoxicity assay [60] and – caused, at the dose less than 0.01 μg/ml, more than 50% cell death in human oral epidermoid carcinoma cells. Cucurbitacin B obtained in both pure and glycoside form from the fractionation from root extract of *Casearia arborea* showed potent cytotoxicity against glio-sarcoma and melanoma cell lines [61]; from the chloroform-methanol extracts of *Cucumis prophetarum* it

showed cytotoxicity against tumor derived and virally transformed mouse cancer cells [62]; from the fruiting bodies of the fungal mushroom *Leucopaxillus gentianeus* it showed very strong cytotoxicity against NSCLC, RCC, HCC and HER2-/ER+ breast carcinoma cells [53]; from the stems of *Cucumis melo* it showed significant cytotoxicity against NSCLC and HCC *in vitro* via activation of phospho-STAT3 [63]; from the fruiting bodies of the fungal mushroom *Leucopaxillus gentianeus* it showed cytotoxicity against NSCLC, RCC, HCC and HER2-/ER+ breast carcinoma cells [53]; and from the methanol extract of *Trichosanthes kirilowii* Cucurbitacin B and its close relatives demonstrated potent anticancer activities mediated through HIF-1α and NFκB suppression [64]. From the air-dried rhizomes of *Begonia nantoensis* it not only showed cytotoxicity against NSCLC, HER2-/ER+ breast carcinoma, gastric adenocarcinoma and non-neoplastic nasopharyngeal epithelial cell carcinoma cells, but also inhibited HIV replication in human T-lymphocytes, flaunting its potential as an anti-viral molecule [65].

Many studies have shed light on other medicinal properties of Cucurbitacin B. Yesilada et al. showed potent anti-inflammatory activity in a fraction from the freeze-dried fruit juice of squirting cucumber *Ecballium elaterium* L. Rich [66]. Rawat et al. demonstrated the anti-oxidant and anti-inflammatory potential of extracts of cucurbits *Lagenaria siceraria*, *Cucurbita pepo*, *Luffa cylindrical* [67]. Overall, in last 50 years, Cucurbitacin B has been shown to possess therapeutic value for ailments like cancer, HIV-AIDS, and inflammatory disorders. Indeed, methods for preparing Cucurbitacin with longer shelf life have been developed [68]. More recently, several studies, using *in vitro* and *in vivo* approaches, have reported its mechanism of action.

3.3 Cucurbitacin B - anticancer activity

Many researchers around the world have based their research questions on the activity of Cucurbitacin B in cancer cells. Cucurbitacin B has been shown to possess strong anticancer activity in a variety of cancer cell lines *in vitro* and *in vivo* (Fig. 9).

3.3.1 Breast cancer

Tannin-Spitz et al. isolated Cucurbitacin glycosides from the leaves of *Citrullus colocynthis* and found that the combination (Cucurbitacin B/E glycosides 1:1) inhibited the growth of breast cancer cells in a dose and time dependent fashion, and forced the cells into G_2/M phase cell cycle arrest furthering into apoptosis [36]. Growth arrest was elucidated by the downregulation of $p34^{Cdc2}$/cyclin B1 protein complex and upregulation of phospho-STAT3 and $p21^{WAF1}$. Breast cancer cells treated with the combination of Cucurbitacin B and glycosides showed remarkable annular appearance representative of actin filament disruption. This led to ER status independent inhibition of PKB protein phosphorylation and reduction in the expression of Survivin, contributing to apoptosis. Wakimoto et al. confirmed that Cucurbitacin B induced dose dependent disruption of actin microtubules and filaments to illustrate rapid morphological changes in breast cancer cells, as soon as 15-20 minutes after exposure to the compound [69]. These were due to the disruption of F-actin within 3-5 minutes after exposure, followed by disruption of microtubules over 15-20 minutes. These findings were verified using nude mice, in which tri-weekly orthotopic 1 mg/kg intra-peritoneal injections of Cucurbitacin B resulted in about 50% tumor size growth suppression.

Duangmano et al. (2010) reported that Cucurbitacin B inhibited the telomerase activity in the breast cancer cells [70]. Telomere erosion and telomerase inhibition was supported with the inhibition of hTERT and cMYC proteins and consequential cell cycle arrest into G_2/M phase [70, 71]. Two years later they reported downregulation of cyclin B1 (key cell cycle regulatory protein)

by Cucurbitacin B [10]. They also showed inhibition of phosphorylation of GSK-3β, resulting in enhanced activity of the β-catenin-degradation complex, accompanied with downregulation of galectin-3. These results indicated an over obstruction of canonical Wnt/β-catenin signaling axis. They also reported the role of neucleophosmin/B23 in breast cancer cells [48]. Nucleophosmin/B23 protein plays an important role in controlling cellular cycling activities, and continuously patrols from nucleolus to cytoplasm and back. Microtubules are cytoskeleton builders consisting of α- and β-tubulin subunit chains, and have fundamental role in maintaining cell structure, motility, trafficking and division. Shortage of nucleophosmin/B23 may lead to disruption of tubulin subunit polymerization. The authors found that Cucurbitacin B treatment caused strong anti-proliferative and apoptotic effects in breast cancer cells through downregulation of nucleophosmin/B23 and disruption of microtubule polymerization. They investigated the effectiveness of Cucurbitacin B in BRCA1-defective breast cancer cells [72], where it counterpoised uncontrolled proliferation and drug resistance of cancer cells. Additionally, it caused up regulation in the expression of cell cycle inhibitors $p21^{WAF1}$ and $p27^{KIP1}$, driving the cells into apoptosis.

HER2 status and integrins play a vital role in the carcinogenesis in breast cancer cells. HER2/neu, a proto-oncogenic protein, is a mitogenic tyrosine kinase receptor, which directly participates in cell transformation, survival and proliferation. Integrins are a large family of extracellular matrix (tumor cell microenvironment governing) receptor proteins, composed of two α- and two β-glycoprotein units linked with non-covalent bonds. There are about 24 popular integrin dimers, distinctly mended by at least 18α and 8β subunits. Integrins ITGAVB3 and ITGA6B4 specifically foster survival and cell motility [73-75], whereas ITGB1 and ITGB3 induce apoptosis (integrin-mediated cell death) [76]. Gupta and Srivastava (2014) reported that

Cucurbitacin B treatment inhibited HER2 receptor and cell adhesion integrins, and triggered integrin-mediated cell death via B1 and B3 upregulation through a dose and time dependent BAX and caspase 8 cleavage [77, 78]. They also reported that Cucurbitacin B treatment in HER2+ breast cancer cells reduced their invasiveness by EMT reversal. HER2+ cells acquire mesenchymal properties via upregulation of TGFβ and downregulation of E-cadherin [79]. Cucurbitacin B inhibited the expressions of TGFβ, SMAD, SNAIL, SLUG, ZEB1 and N-cadherin, and abrogated the expression of E-cadherin in HER2+ breast cancer cells. Cucurbitacin B treatment induced autophagy in breast cancer cells [80]. It caused DNA damage in HER2- breast cancer cells via ROS mediated upregulation of γH_2AX and phosphorylation of ATM/ATR resulting in p53-dependent cell apoptosis. Autophagy induction was confirmed by the appearance of autophagic vacuoles in monodansylcadaverine (MDC) staining and upregulation of Beclin1, ULK1 and LC3 in a time and dose dependent manner. The effects of ROS reversed if the cells were pretreated with NAC. Cucurbitacin B also reduced the metastatic potential of the breast cancer cells [81]. At the non-apoptotic dose, Cucurbitacin B delayed migration and invasion potential of the breast cancer and human vascular endothelial cells in a time and dose dependent manner. It was further accompanied by inhibition of angiogenesis potential and a dose dependent suppression of VEGF/FAK/MMP9 signaling axis. These results were validated via retrograde inhibition of FAK using its inhibitor FI14 and genetic silencing, and *in vivo* studies.

3.3.2 Lung cancer

Lang et al. tested the effect of Cucurbitacin B on NSCLC cells [82]. They showed that the highly oxygenated bitter triterpene (Cucurbitacin B) caused moderate to potent cytotoxicity with IC_{50} 0.13 μM in 48 h and 0.04 μM in 72 h. Thiols are one of the crucial redox regulators for

cytoskeleton remodeling, cell cycle progression, mitochondrial apoptosis and regulation of redox sensitive signal transducers and activators of transcriptors. Kausar et al. (2013) showed that the thiols act as the intermediate between Cucurbitacin B and its toxicity in lung cancer cells [40]. All cytotoxic effects were attenuated with thiol anti-oxidant NAC pretreatment, whereas exacerbated with GSH synthesis inhibitor BSO. They demonstrated the physical interaction of Cucurbitacin B with NAC and glutathione (GSH) extracellularly using ultraviolet (UV) and FTICR mass spectrometry. Furthermore, Guo et al. reported that Cucurbitacin B in lung cancer cells also caused DNA damage via ROS formation, and let cells into G_2/M cell cycle arrest [83]. ROS caused double strand DNA breaks, which led to ATM-mediated activation of Chk1-Cdc25C-Cdk1 and p53-14-3-3-σ-CDC-25C-CDK1 pathways leading to mitotic interruption in parallel. Lung cancer when treated with Cucurbitacin B inhibited phosphorylation of STAT3 to cause growth arrest and apoptosis in dose and time dependent manner [84]. It inhibited STAT3 pathway leading to downregulation of cyclin B1 and BCL2. Shukla et al. (2015) reported global DNA methylation-associated epigenetic modifications due to Cucurbitacin B treatment in highly aggressive NSCLC cells [85]. They reported that the altered histone modifications at the respective promoter sites caused upregulation of $p16^{INK4A}$and $p21^{WAF1}$ and downregulation of hTERT to cause replicative senescence, growth arrest, and apoptosis. They also found that Cucurbitacin B caused downregulation of cMYC/kRAS at only protein and not transcriptional level. 5-mC reduction was accompanied with downregulation of DNMTs, HDACs and SIRT, and upregulation of CBP and PCAF. The results were validated using carcinogen NNK-induced lung tumorigenesis in mice, advocating epigenetic modulation to be a significant anticancer mechanism of Cucurbitacin B.

Silva et al. (2016) reported PI3Kinase and MAPK pathway inhibition due to Cucurbitacin B treatment [86]. The treatment delayed cell migration, alleviated invasion potential, and caused

dose and time-dependent apoptosis. It inhibited MMP release and FAK activation, and upregulated (activated) phospho-AKT, -ERK, -JNK and -NFκBp65. In another study, Cucurbitacin B exhibited a strong anti-metastatic potential in the NSCLC cells via down regulation of canonical Wnt/β-catenin signaling axis [87]. In both moderately aggressive and highly aggressive NSCLC cell lines *in vitro*, Cucurbitacin B treatment delayed migration and impeded invasion with downregulation of Wnt3/Wnt3α, FZD7, β-catenin, MMP2, cMYC, cyclin D1, Survivin and VEGF and upregulation of E-cadherin proteins. It also showed potent anti-angiogenic effects. These effects regressed upon the treatment with EMT inducer TGFβ or by retrograde genetic knockdown of Wnt3/Wnt3α. All the results were validated using NNK-induced lung tumorigenesis in mice. Intraperitoneal injections of Cucurbitacin B at 0.1 mg/kg body weight, administered thrice a week, reduced the tumor incidence, frequency, and volume by 80-90% compared to vehicle group.

3.3.3 Skin cancer

In malignant melanoma, Cucurbitacin B inhibited cell proliferation as well as their migratory potential [88]. Treatment in a mouse melanoma cell line caused cell membrane bleb and deformation, and multiploidy, via ROS induction resulting in dose dependent G_2/M phase growth arrest. There was significant depletion and aggregation of G-actin protein from the cellular cytoskeleton, and were reversed using NAC. NAC is a *N*-acetyl derivative of *L*-cysteine, and an established potent antioxidant. Inhibition of growth of subcutaneously implanted melanoma cells was validated using female C57BL/6 mice. Cofilin is an actin-depolymerization factor. It is regulated by phosphatidylinositol phosphate, pH variations, redox balance, and competition with tropomyosins [89], activated by dephosphorylation at its serine residue 3 by chronotropin or slingshot phosphatases, and inactivated by phosphorylation via LIM or TES kinases [90]. Rho-associated kinases indirectly modulate the stress fibers and focal adhesions [91]. Cofilin and actin

form rods and are implicated in the pathogenesis of neurogenerative disorders [92]. Cucurbitacin B dramatically activated cofilin via thiol oxidation, which formed rod like structures co-localizing with the actin (tandem rods) in melanoma cells [93]. Rho kinase and LIMK were downregulated, which were reversed by the treatment of thiol-ROS-scavenger NAC. Cucurbitacin B induced slingshot homolog-1 dependent hyper activation of cofilin and formation of cofilin-actin rods downstream of actin aggregation. VASP, an F-actin barbed end binding protein facilitates actin filament elongation through interaction with G-actin, profilin and other actin regulatory factors [94]. It directly controls the assembly of the actin-filament mesh, transforms the morphology and behavior of membrane protrusion structures, and also contributes in cell migration and adhesion. Cucurbitacin B induced VASP phosphorylation (deactivation) at serine 157 [95]. It was mediated by cAMP independent activation of Gα13/RhoA/PKA pathway, to generate VASP clumps. These clumps co-localized with amorphous actin aggregates, prior to the formation of highly ordered cofilin-actin rods in melanoma cells.

3.3.4 Brain cancer

Cucurbitacin B inhibited growth of human glioblastoma multiforme cells by intense disturbance in its internal cytoskeleton [96]. Within 15 to 30 min of treatment, it caused loss of pseudopodia, multi-nucleation and skirting up of cells associated with disruption of actin and microtubules, but was followed by the activation of cell survival pathways. It also inhibited cell proliferation, decreased migration, and caused cell cycle arrest in G_2/M phase and apoptosis. After 30 minutes of treatment, it caused upregulation of phospho-p38, JNK, JUN and ERK in a time-dependent manner. This was validated using SP600125, a broad-spectrum anthrapyrazolone inhibitor of JNK. SP600125 blocked the effects of Cucurbitacin B. The treated glioblastoma

multiforme cells exhibited marked disintegration and rearrangement of filamentous actin and β-tubulin. Touihri-Barakati et al. recently found that the proliferation, adhesion and migration inhibition due to Cucurbitacin B may be mediated through α5β1 integrins [38]. Laminins and fibronectin are extracellularly present high molecular weight cell adhesion proteins, and constitute major component of basal lamina contributing to cell adherence, dissemination and differentiation. Their upregulation is commonly found in EMT. Authors found significant downregulation of Laminin-1 and fibronectin in human glioblastoma cells. Further introspection in microvasculature endothelial cells demonstrated potent anti-angiogenic activity. Cucurbitacin B also showed remarkable anticancer effects in human neuroblastoma cancer cell lines [97]. It induced G_2/M arrest and apoptosis supported with upregulation of p53, p21 and BAX, and down regulation of BCL2. This was accompanied with the down regulation of proteins (CDK1 and Cyclin B1) essential for cell cycle progression. It also inhibited JAK2/STAT3 signaling cascades and induced JNK/p38MAPK-activation/ERK-inactivation. Shang et al. reported that PTEN activation is crucial and adds positively to the anti-proliferative effects of Cucurbitacin B [98]. Apart from proliferation inhibition, cell cycle restraining and apoptotic trend, they dissected the possible mechanism of inhibition of AKT signaling pathway in human neuroblastoma cells. Although they found that some of the key down-stream factors in the pathway viz., NFκB, AMPK and p38 did not alter; genetically activating AKT using plasmid vector carrying myr-AKT locus revered the toxic effects of Cucurbitacin B. Silencing of activated PTEN resulted in AKT phosphorylation and upregulation of the proapoptotic markers and repression of cyclins.

3.3.5 Liver cancer

Dat et al. (2010) isolated Cucurbitacin B and its close relatives, which demonstrated potent anticancer activities mediated through HIF-1α and NFκB inhibition in hepatic carcinoma cells [64]. Cucurbitacin B inhibited the activation of HIF-1α in an artificially induced hypoxia cell-based reporter assay, and inhibited NFκB in secreted alkaline phosphatase reporter assay. VEGF-specific ELISA validated its anti-angiogenic potential. Chan et al. (2010) explored the activity of Cucurbitacin B in human hepatocellular carcinoma *in vitro* and *in vivo*, where they reported that it caused dose and time dependent clonogenic inhibition via STAT3 independent S-phase arrest [99]. This phenomenon occurred probably via ERK1/2 activation and suppression of Cyclin D1, CDC2, and c-RAF phosphorylation. Cucurbitacin B induced ROS-mediated DNA damage leading to apoptosis and autophagy in hepatocellular carcinoma cells [100]. It was supported with increased upregulation of γH_2AX, phosphorylation of ATM/ATR and CHK1/CHK2, modulations in BCL2 family proteins and cleavage of caspases-7 and -9). They also ascertained Cucurbitacin B-induced autophagy, which was marked by vacuolization, upregulation of LC3II and ULK1, downregulation of AKT and mTOR proteins and activation of PTEN. They dissected that the contemporary activation of PTEN protein, which probably led to AKT/mTOR inhibition, had indirect correlation with autophagy. They used silencing RNA to genetically knockdown PTEN gene to confirm inhibition of AKT and upregulation of autophagy specific proteins.

3.3.6 Blood cancer

Cucurbitacin B with variable IC_{50} value induced cell cycle arrest and cellular differentiation in acute promyelocytic and myeloid leukemia [101]. It induced S phase growth arrest, swollen morphology of cells, altered cytoskeleton due to rapid and haphazard polymerization of filamentous actin into globular aggregates, and decreased clonogenicity in the immature blasts. It

also caused upregulation of monocytic-/granulocytic- specific CD11b, signifying cell differentiation. Cucurbitacin B suppressed the activated MAPK/ERK pathway and inhibited STAT3 activation in various human chronic myeloid leukemia cells [102]. Protein expression analysis showed activation of STAT3, RAF, MEK and ERK proteins is inhibited. STAT3 activation modulation ensued through a crosstalk mechanism, which also resulted into G_2/M arrest and apoptosis. Similar findings were noted in human leukemic *Jurkat* cells [101]. Cucurbitacin B caused cofilin dephosphorylation and actin dynamics intrusion, prompting into cell volume increase and simultaneous multi-nucleation. It also induced autophagosomes and LC3II upregulation as a compensatory protective response. Constitutive suppression of autophagy led to dramatic increase in caspase-3 mediated autophagy.

3.3.7 Others

Gao et al. (2014) reported the anticancer effects of Cucurbitacin B in prostate cancer cells [103]. Cucurbitacin B caused selective toxicity human epithelial type prostate cancer cells. ACLY is an enzyme, which metabolically converts mitochondrial citrate into acetyl coenzyme A [104, 105]. Acetyl coenzyme A is a major precursor and constituent responsible for synthesis of fatty acids and mevalonate, which promote carcinogenesis. Cucurbitacin B downregulated the expression of acetyl coenzyme A, fatty acid synthesis and mevalonate, supplemented with mitochondrial ROS production. It was suggested that the inhibition of the acetyl coenzyme A signaling might be one of the downstream mechanisms of ROS-mediated intracellular insults leading into apoptosis. Cucurbitacin B exhibited significant toxicity in human laryngeal cancer cells leading to G_2/M phase arrest [37, 106, 107]. This was supported with downregulation of cyclin B1, phospho-STAT3 and BCL2, associated with chromatin condensation, nuclear fragmentation, and appearance of apoptotic bodies in a dose and time dependent manner. Cucurbitacin B inhibited

proliferation and induced G_0/G_1 cell cycle arrest in a dose and time dependent manner in gastric cancer cells [108]. It suppressed the expression of cyclin D1, cyclin E, CDK4 and CDK2, and upregulated the expression of p27, all of which are indicated in inhibition of cell cycle progression. It also inhibited phosphorylation of JAK2 and STAT3, and caused apoptosis. It also induced caspase dependent apoptosis and autophagy in SGC7901/DDP DDP-resistant gastric cancer cells [109]. It suppressed cell proliferation and induced apoptosis and autophagy via inhibition of activation of CIP2A-PP2A-mTORC1 axis. Cucurbitacin B was shown to cause cytotoxicity to a variety of bone cancer and normal cells at nanomolar doses [29]. It forced osteoblastoma and normal lung fibroblasts into G_2/M phase growth arrest, and unanimously activated p53 and pRB tumor suppressor pathways, leading to characteristic senescence like growth arrest and/or apoptosis. At 20-100 μM dose it suppressed cell proliferation and induced apoptosis in U-2OS human osteosarcoma cells [110]. It inhibited JAK2/STAT3 and MAPK pathways leading to BH3 domain and caspase family protein modulation to induce cell cycle arrest, along with MMP2, MMP9, VEGF inhibition adding up to delay in migration potential of the cells and angiogenesis inhibition. Cucurbitacin B showed anticancer activity in paclitaxel-resistant A2780/Taxol ovarian cancer cells [111]. It caused growth inhibition in G_2/M phase and apoptosis via upregulation of p53 and p21, downregulation of BCL2, activation of caspase 3, and suppression of P-gp, suggesting potential role against multidrug resistance clinical cancer. Ma et al. (2014) monitored hypoxia-induced signaling and modulation by Cucurbitacin B in various cell lines *in vitro* [112]. They found that the activation of HIF-1α-monomer was suppressed due to Cucurbitacin B treatment in a dose dependent manner. They also found that this effect co-existed and correlated with strong dephosphorylation of mTOR, p70S6K, 4EBP1, and ERK1/2 proteins. It also downregulated the HIF-1 targets, VEGF and erythropoietin. Contemporary treatment with a known proteasomal

inhibitor MG-132 overshadowed the hypoxia signaling suppression, implying that Cucurbitacin B did not affect transcriptional coding, but regressed its ubiquitin-mediated proteasomal degradation. It also altered microtubule structures in human cervical cancer HeLa and osteosarcoma U-2OS cells [113]. It affected mitotic spindles and induced G_2/M cell cycle arrest. Zhang et al. (2012) showed that Cucurbitacin B induced caspase-independent autophagy reflux in a variety of cell lines [114]. It suppressed cell growth and proliferation, and inhibited interleukin-6 mediated phosphorylation of STAT3 in a dose dependent manner. Increase in mitochondrial-derived ROS and activated ERK1/2 and JNK proteins were also observed. It induced autophagy as evidenced by appearance of autophagosomes and upregulation of lipidated LC3 II. However, inhibition or knockdown of ATG5 and Beclin1 proteins did not rescue the cells from death. Instead, it forced cells to undergo caspase-dependent apoptosis, suggesting a competitive cross relation between autophagy and apoptosis.

3.4 Cucurbitacin B - as combination therapy

Cucurbitacin B and its derivatives have shown synergism with other anticancer agents. Marostica et al. (2015) presented DACE, a novel semisynthetic derivative of Cucurbitacin B and tested its effect in NSCLC cells as individually and in combination with either cisplatin (9 μM), irinotecan (4.25 μM), or paclitaxel (0.125 μM) [115, 116]. Cucurbitacin B (20 mg) was made to react with *p*-toluenesulfonyl chloride (34 mg) and DABCO (20 mg) in dichloromethane (200 μl) to obtain tosylated intermediate (20 mg), which was then made to undergo nucleophilic substitution using sodium azide (18.2 mg) in dimethylformamide (250 μl) to finally attain DACE. Cisplatin, an inorganic water-soluble platinum complex, reacts with and alters DNA after undergoing hydrolysis to produce crosslinks. Crosslinks impair DNA replication, and forces the cells into G_2 phase arrest.

Irinotecan is a topoisomerase inhibitor. Paclitaxel is a cyclodecane isolated from the bark of *Taxus brevifolia*. It stabilizes microtubules when they are in polymerized form, which causes cell death. In combination with either one of three accomplices, DACE (0.125 μM) reduced the risk of drug resistance, which is one of the major hurdles today in anticancer therapy by synthetic agents. It also showed selective toxicity to the cancer cells, forced them into G_2/M phase cell cycle arrest via STAT3 activation suppression and AKT downregulation, filamentous actin aggregation, nuclear fragmentation, inactivated cofilin1 suppression and E-cadherin substantiation. DACE also interfered with the activation of EGFR and its downstream factors AKT, ERK, STAT3 and survivin, contributing to growth arrest and caspase 3-mediated apoptosis. Efficacy in combination with cisplatin has also been checked in cutaneous squamous cell carcinoma [117]. Cucurbitacin B (0.1-2.5 μM) with cisplatin (5-20 μM) was pulse exposed to the cells i.e., exposed for a limited duration followed by culture in usual growth medium. The combination synergistically downregulated cyclin B1 and CDC2 expressions, with reduction in migratory and invasive potential of the cells. In laryngeal squamous cell carcinoma, the combination (0.1 μM Cucurbitacin B, 10 μM cisplatin) interdependently suppressed activation of STAT3 and translational expression of cyclin B1 and BCL2 [106]. In ovarian cancer, Cucurbitacin B sensitized cells to cisplatin (El-Senduny et al. 2016). Cucurbitacin B (2 μM) pretreated with cisplatin (10 μM) resulted in enhanced cytotoxicity than that by cisplatin alone in both cisplatin sensitive and insensitive ovarian cancer cells, via depletion of glutathione and increase in ROS production. It downregulated Dyrk1B, phosphorylated ERK1/2 and STAT3, and cyclin B1, leading to G_2/M phase growth arrest. It also downregulated BCL2 and APAF1, and upregulated caspase 9 - indicating apoptotic induction. These effects afforded by the combination had Cucurbitacin B at the dose of just a fourth of its IC_{50}. Cucurbitacin B (1 mg/kg) in combination with paclitaxel (10 mg/kg) injected intravenously

suppressed tumor growth in Balb/c nude mice [118]. Treatment was well tolerated by the animals and no evident damage in liver and kidneys was observed.

Docetaxel is a microtubule inhibitor. It prevents formation of microtubules leading to failure of growth and cell division. Gemcitabine, a nucleoside metabolic inhibitor, prevents the synthesis of genetic element, hence preventing DNA replication. Cucurbitacin B (0.001-0.05 μM) synergistically enhanced the anti-proliferative and apoptosis effects of docetaxel (0.001-0.005 μM) or gemcitabine (0.001-0.1 μM) in breast cancer cells *in vitro* and *in vivo*, at much low dose of either drugs than that are used in chemotherapy, indicating minimum adverse effects [119]. However, even with combination, but at only high dose, myelosuppression, hepatotoxicity and leukopenia with gemcitabine combination was encountered. In another study, combination of Cucurbitacin B (1 μM) and docetaxel (0.025 μM) caused cell cycle arrest at G_2/M phase and apoptosis via synergistic suppression of phospho-STAT3, BCL2, and Cyclin B1 in laryngeal cancer cells [37, 107]. Thoennissen et al. reported synergism of Cucurbitacin B with gemcitabine in pancreatic cancer [120]. Cucurbitacin B (0.01-0.1 μM) and gemcitabine (0.001-0.01 μM) combination caused dose-dependent multi-nucleation, G_2/M arrest and apoptosis, associated with inhibition of activated JAK2, STAT 3/5, Cyclin A/B1, and BCL-XL, and activation of $p21^{WAF1}$ and Caspases, more than Cucurbitacin B (0.05-0.2 μM) alone. Same group in another study in 2010 showed that this combination also inhibited BCL2 and cMYC adding up to apoptosis in pancreatic cancer cells *in vitro*. These effects were positively validated *in vivo* with only mild toxicity [121]. Protein kinase activity is crucial for a majority of intra-cellular signaling pathways. Prevention of protein kinase results into cell growth arrest. Gefitinib is a protein kinase inhibitor and known to be orally active selective inhibitor of EGFR, which inhibits autophosphorylation of intracellular tyrosine residues. Cucurbitacin B at safe dose (0.5 μM) offered synergistic anti-proliferative affects to benign dose

of gefitinib (10 μM) in human colorectal cancer cells *in vitro* [122], as validated via LDH assay. There was more significant down regulation of BCL2, Cyclin D1, and phospho-EGFR and STAT3, and upregulation of BAX, BAK and $p27^{KIP1}$, indicating stronger growth arrest and apoptotic signaling. Thymidylate is one of the important building blocks of DNA. Its synthesis is mainly stimulated by tetrahydrofolate. Methotrexate, an antineoplastic antimetabolite with immunosuppressant properties, is an inhibitor of tetrahydrofolate dehydrogenase. Cucurbitacin B (0.07 μM) and methotrexate (0.05 μM) combination caused G_2/M growth arrest and apoptosis in human osteosarcoma cells [39]. This was corroborated by inhibition of protein expression of ERK, AKT, and mTOR in JAK/STAT inactive cells. Further *in vivo* validation exhibited tumor suppression by combination (Cucurbitacin B 0.5 mg/kg body weight, methotrexate 150 mg/kg body weight) by 60-80%, which held at 66% after methotrexate withdrawal. Doxorubicin, a topoisomerase inhibiting anthracycline, intercalates DNA and exerts its anticancer activity by the suppression of DNA polymerase, topoisomerase II, and methyltransferase [123]. Doxorubicin resistant cells are known to entail survivin super-expression [124]. Cucurbitacin B (0.2-1 μM) and doxorubicin (1-5 μM) showed synergism against the progression of anaplastic thyroid cancer [125]. They synergistically enhanced ROS production, with consequential upregulation of cleaved PARP, COX2 and phospho-ERK1/2, and downregulation of BCL2, survivin, and JAK/STAT-signaling axis. In a recent study, Cucurbitacin B (up to 0.2 μM) with doxorubicin (up to 0.2 μM) showed synergistic anti-tumor activity via inhibition of aurora A leading to G_2/M phase cell cycle arrest, and IL10-induced STAT3 phosphorylation inhibition [126]. It also induced cofilin dephosphorylation and caspase-mediated apoptosis.

Valproic acid, popular anti-convulsion and mood stabilizing fatty acid, is inhibited by histone deacetylase (drug resistance). Histone deacetylase activates tumor suppressors p53, p21

and CDKs, and increase histone acetylation, which suppress the activation of many protoncogenes [127]. Cucurbitacin B caused dose dependent toxicity in mouse melanoma cells, followed by multiploidy, autophagy and BCL2 upregulation for cell survival [128]. This demonstrated the prosurvival role of autophagy in cancer cells after treatment with Cucurbitacin B (1 μM). When administered in combination with valproic acid (1-5 mM), it showed synergism to sensitize the cells to the toxicity due to valproic acid. It henceforth caused cell apoptosis and tapered multiploidization. Curcumin, obtained mainly from *Curcuma longa*, a yellow-orange phytopolyphenolic pigment commonly known as turmeric, is known for its medicinal properties such as anti-oxidant (prevention of ROS production), anti-inflammatory (COX inhibition), and anticancer (suppression of protein kinase C). It showed potency against alcoholic liver injury and insult due to lipopolysaccharide, D-(+)-galactosamine and heavy metals [129-131]. It fundamentally operates via mitochondrial invasion and is relatively safe to the healthy tissue [132]. Combination of Cucurbitacin B (143.2 μM) and curcumin (108.6 μM) showed synergism dose and time dependently against the human hepatocellular carcinoma [35], forcing the cells into G_0/G_1 phase arrest and apoptosis. It decreased the sensitivity of the cells to p-glycoprotein and reversed the resistance to 5-fluorouracil, indicating reversal of multidrug resistance. *In vivo* validation using Cucurbitacin B (10 mg/kg body weight) and curcumin (5 mg/kg body weight) combination resulted in greater suppression in tumor growth than with either molecule alone, with enhanced caspase 3 activity and reduced ATP contents. Cucurbitain B in combination with glycosides exhibited excellent antioxidant properties in a dose dependent manner [36, 133]. The combination inhibited hydroxyl radical-dependent DEPMPO-hydroxyl radical adduct formation, superoxide radical anion-dependent DEPMPO-hydroxyl radical addict formation and singlet oxygen-dependent TEMP-singlet oxygen addict generated in the photoradiation-porphin system. Duangmano et al.

(2012) reported that Cucurbitacin B increased the sensitivity of HER2 negative breast cancer variants to radiotherapy [49], and caused dose dependent G_2/M phase arrest and apoptosis *in vitro* via progressive up regulation of the p21 mRNA. Further augmentation with radiation resulted into rapid cell death. Cucurbitacins - Picracin and deacetylpicrscin from *Picrorhiza scrophulariiflora* inhibited mitogen-induced T cell proliferation and IL-2 [134]. Authors regarded picracin as more active in inducing apoptosis of non-stimulated T cells than the other.

3.5 Cucurbitacin B - other biological systems

Potential of Cucurbitacin B against cardiac, liver, lung, neuronal and skin injuries, systemic infections, inflammation, sex-related behavior and adipocyte differentiation has also been explored. Cucurbitacins exhibit a broad range of pharmacological properties such as anti-inflammatory, antioxidant, antiviral, antipyretic, analgesic and anti-malarial [54, 135, 136]. Cucurbitacin B (0.2 mg/kg) offered protection against pressure-overload cardiac hypertrophy with potent anti-hypertrophy and anti-fibrosis [137]. Male C57/BL6 mice were undertaken surgical aortic banding to induce cardiac hypertrophy. Cucurbitacin B fed mice demonstrated a significant reduction in heart weight, myocardial cell cross sectional area and interstitial fibrosis, etc. These effects were further accompanied with inhibition of hypertrophy in phenylephrine stimulated cardiomyocytes attributed to inhibition of AKT/mTOR/FOX03A axis and autophagy. Cucurbitacin B may be indicated in sepsis-induced acute lung injury (ALI) [138]. A rat ALI model following abdominal septic puncture was treated with Cucurbitacin B intraperitoneally. Cucurbitacin B-treated rats showed an increase in arterial oxygen partial pressure, and reduction in lung effusion, protein content, neutrophils and lymphocytes, and cytokines in a dose dependent manner, with 3-5-fold increment in survival. Histological examination revealed that the pulmonary

destruction alleviated with Cucurbitacin B treatment, endorsing its anti-oxidant and anti-inflammatory properties. Cucurbitacin B offered hepatoprotective and anti-inflammatory effects in artificially induced acute liver damage in outbred albino male Wistar rats [139]. Flower-squeezed-sterile-juice of Cucurbitacin B administered orally at 200-700 μL/kg body weight for three days before artificial induction of carbon chloride mediated hepatotoxicity resulted into mild and reversible damage in the liver parenchyma and liver function tests. However, higher dose showed signs of irreversible hepatotoxicity. Psoriasis is a chronic keratinocyte inflammatory adaptive immune-mediated disease, involving Th1-type immune cells and cytokines, encompassing about 0.5 to 3% human population globally. It is characterized by hyperproliferation, inflammation and abnormal keratinocyte differentiation. Keratinocytes act as the first line barrier in immune surveillance, and govern innate immunity via inflammation-associated molecules like NFκB. Imiquimod is an analog of adenosine, a chemical stress inducer. Topical application of Cucurbitacin B inhibited imiquimod-induced pathogenesis of psoriatic dermatitis [140]. It caused growth inhibition of keratinocytes, which was mediated by inhibition of NFκB and STAT3 signaling leading to reduced expression of psoriatic IL8 and CCL20 cytokines, thus reducing epidermal hyperplasia and psoriatic pathogenesis. Yesilada et al. (1988) indexed anti-inflammatory property of Cucurbitacin B using Whittle method, using a fraction from the freeze-dried fruit juice of squirting cucumber *Ecballium elaterium* [66]. They estimated dye leakage from the vascular tissue in orally fed the mice. Vascular leakage corresponded to permeability and inflammatory response. Authors recorded an increase in permeability with Cucurbitacin B dose; however, 400 mg/kg body weight (highest) also imposed severe toxicity to the animals.

Likewise, the ameliorative anti-oxidant effects of Cucurbitacin B and its relatives were shown as beneficial against the neuronal injury [141]. It significantly inhibited neuroinflammatory

mediators in TLR2/4 agonist-stimulated microglia. Excess TLR activated cytokine and complement proteins may result into neuronal injury and consequentially cell death, mediated through pro-inflammatory cytokines (TNFα and IL1β/6), and JAK/STAT and NFκB pathways. Pretreatment with Cucurbitacin B suppressed the phosphorylation of JAK1, STAT1 and STAT3, NFκB transactivation and cytokines' release, resulting into attenuation of expression of iNOS and COX2. It enhanced the activity of Nrf2/ARE pathway to upregulate HO1 and NQO1, and inhibited caspase activity to offer significant neuroprotection. Rawat et al. also evaluated the anti-oxidant and anti-inflammatory potential of Cucurbitacin B containing plant extracts [67]. Extracts of cucurbits from *L. siceraria*, *C. pepo* and *L. cylindrical* by means of superoxide radical scavenging activity assay and catalase activity assay in the presence of xylene orange and Amplex® Red demonstrated potent radical scavenging activity. They also inhibited inflammation specific cytokines COX-1 and COX-2 in lipopolysaccharide-induced mice serum. Cucurbitacin B with Cucurbitacin E in the dichloromethanolic extract from the roots of *Wilbrandia ebracteata* Cogn. protected against inflammation and algesia in rats [142]. Male Wistar rats were injected with inflammatory agent carrageenan in paws, which developed into inflammation. Inflammation was relatively and significantly less in rats fed with the extract. Furthermore, pain felt with acetic acid application in the inflamed area was significantly faint as compared to the vehicle group.

Cucurbitacin B reduced the likelihood of onset of hepatocellular carcinoma by preventing STAT3 phosphorylation and consequent adipocyte accumulation [143]. Phospho-STAT3 stimulates the regulation of pro-proliferative cyclin D1 and adipogenesis markers PPARγ, aP2, C/EBPα, adiponectin and CD36 proteins, and inhibits adipocyte differentiation inhibitor KLF5. Seo et al. (2014) showed that Cucurbitacin B suppressed the activation of STAT3, henceforth suppressing adipocyte differentiation and accumulation. Prevention of adipogenesis and lipid

accumulation by 0.2-0.3 μM Cucurbitacin B was more promising than by 20 μM resveratrol (standardized anti-adipogenic compound). Genetic silencing of STAT3 significantly attenuated the anti-adipogenic activity. Cucurbitacin B showed synergistic antibacterial and antiviral potential against *Staphylococcus aureus* and *Herpes simplex* virus -1 [144]. Within a range of dose, Cucurbitacin B in synergism with other antibiotics such as tetracycline and oxacillin inhibited the growth of clinical drug resistant variant of *Staphylococcus aureus*, as determined by microdilution method and checkboard assay. By means of plaque number reduction assay, it showed potent anti-HSV-1 potential, comparable to acyclovir. Cucurbitacin B treatment, however, led to decline in the sexual hormone and behavior in male moth *Agrotis ipsilon* [145]. Cucurbitacin B as an antagonist of 20E/EcR/USP complex and signaling pathway staging crucial for sexual behavior from the male antennal lobe reduced the amount of AipsEcR and AipsUSP in a dose dependent manner, which inhibited central pheromone processing in the adult sexually mature male moth.

3.6 Toxicity

Cucurbitacin B to the best of our knowledge has not been included in toxic or restricted use by any of the drug and safety bureau across the world, nor there is any report claiming its toxic role *in vivo* across the world [146], except an FDA report from 1955 and follow-up in 1983, where the authors reported that the median lethal dose of Cucurbitacin B via intraperitoneal route was about 1 mg/kg in male albino mice at the end of three doses [147]. Cause of death was acute pulmonary edema and respiratory arrest. Smit in 2000 reported that in rabbits the median lethal dose of Cucurbitacin B was 0.5 mg/kg body weight after intravenous administration [134, 148]. Ferguson et al. also reported of poisoning after human consumption of 700 grams of commercially produced *Cucurbita pepo* L. within 6 h period [149]. Toxic symptoms included bitter taste in mouth,

abdominal cramps, diarrhea, and occasional vertigo and syncope. Australian Therapeutic Goods Administration has listed Cucurbitacin B free from restricted use and encourages its use in combination with other agents [150].

Cucurbitacin B in its pure form had median lethal dose of about 5 mg/kg (oral route) [151] and 1 mg/kg (intraperitoneal) [147] mice, 0.5 mg/kg (intravenous) [152] in rabbit, and 0.32 mg/kg (intravenous) [153] in cat, recorded so far. Deaths at this dose were accompanied with symptoms such as pulmonary edema, however, with no mentioned additional symptoms. Furthermore, severe toxicity leading to death following oral administration were reported in various studies reporting the use of plant and extracts - *Ecballium elaterium* in rabbits caused nervousness, restlessness, seizures, anorexia, tachycardia, tachypnea, dyspnea, cyanosis, and diarrhea eventually leading to death [154, 155]; *Cucurbita texana* in Swiss Webster mice caused severe anemia followed by death [156]; *Citrullus colosynthis* and *Lagenaria siceraria* in goats caused restlessness, anorexia, diarrhea, dehydration, anemia, dyspnea, kinetic latency, internal hemorrhages, pulmonary emphysema, enteritis, multi-organ failure, and eventually death [157]; and *Citrullus colocythis* in Bovans-type chicks led to hepatic fatty changes and toxicity, catarrhal enteritis, pulmonary emphysema, renal tubular necrosis, but these symptoms reversed after 4 weeks of withdrawal [158].

Various human toxicity complaints have been reported from around the world after accidental or intentional consumption of fruit juice or zucchini squash [154, 159, 160]. Symptoms reported were similar to those in the *in vivo* studies pivoting digestive and neurological systems. However, following topical application with the same extract the human subjects remained asymptomatic [161]. Since the median lethal dose via oral route was significantly higher that the parenteral - possibly digestion, emergence of metabolites and their absorption from the gut before

reaching systemic circulation is crucial to alleviate its toxic effects and liberate its medicinal potency. Moreover, the oral feeding led toxicities and deaths involved components additional to the Cucurbitacin B, advocating bail for Cucurbitacin B off severely toxic profile. Therefore, oral administration of purified form of Cucurbitacin B as an independent executor may be justified, as long as the dosage is conscientiously tailored and the symptoms are cautiously checked.

3.7 Cucurbitacin B - Biological supply chain and future scope

The natural origin and synthetic production of Cucurbitacin B have been extensively studied over the last few decades. Jung and Lui (2010) presented the artificial convergent edifice efforts [162]. Razavilar and Choi (2014) found that the diffusivity of Cucurbitacin B depends on wiggling motion of the block copolymers to diffuse while the contemporaneous water molecules diffused via a hopping mechanism [163]. Toker et al. (2003) proposed a novel method to naturally increase the yield of Cucurbitacin B using *Ecballium elaterium* callus culture technique [164]. They showed that the subculture calluses of stem explants incubated in medium supplemented with 1 mg/l benzyl adenine and 0.1 mg/l naphthalene acetic acid could competently accrue the compound. Mei et al. (2016) suggested a process for Cucurbitacin B bioproduction from one of its parent glycoside using a specific *Streptomyces sp*. [165], using enzyme broth incubation and extraction ethyl acetate. The process was mild, simple and prolific; nevertheless, its hydrophobic and electrostatic structure left it prognostically difficult. Quick exploitation followed by attenuated performance of Cucurbitacin B may abet solid doubts about the treatment modality and dosage in practical use. Cucurbitacin B is hydrophobic, hence suffers *in situ* absorption. Its absorption from carboxymethyl chitosan films loaded with phospholipid-bile salts-mixed micelles as mucoadhesive buccal films resulted in 2.69-fold increase in bioavailability [166], with no toxic effect on buccal

mucosa. Molavi et al. (2008) prepared polymeric micelles of less than 90 nanometers by encapsulating Cucurbitacin B in PEO-*b*-PCL and PEO-*b*-PBCL [167]. PEO-b-PCL micelles showed superiority in maintaining a sustained release of hydrophobic Cucurbitacin B, thereby limiting the rate of STAT3 activation in murine cancer cell line. Patel et al. with the help of molecular dynamics simulation studies predicted that the increasing PCL/PEO ratio in PEO-b-PCL-Cucurbitacin B micelles would reduce the drug release rate [168], due to polar intermolecular interactions. Docking energy analysis showed that the increase in ratio would further favor additional hydrogen bond formation between the molecule and poly(ε-caprolactone). Cheng et al. prepared berberine hydrochloride modified phospholipid complex loaded Cucurbitacin B (CUB-PLC-BER) as a formulation and tested its delivery and efficacy against cholangiocarcinoma in 2015 [169]. Berberine hydrochloride is known for stimulating bile release, hence was believed to contribute to sustained and prolonged drug release. Cucurbitacin B loaded with phospholipids and berberine hydrochloride had higher drug delivery rate, and was more cytotoxic to the cancer cells in both *in vitro* and *in vivo*. Wang et al. encapsulated Cucurbitacin B in glycosylated solid lipid nanoparticles [170]. Administration of the formulation resulted into significant increase in targeted cytotoxicity, with overall target specific efficiency of nearly 64%, where the conventional formulations showed only 23-26%.

You et al. (2015) predicted direct relation between STAT3 protein localization and autophagy [171]. STAT3 in cytoplasm inhibited autophagy via sequestration of EIF2AK2 and interaction with FOXO 1/3. Cytoplasmic localization initiated direct protein-to-protein interaction and impeded autophagy by countervailing autophagy related proteins. Nuclear STAT3 attuned autophagy via transcriptional regulation of autophagy-related genes such as the BCL2 family. It is mediated at the genetic level where STAT3 activation may prompt genetic remodeling and

attenuation of autophagy. Mitochondrial translocation of STAT3 constitutively suppressed autophagy. Studies reported that Cucurbitacin B and derivatives interfered with the activation of STAT3 [37, 40, 48, 84, 95, 102, 106-108, 114, 115, 120-122, 125, 126, 143, 172]. Autophagy signaling is a fairly new subject. Cucurbitacin B and its role in autophagy is mostly unexplored, hence the field is wide blank to fill in.

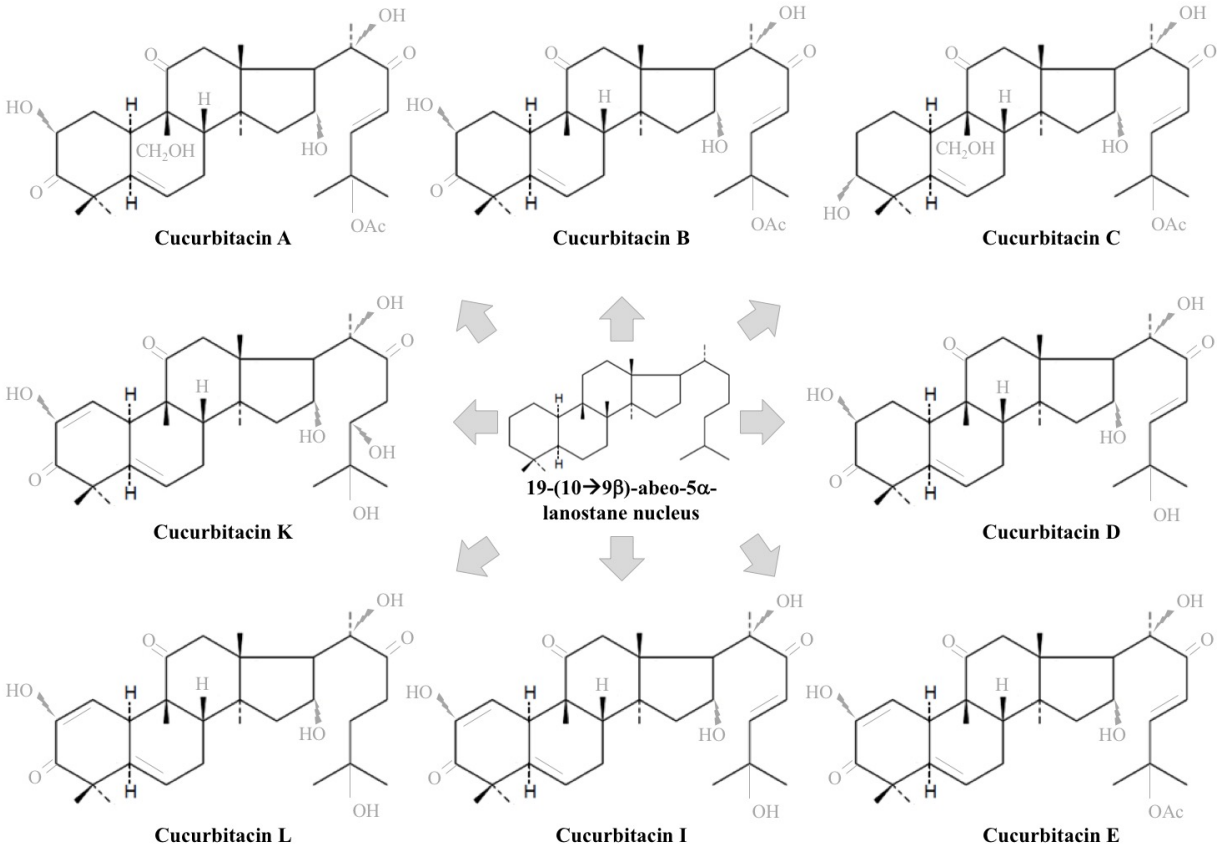

Fig. 8. Two-dimensional chemical molecular structures of Cucurbitacins and Cucurbitacin B. Differences between various subtypes.

Garg et al. 2018 International Journal of Oncology 52(1): 19-37

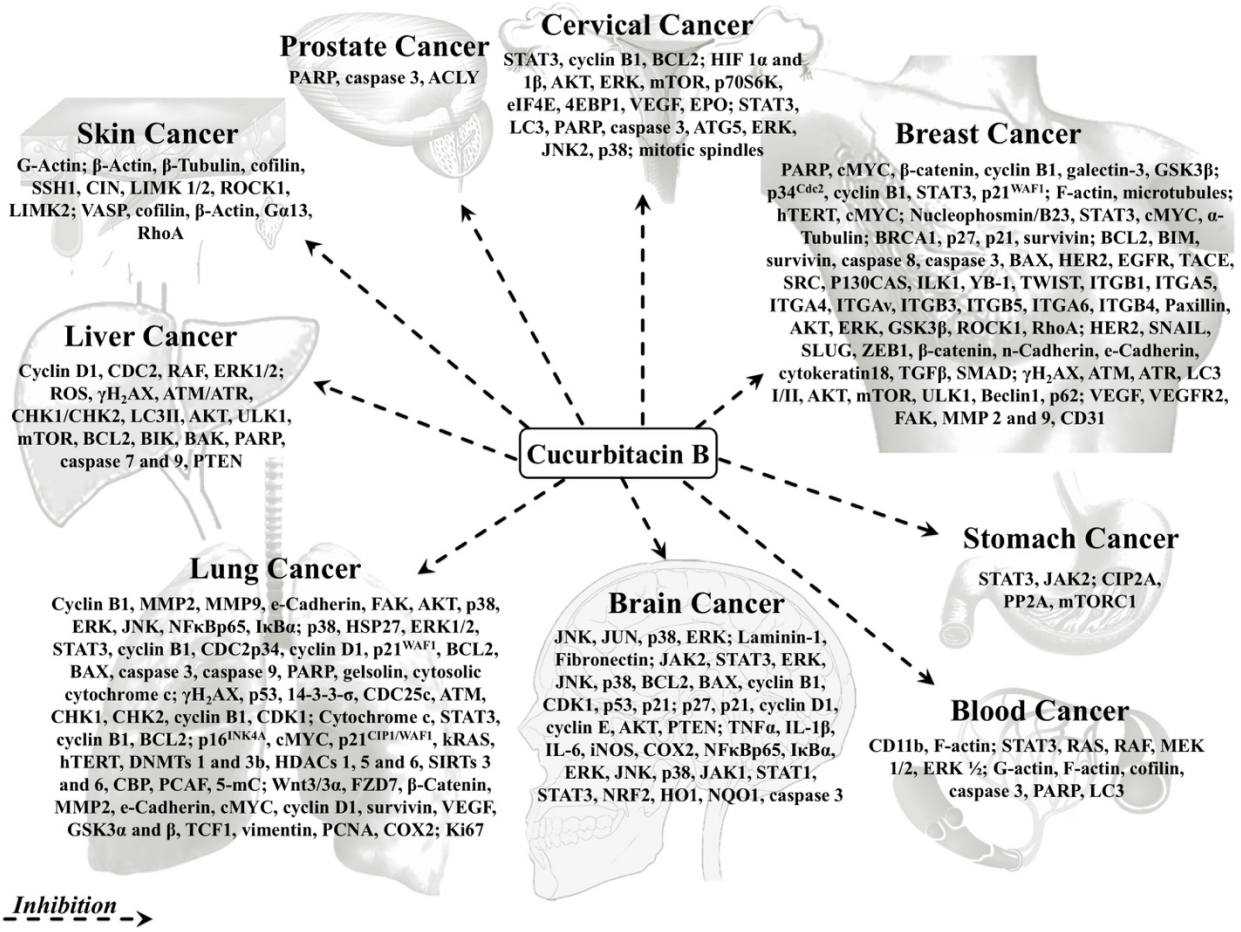

Fig. 9. Summary of anticancer molecular mechanisms (tissue specific) by Cucurbitacin B. All stated proteins are either upregulated or downregulated, contributing to the inhibition of cancer development.

Garg et al. 2018 International Journal of Oncology 52(1): 19-37

3.8 Summary

Cucurbitacins, steroids derived from triterpene hydrocarbon, found in a number of plant families, are some of the principle compounds, which attribute medicinal qualities to the plant. Cucurbitacin B, the bitter toxin, in previous few decades has splendidly verified its cytotoxic potential against cancer and other medical conditions. Through various mechanisms, it suppressed the pathogenesis and inhibited the spread of cancer *in vitro* and *in vivo*. It did so via onset of tumor suppressor p53 pathway and inhibition of tumor progression Wnt/β-catenin, phospho-RB, NFκB, JAK/STAT, PI3K-AKT, and MAPK/ERK pathways. Treatment with Cucurbitacin B consistently upregulated DNA damage and pro-apoptotic protein markers, while downregulated pro-survival markers, growth receptors and cell cycle progressors at either transcriptional level or via ubiquitination and proteasomal degradation. Consequently, it caused growth arrest, apoptosis, cellular differentiation, and inhibition of proliferation in cancer cells. It also showed significant efficacy against the developing detrimental effects of cardiac, pulmonary, neurological and hepatic injuries, psoriasis, infections and lipogenesis. It also caused STAT3 dependent autophagy. Bio-production, efficacy and metabolism of the compound may be improved by means of slight chemical modulation such as the use of hydroponics, bio-transformers, micelles and nanomaterials. It is not difficult to categorize Cucurbitacin B as an effective anticancer molecule. It has the potential to prevent cancer, delay its progression, and might be able to completely cure it. Since it is procured from the natural sources, it could significantly economize the expenditure against the continuously growing disease. Surprisingly, not one human study to explore the efficacy of the molecule has been conducted so far. Clinical trials for Cucurbitacin B as the mainline-targeted anticancer therapy either as an independent effector or as a supplement is warranted.

Chapter 4

Withania somnifera and Withanone

4.1 Introduction

Withanone ($C_{28}H_{38}O_6$), 6,7-epoxy-5,17-dihydroxy-1-oxowitha-2,24-dienolide, is a C_6, C_7 epoxy steroidal lactone with hydroxyl groups at C_5 and C_{17} [173-175]. It is one of the major bioactives of the leaves and roots of plant *Withania somnifera L.*, and was first isolated, identified and reported 2004. Authors isolated Withanone from *Withania somnifera* root extracts by means of positive ion electrospray ionization-mass spectrometry, and characterized using the external standards. Upon analysis using LC-ES-MS chromatography, they found that the Withanone content within the extract had retention time of 311.01 minutes, molecular ion 492.8 m/z bound to sodium ion, and diagnostic molecular fragments at 470.7, 280.8, and 252.6 KDa each. While the most of the operational exploration has been conducted on its close relative Withaferin A due to its distinct differential toxicity, Withanone has gained attention recently. Withanone in the recent years of wet and dry laboratory exploration has been known for the selective protection that it offers to the normal tissue, as discussed later in the below paragraphs.

Joshi et al. prepared derivatives of Withanone and Withaferin A by modifications at their respective 5, 6, and 7 carbons of ring B to study the effect of epoxide group and further modified thiiranes, amino alcohols and alcohols [176]. They checked *in vitro* toxicity against cancer cell lines WRL68, CaCO-2, PC-3 and MCF7, and built derivations in order to establish the relationship between toxicity and compound chemistry. They showed that Withanone nucleus is comparatively less active than Withaferin A, as the latter binds more strongly to its targets. Withaferin A has oxidation on 4, 5, and 6 carbons, and has strong anticancer activity, whereas Withanone has oxidation at 5, 6, and 7 carbons, and had almost negligible activity against any cancer cell line. It did not react significantly for either thiiration or amination reactions. Comprehensively speaking, Withanone nucleus showed weak binding. Whereas Srivastava et al. hypothesized and debated that

the differential activity of withanolides such as Withanone might be due to the differential channel and reaction mechanisms of the catalytic activity of cytochrome p450 within the *Withania somnifera* plant [177]. Besides various pharmacokinetic factors, medicinal efficacy of any compound depends upon its absorption and assimilation within the living body. Devkar et al. tried to demonstrate this for withanolides using double stage apparatus [178]. They loaded the test samples comprising a mixture of major withanolides in the top stage, and separated it from the bottom chamber via an epithelial cell monolayer. After an hour of permeabilization, they measured the test sample concentration in the permeabilized mixture by HPLC for withanolide concentration. Withonone and Withanolide A are non-polar and have low molecular weight, thus were found to be highly permeable. On the other hand, highly reactive Withaferin A was completely impermeable to intestinal epithelium.

4.2 Sources and Content Manipulation

Several studies have been conducted to explore withanolide production and transcriptional modulation. In 2017 a fungi-elicited cell suspension culture of *Withania somnifera* was recruited to study the same [179]. The authors found that the principle withanolide production was maximum when the plant was co-cultured with cell homogenates of 3% *P. indica*, 5% *V. dahliae*, 3% *A. alternate*, and 3% *F. solani* (10.8, 5.8, 4.9, and 3.3 folds higher respectively, against control. They elucidated transcriptional changes and found that the key genes of MVA, MEP and biosynthetic pathways i.e., HMGR, SS, SE, CAS, FPPS, DXR and DXS were significantly up regulated. They found that along with the biomass and other withanolides, there was about 1.5-fold enhancement in the synthesis of Withanone. Pathological agents reduce the bioactivity of *Withania somnifera* plant [180]. Leaf spot disease was induced in *Withania somnifera* plant, which resulted into a

significant reduction in total polyphenolic compounds in the plant and a dip in its antioxidant potential. They witnessed a decrease in the production of the contents of major withanolides, especially Withanone. This was a result of downregulation of genes HMGR, FPPS, SS, SE, CAS, PGT, P450, DXS, DXR and PAL, which are some of the key genes involved in withanolide biosynthesis in MEP and MVA pathways. WsSGTL1 is a 3β-hydroxy specific sterol glucosyltransferase gene, and has catalytic specificity to glycosylate withanolide and sterols [181]. Glycosylation stabilizes and alters physiological activities contributing towards the milieu interior. Authors induced ectopic overexpression of the gene in *Withania somnifera* plant, which resulted into enhances leaf growth, increased production and reduced accumulation of withanolide content, better tolerance against biotic and abiotic stresses, and enhanced recovery after cold stress.

Sivanandhan et al. in 2012 used methyl jasmonate and salicylic acid based hydroponic medium to grow *Withania somnifera* plant and enhance its withanolide content [182]. Methyl jasmonate is a volatile organic compound and has been implicated to play a significant role in seed germination, root growth, flowering, fruit ripening and plant senescence. Salicylic acid is a lipophilic monohydroxy benzoic acid and a beta hydroxyl acid. It is a stress-signaling plant hormone and plays a significant role in defense, growth and development, ion uptake, photosynthesis and transpiration. The authors found that supplementation of culture medium with 150 μM salicylic acid or 15 μM methyl jasmonate for 4 hours resulted in maximum (at least 28-fold) enrichment of Withanone in the plant roots. The effects due to salicylic acid was superior than due to methyl jasmonate. Over-expression of squalene synthase (4-fold) in the tissue cultures of *Withania somnifera* using *A. tumifaciens* as the transformation vehicle also would have resulted in a significant increase in the withanolide content [183]. Co-cultivation of *Withania somnifera* from 6 day old nodal explants alongside with *A. tumefaciens* for 3 days, and testing of injury

treatments, sonication, vacuum infiltration and their combinations was conducted [184]. Transformed plants with vacuum infiltration, sonication, L-cysteine, sodium thiosulphate and dithiothreitol exhibited higher b-glucuronidase expression, fertility and withanolide production. Chaurasiya et al. clustered a collection of *Withania somnifera* plant from different geographical locations, through DNA, enzymes, and withanolide profile [185]. They found that geographical diversity of the plant has little to do with the *Withania somnifera* bioactives distribution. Bharti et al. in 2011 performed the metabolic profiling of fresh leaf and tissue specimens of *Withania somnifera* by high-resolution magic angle spinning nuclear magnetic resonance spectroscopy [186]. They identified 41 metabolites, including withanone as one of the principle bioactives.

Chaurasiya et al. using linear binary gradient solvent system assisted revered-phase HPLC analyzed withanolide content in the leaf and root extracts of *Withania somnifera*, and found that Withanone was one of the major constituents in the tissue [187]. They validated their findings via photodiode array, evaporative light scattering detection and on-line UV spectra. *Withania somnifera* has five principle developmental stages i.e., vegetative, flowering, fruit-set, fruit-maturation, and over-maturation [188]. *WsSQS*, *WsSQE*, *WsCAS*, *WsCPR1* and *WsCPR2* are some of the key genes involved in the withanolide biosynthesis in the plant organs. Authors found that within the roots, Withanone content was highest in the vegetative stage in two distinct morpho-chemo-variants of the plant, and this stage was associated with marginal downregulation in the expression of all five associated above-mentioned genes. Supplementation of sucrose and nitrogen sources like L-glutamine, adenine sulphate, ammonium nitrate, potassium nitrate and sodium nitrate in combination with cytokines kinetin and indole acetic acid resulted in higher frequency of flowering and fruiting, with uniform distribution of Withanone [189]. Sabir et al. in 2013 inoculated *Withania somnifera* leaves in culture supplemented with growth promoting

auxinsindole-3-acetic acid, indole-3-butyric acid, α-naphthalene acetic acid, and 2,4-dichlorophenoxy acetic acid alone or in combinations, and witnessed the increase in overall withanolide content upon organogenesis [190]. They found that while the overall withanolide expression was highest in shoot and related directly to the stage of organogenesis and green flesh, however, the content of Withanone related in the inverse proportion in all aspects. Withanone was mostly found in roots, and its expression reduced with growth promoting auxin supplementation. Tong et al. in 2011 isolated chlorinated withanolides, including derivatives of Withanone, from *Withania somnifera* and elucidated their structures by spectroscopic methods and X-ray crystallography [191].

Authors estimated biomass accumulation and withanolide content production by *Withania somnifera* cell suspension culture on supplementation with various chemical or physical parameters like auxins, cytokines, carbon sources, agitation speed, organic additives, and seaweed extracts [192]. They encountered an overall increase in withanone production with auxinspicloram, 2,4-dichlorophenoxy acetic acid, indole-3-butyric acid, indole-3-acetic acid and a-naphthaleneacetic acid, cytokines kinetin and 6-benzyladenine, increased agitation speed, organic additives l-glutamine and casein hydrolysate, and seaweed extracts *G. edulis* and *S. wightii*. Biosynthesis of withanolides in cell suspension culture using shake-flask and bioreactor against time and supplementation with chemical elicitors was investigated [193]. They found the maximum production of Withanone was achieved on 28th day, when supplemented with 100 mg/L chitosan, 10 mg/L aluminum chloride, 15 mg/L cadmium chloride, and 6 mM squalene. Upon supplementation of *Withania somnifera* hairy root suspension culture with seaweed extracts *G. edulis* and *S. wightii*, authors noted 2-3-fold increase in the production of biomass and withanolides [193]. Withanone content enhancement was more significant on the supplementation with *G. edulis*

(about 2-3) fold, than with *S. wightii* (1.2-1.5 fold). We, in 2016 developed a novel method to enhance the bioproduction of withanolides by using hydroponics and light manipulation [194]. We found that Withanone production may be enhanced by nutrient rich hydroponic cultivation of the *Withania somnifera* and manipulating light conditions. We also found that its total content is higher in leaves compared to the roots. Furthermore, recruitment of cyclodextrin as vector for encapsulation could significantly improve *in vitro* delivery of the compound, and should be implicated in anticancer treatment.

4.3 Anticancer Activity

Withania somnifera leaf extract induced selective killing in the cancer cells, with involved ROS induction [43, 47]. Widodo et al. in 2010 found that the *Withania somnifera* leaf extract, having Withanone as one of the major constituents, selectively killed the cancer cells at the dose of 40 μg/ml. Negligible toxicity was noted in the normal cells. Upon further elucidation into molecular mechanism, authors found that Withanone induced oxidative stress in cancer cells via ROS induction, along with selective upregulation of $p21^{WAF21}$ and γH2AX, and altered membrane potential in the cancer cells. In 2008, they obtained purified Withanone (i-Factor) from *Withania somnifera* leaf extract (i-Extract) and subjected it to elucidate its anticancer potential [44]. High polarity crystal fraction achieved after hexane/ethyl acetate gradients by silica gel column chromatography was named as i-Factor. The authors found that Withanone was highly selective in killing osteosarcoma cells. Normal to cancer cell IC_{50} dose ratio was 26.97:32.64. At this dose, Withanone significantly suppressed the subcutaneous tumor growth in balb/c neu mice model. *In vitro* analysis suggested that Withanone interrupted with DNA replication and repair, disturbed

cellular assembly and organization, caused G_2/M phase arrest, abrogation of mortalin-p53 interaction and induced p53-mediated apoptotic death signaling in cancer cells.

Vaishnavi et al. in 2012 explored the differential molecular interactions of Withanone and Withaferin A with their potentially target proteins by means of *in silico* studies and further *in vitro* validation [175]. They found that Withaferin A had strong affinity to mortalin, p53, p21 and Nrf2, all of which are implicated in stress related apoptotic signaling. On the other hand, Withanone had weak affinity and had minimal toxicity effects. Withanone was therefore safe to use for the normal cells. Molecular validation confirmed that Withanone downregulated mortalin and Nrf2 and upregulated p53, p21, γH2AX at a relatively higher dose than Withaferin A, yet in a dose dependent manner. Corresponding genes were not affected, showing that these effects were post-translational. In the normal cells, as a result of stress stimuli, p53 tumor suppressor is induced which leads ultimately to apoptosis [195]. p53 is a cytosolic protein, which translocates into the nucleus upon activation for its function. Exact mechanism of action of mortalin protein is still unknown, but it was previously shown to form a complex with p53, thus delaying or preventing apoptosis. Grover et al. in 2012 showed by means of *in silico* model that Withanone could competitively bind to mortalin, at the site which is usually the target for the protein-to-protein interaction between mortalin and p53. This interaction is over-expressed in cancer cells, and is minimal in the normal cells. Thus, the treatment of normal cells with Withanone was predicted to inhibit apoptosis by abrogating mortalin-p53 complex leading to delay in senescence. Same mechanism could be applicable to caused nuclear translocation and functional reactivation of p53 in the cancer cells due to the low dose treatment with Withanone.

Aurora A kinase is a serine/threonine kinase protein that has critical role during mitosis and cytokinesis [196]. It is found to be upregulated in various cancer types and adds to genetic stability.

It functions through its interaction with TPX2, which was also found to be upregulated in cancer models. Authors via *in silico* model found that Withanone could specifically target and disrupt the TPX-Aurora A complex. Thus, its treatment resulted into dissociation of the complex and disruption of normal mitotic spindle assembly, thereby causing genetic instability and proliferative failure. *In vitro* model validated the results that Withanone treatment led to simultaneous downregulation of Aurora A and TPX2 in HER2-/ER+ breast cancer cells. Moreover, survivin is one of the hallmark proteins associated with the survival of tumor cells. It is often found to be activated in major cancer subtypes such as breast, prostate and colorectal cancer. It inhibits caspase cleavage that could lead to apoptosis in cancer cells. Withanone inhibited survivin [197]. Withanone according to the *in silico* studies was shown to be docking with BIR5 domain of survivin protein.

Withanone and Withaferin A are close relatives different by only one epoxy and two hydroxyl position, yet contrast tremendously in their cytotoxicity and molecular mechanism of action. Withanone promotes survival to the normal cells, whereas Withaferin A is highly toxic to the cancer cells. While Withaferin A downregulated Notch proteins through their cleavage and antagonist transcriptional activation of associated proteins, these effects were absent when the cells were treated with Withanone [198]. Similarly, while Withaferin A caused severe disruption of normal spindle morphology during the M-phase leading to inhibition of normal mitotic division and growth arrest in the breast cancer cell lines, Withanone had no such effect [199, 200]. Withanone also had no effect on experimentally-(TNFα/TGFβ)-induced epithelial to mesenchymal transformation of the breast epithelial cell line, while its toxic relative had therapeutic effect [201]. Gao et al. in 2014 developed a combination of both in the ratio of 20:1 by weight, respectively [202]. They found that the combination showed synergism. Withaferin A pre-possessed with anti-

migratory, anti-invasive and anti-angiogenic effects, acquired selectivity in cytotoxicity in combination with Withanone. It caused significant downregulation in hnRNP-K, VEGF, mortalin, p44, and MMP2 protein expression. These results were validated using *in silico* model and *in vivo* model.

Shah et al. tested the anticancer effects of alcoholic extract of *Withania somnifera* leaves in glioblastoma cells [203]. Withanone is one of the major constituents in the *Withania somnifera* leaf extracts. They found that the Withanone caused G_2/M-S phase cell growth arrest, delayed the wound scratch cell migration, and induced astrocytic differentiation in rat and human glioma cell lines, with upregulation of GFAP and NCAM. There was evidence to suggest pancytoplasmic redistribution of mortalin protein from perinuclear sites, suggesting the role of mortalin in the dynamics of glio-differentiation. They also tested if the low dose of Withanone could have stress protective and differentiation inducing potential in glioblastoma and neuroblastoma cells [204]. Brain cancer cells treated with 2-5 μg/ml Withanone demonstrated significant reduction in cell viability with increased LDH release in H_2O_2 stressed cells. They also exhibited downregulation of stress-induced ROS generation and γH2AX expression, and upregulation of GFAP, NF200, MAP2 and mortalin levels. Kataria et al. developed an aqueous based extract of *Withania somnifera* leaves, and screen it to check differentiation induction from immortalized rat hypothalamic GnV-3 cell line into neuroendocrine variety [205]. The extract caused a dose-dependent toxicity in the cells. At the sub-toxic doses, the authors found that the cells treated with the extract acquired a differentiated morphology close to preoptic GnRH neurons. This was associated with an upregulation of PSA-NCAM and MAP2, with GnRH expression upregulation and release.

4.4 Toxicity Revocation

In the normal cells, Withanone delayed induction of senescence [206]. While selectively toxic to the cancer cells, Withanone protected the normal cells against various toxic stimuli. It protected the normal cells against the toxicity caused by its own close cytotoxic relative Withaferin A. It increased the mitotic potential of the cells via decrease in accumulation of $p21^{WAF1}$ expression, protection against hydrogen peroxide and ultraviolet radiation mediated oxidative stress, and induction of proteasomal activity. Morphologically in the absence of any stress, there was no cell toxicity visible in the normal cells. in cancer cells, however, after exposure to the UV/H_2O_2/epoxomyxin, the induced stress resulted into suppression of cell proliferation, effects of which were significantly abrogated with Withanone treatment. Treated cells exhibited induction of ROS, downregulation of p53 and γH2AX and upregulation of proteasomal activity. Withanone possesses immunostimulatory potential [207]. Khan et al. in 2009 found that the *in vitro* treatment of T cells ($CD3^+$, $CD4^+$, $CD8^+$, and $CD19^+$) with *Withania somnifera* leaf extract caused dose dependent proliferation (up to 25 mg/kg *Withania somnifera* L.) and increased their ability to secrete IL2 and INF-γ. In Con A primed splenocytes, it enhanced Th1 cytokine IFN-γ expression, hence positively contributing to immunity. Further chemical and molecular characterization showed them that these effects were due to 2,3 dihydro-3-sulphonile Withanone derivative present within the extract. Withanone derivative was responsible for skewing to Th1 immune polarization via stimulation of the expression of IFN-γ and B cell switch over for the secretion of IgG2α, coupled with enhanced expression of integrins and co-stimulatory molecules.

Leishmaniosis is a vector-borne parasitic disease, encircling about 0.7 to 1 million global new cases, claiming the most risk with poverty, malnourishment and poor hygiene status. It kills about 20000-30000 patients, each year [208]. Most pharmacotherapy strategies to its cure at present have failed. Although the structure of protozoan protein kinase C is difficult to predict, it is

implicated in some of the vital enzymatic reactions in the parasite that lead to disease according to the previous studies. Grover et al. in 2012 predicted and developed the structure of Leishmanial protein kinase C, and via *in silico* tools found that Withanone holds promising docking capacity to inhibit its activity [209]. They found that the Withanone showed a significantly high binding affinity (-22.57 kCal/mol) with stable molecular docking simulations. It was suggested that treatment or supplementation to Leishmanial patients with Withanone could significant contribute to control the disease and associated deaths. Wube et al. in 2008 shed light to the implications of the variations in the structural differences within withanolides [210]. Certain cyclooxygenase (COX) and Leukotriene (LTB) enzymes are known to promote inflammation, cell proliferation and angioneogenesis. COX-2/LTB_4 inhibitors are hence directly indicated in suppression of inflammation. Withanolides' interaction with these enzymes was studied via *in vitro* bioassay at 50 μM molecular concentration. Authors found that few withanolides derived from the bark of *Discopodium penninervium* demonstrated superior COX-2 and LTB_4 inhibition than the others. However, Withanone was not one of them.

Scopolamine is a cholinergic antagonist, known to contribute to amnesia [211]. It caused cytotoxicity in human neuroblastoma and rat glioma cells, associated with downregulation in the expression of BDNF, GFAP, NF-H, MAP2, PSD95 and GAP43 and upregulation in the expression of γH2AX and ROS markers in a dose and time dependent manner. Treatment with Withanone reversed the scopolamine induced cell toxicity and associated molecular expression of proteins. Methoxyacetic acid is an industrial product used as gelling and stabilizing agent and is a major metabolite of ester phthalates [212]. It was shown to cause premature senescence in normal cells, associated with ROS induction and DNA and mitochondrial damage. Normal cells treated with Withanone before and after exposure to methoxyacetic acid exhibited a decrease in ROS generation

and associated intracellular damage. This was supported by molecular elucidation of Nrf2 mediated cell defense pathway and proteasomal degradation. N-methyl-D-aspartate (NMDA) is water-soluble glutamate neurotransmitter mimicking amino acid derivative, an excitotoxin, which induces accumulation of calcium ions intracellularly leading to ROS generation, loss of mitochondrial membrane potential, cytochrome c release, caspase and PARP upregulation and cleavage, lipid peroxidation, indicating DNA damage and prompting of death signaling [213]. Withanone pretreated in neuron-like (N2α) cells offered protection against NMDA-induced excitotoxicity and prevented their dose dependent cell death. It alleviated BAX/BCL2 ratio, prevented ROS generation, attenuated calcium ion release and accumulation, normalized mitochondrial membrane potential, downregulated cytochrome c release, caspase/PARP activation, and malondialdehyde levels.

4.5 Anti-inflammatory potential

Gupta and Kaur proposed the anti-inflammatory potential in extract from *Withania somnifera* leaves [214]. They prepared a water extract from the leaves, and pretreated it to β-amyloid and lipopolysaccharide-stimulated primary microglial and BV-2 microglial cells. The pretreatment resulted into extensive morphological changes in the cells, proliferation suppression, and G_0/G_1 and G_2/M phase growth arrest in activated microglia, with associated downregulation of PCNA, cyclin D1, $AKT^{phospho}$, MHC II, Ibα1, NFκB, AP1 and ROS generation, and attenuation of TNF1, IL1B, IL6 and RNS. *Withania somnifera* leaf extract also delayed migration of activated microglia and downregulated associated MMPs. They hypothesized that these effects were attributed mainly due to the presence of Withanone. Toll-like receptors are the proteins critically involved in the development and regulation of the innate immune system [215]. They recognize

and act on the pathogen after they have entered the parenchyma after crossing the guarding mucosal epithelium. They can be classified from TLR1 to TLR13, out of which TLR4 is a transmembrane protein and its activation stimulates cytokines and complement proteins. Excess stimulation may lead to cellular injury and eventually death. This mechanism operates through modulation of proinflammatory cytokines and proteins such as MAPK and NFκB. Purushotham et al. by computational studies showed that Withanone could suppress TLR4-activated inflammatory process, through suppression of LPS-induced cytokines in leukocytic macrocytes. They validated their results experimentally and showed that Withanone suppressed inflammatory process in TLR4-associated system via downregulation of MAPK and NFkB pathways. This was further supported by downregulation of TNFα, IL6, $ERK^{phospho}$, $p38^{phospho}$, $JNK^{phospho}$ and IκBα in a dose dependent manner. Recently Pandey et al. (2017) demonstrated that Withanone attenuated inflammatory cytokines TNFα, IL-1β, IL-6, MCP-1 and nitric oxide, lipid peroxidation and β- and γ- secretase enzymatic activity, and reversed the decline in acetyl choline and glutathione activity, demonstrating its cognitive skill improvement and multifunctional neuroprotective effect [216].

Chapter 5

CucWi-N

5.1 Introduction

Cancer is a highly complex disease arising from a single mutated cell, characterized by its immortalization, rapid and uncontrolled proliferation to form a clinical lump, and compromise in the function of various organ systems including cytoskeleton rearrangements and hormonal dysregulation. World health organization has already labelled cancer as the largest life taker in the world, especially in the developed counties, which is likely to rise to more than 26 million annual new cases by 2026 and cause global epidemic (WHO 2018). Cancer cells are most consistently defined by continued proliferation, insensitivity to stress and DNA damage induced growth arrest that are tightly controlled in normal cells. At molecular level inactivation of one or more tumor suppressor proteins and activation of a variety of oncogenic signaling have been reported with carcinogenesis [217-219]. Malignantly transformed and metastatic cancer cells exhibit enrichment of proteins including MMPs, Vimentin, VEGF, mortalin and hnRNP-K [220, 221]. hnRNP-K protein has been shown to regulate MMPs and VEGF and cancer cell phenotypes including neoplastic stage, genomic instability and cell migration/invasion [220, 222, 223]. Mortalin is a hsp70 family stress chaperon implicated in carcinogenesis, metastasis, EMT and stemness of cancer cells and has been shown to regulate hnRNP-K [224-228]. Mortalin was shown to inhibit transcriptional activation and apoptotic functions of p53 by its retention in cytoplasm [229-231]. Remarkably, anti-mortalin molecules were shown to cause growth arrest, and decrease in EMT and migration characteristics [195, 225, 229, 231-236].

Replicative senescence is an irreversible growth arrest that normal cells enter as they exhaust their predetermined proliferative capacity [237]. It acts as a strong tumor suppressor mechanism and may serve as an effective anticancer strategy [238]. Lamin A & C are often upregulated in cancer cells and responsible for nuclear strength and enhanced DNA repair [239]

that is tightly regulated by MRN (MRE11-RAD50-NBS1) complex (enriched in cancer cells) [240]. Depletion of lamin A and MRN complex proteins have been shown to cause senescence like growth arrest in cancer cells and have been predicted as potential targets for cancer therapy.

Cucurbitacin B (19-(10→9β)-abeo-10-lanost-5-ene triterpene) is a steroid bioactive with peculiar bitter taste and cytotoxic properties commonly found in the plants of Cucurbitaceae and other families such as Brassicaceae, Salicaceae, Chrysobalanaceae, Tricholomalaceae and Begoniaceae. It has been acknowledged to possess potent anticancer properties [29, 40, 82-87, 241]. However, it caused acute toxicity to animal tissues in *in vivo* assays [53]. An FDA report from 1955, follow-up in 1983, and several other assessments have reported that the overdose of Cucurbitacin B in animals caused abdominal cramps, diarrhea, and occasional vertigo, syncope, acute pulmonary edema and respiratory arrest and death [241]. To corroborate this information, we previously showed that Cucurbitacin B was not only toxic to the cancer, but also to normal, cells [29].

Withanone (6,7-epoxy-5,17-dihydroxy-1-oxowitha-2,24-dienolide) is a C_6, C_7 epoxy steroidal lactone with hydroxyl groups at C_5 and C_{17}, and one of the major bioactives of the plant *Withania somnifera L*. [173, 175]. [44, 47] found that Withanone was selectively toxic to the osteosarcoma cells and caused irreversible damage via interruption of DNA replication and repair, disturbance in cellular assembly and organization, mortalin-p53 interaction abrogation, and p53-mediated apoptotic death signaling in cancer cells. Several other studies have advocated anti-inflammatory and anti-stress potential of Withanone [204, 212, 215, 216]. It has been shown to be less active than its toxic relatives due to oxidation at 5, 6, and 7 carbons in its chemical structure [176]. This property could translate into weak binding affinity of Withanone to the cellular stress-related proteins in cancer cells [195]. It was shown to delay the replicative and stress-induced

premature senescence in normal cells [206, 212]. It was shown to protect brain derived cells from oxidative and glutamate stresses [204, 205, 242, 243] and was found responsible for recovery from scopolamine induced memory loss in mice model [211, 244, 245]. When used in combination with Withaferin A, it was shown to reduce the toxicity of normal cells; the combination retained the anti-migration, anti-angiogenesis and anti-tumor potentials *in vivo* [202].

In this study, we formulated combinations of Cucurbitacin B and Withanone (CucWi-N) and achieved one with selective toxicity to cancer cells as well as potent antitumor and anti-migration activities. Bioinformatics analyses endorsed higher affinity of CucWi-N to mortalin as well as hnRNP-K proteins, and was supported by cellular and molecular assays. We report that CucWi-N caused induction of replicative senescence in cancer cells selectively by targeting proteins involved in proliferation and migration and translated well to effective inhibition of tumor growth and metastasis *in vivo*.

5.2 Materials and Methods

5.2.1 Cells and reagents

A549 (non-small cell lung cancer) and TIG-3 (normal skin fibroblast) cells were cultured in Dulbecco's modified Eagle's medium (DMEM) (Invitrogen) supplemented with 5% fetal bovine serum and 1% penicillin/streptomycin in a humidified incubator (37°C and 5% CO_2). Cucurbitacin B (Sigma-Aldrich, Tokyo, Japan) and Withanone (Funakoshi) were dissolved in DMSO to prepare 100 mM and 50 mM stocks, respectively. Working solutions (10 µM for Cucurbitacin and 5 mM for Withanone) were also prepared in DMSO and stored at -20^{o}C in small aliquots. Antibodies against Caspase 3 (SC-7148, Santa Cruz), Caspase 9 (SC-7885, Santa Cruz), CDK2 (SC-163, Santa

Cruz), CDK4 (SC-260, Santa Cruz), Cyclin D1 (SC-20044, Santa Cruz), Cyclin E (SC-481, Santa Cruz), Fibronectin (SC-52331, Santa Cruz), hnRNP-K (4675S, Cell Signaling), Lamin A/C (4777S, Cell Signaling), MMP2 (SC-10736, Santa Cruz), MRE11 (NB100-142, Novus Biologicals), NBS1 (NB100-143, Novus Biologicals), NFκBp50 (SC-7178, Santa Cruz), $p38^{phospho}$ (4511S, Cell Signaling), $p44^{phospho}$ (4370S, Cell Signaling), p53 (SC-6243, Santa Cruz), p70S6K (SC-8416, Santa Cruz), PI3K (SC-1637, Santa Cruz), $pRB^{phospho}$ (9307S, Cell Signaling), Rad50 (Ab89, AbCam), Survivin (SC-10811, Santa Cruz), VEGF (SC-507, Santa Cruz), Vimentin (SC-6260, Santa Cruz), α-Tubulin (SC-53646, Santa Cruz), β-Actin (ab49900, AbCam) were used for immunoblotting and immunostaining. Mortalin and CARF antibodies [228, 246], and recombinant mortalin protein [247] were generated in our laboratory.

5.2.2 Cytotoxicity assays

Cytotoxicity of Cucurbitacin B, Withanone and their combination (CucWi-N) to A549 and TIG-3 cells was determined by MTT (3-(4,5- dimethylthiazol-2-yl)-2,5-diphenyltetrazolium bromide) assay. Cells ($2X10^3$/well) were plated in 96-well plate and allowed to settle overnight, followed by treatment with varying doses of the compounds. The control (DMSO) or treated cells were incubated at 37°C and 5% CO_2 for 48 hrs followed by addition of 10 µL of phosphate buffered saline (PBS) dissolved 5 mg/mL MTT (M6494, Life Technologies) and continued with incubation for 4 hours. Media containing MTT was aspirated out and replaced with DMSO. The plates were placed on a shaker for 5 min followed by measurement of optical density at 570 nm using Tecan infinite M200® Pro microplate reader (Tecan Group Ltd., Mannedorf, Switzerland). Cell viability was calculated in percentage against the DMSO-treated control.

5.2.3 Crystal Violet staining

A549 and TIG-3 cells (10^5 /well) were plated in 6-well plates, and cultured either in control or CucWi-N-supplemented medium for 48 hrs. The cells were then fixed in 100% methanol and stained with 0.5% Crystal Violet stain for 2 hours. The plates were washed and dried, and visualized under Nikon Eclipse TE300 inverted phase contrast microscope at X400 magnification.

5.2.4 QCV assay

A549 cells ($5X10^2$/well) were plated in a 6-well cell culture dish and cultured either in control or CucWi-N-supplemented medium for 8-10 days (until colonies appeared in control cultures) with regular change in medium on every alternate day. Colonies were fixed in methanol:acetone (1:1) and stained with 0.5% Crystal Violet for overnight followed by washing with ultrapure water to remove the excess stain. The plates were air-dried and photographed under Nikon Eclipse TE300 inverted phase contrast microscope at X400 magnification. Colonies from three wells and three experiments were counted and analyzed for size in three independent experiments i.e., clonogenicity, long-term cell viability and cellular morphology.

5.2.5 Immunoblotting

A549 and TIG-3 cells ($5X10^5$/well) were plated in 6-well plates and allowed to settle overnight, followed by culture either in control or CucWi-N-supplemented medium. At the end of 48 hrs, cells were harvested and washed with PBS twice, followed by lysis in RIPA buffer (89900, ThermoFisher) containing complete protease inhibitor cocktail (4693159001, Roche Applied Science) on ice for 45 mins. Cell (or tumor) lysates (containing 10-40 µg protein) were separated

on a SDS-polyacrylamide gel using Mini-Protean® Tetra cell equipment (Bio-Rad, Hercules, CA), and transferred onto PVDF membrane (Millipore, Bedford, MA) by Mini Trans-Blot® Electrophoretic Transfer Cell (Bio-Rad). Membranes were washed with TBST (0.1% Tween 20 in TBS) for 5 mins, blocked with 3% bovine serum albumin protein dissolved in TBST for 45 mins, incubated with primary antibodies diluted in 0.05% TBST for overnight at 4°C, washed with TBST thrice for 10 mins each, incubated with horseradish peroxidase-conjugated secondary antibody (goat anti-mouse HRP (31430, ThermoFisher) or goat-anti-rabbit HRP (31460, ThermoFisher) diluted in 0.05% TBST for 3 hrs at room temperature, washed with TBST thrice for 10 mins each, and finally developed using chemiluminescence solution (GE Healthcare, UK) and visualized using Lumino Image Analyzer equipped with CCD camera (LAS3000-mini; Fuji Film, Tokyo, Japan).

5.2.6 Immunocytostaining

A549 and TIG-3 cells ($2.5x10^4$/well) were plated on coverslips in 12-well plates and allowed to settle overnight, followed by culture either in control or CucWi-N-supplemented medium. At the end of 48 hrs, cells were fixed in methanol:acetone (1:1) on ice for 5 minutes, rinsed with PBS thrice, permeabilized with 0.2% PBST (0.2% Triton-X in PBS) for 20 mins, washed with PBS for 15 mins, and blocked with 2% bovine serum albumin protein dissolved in PBST for 45 minutes. Fixed cells were incubated with primary antibodies diluted in blocking solution against various proteins overnight at room temperature, washed with PBS-PBST-PBS for 15 mins each, incubated with either Alexa-Fluor 488 goat anti-mouse IgG (A11029, Life Technologies) or Alexa-Fluor 594 goat anti-rabbit IgG (A11037, Life Technologies), depending upon the source of the primary antibodies, diluted in blocking solution for 3 hrs in dark, washed with PBS-PBST-PBS for 15 min each, incubated with Hoechst 33342 antibody (H3570, Invitrogen

Molecular Probes) for 10 min in dark, washed with PBST-PBS for 15 min each, rinsed with ultrapure water twice and mounted on glass slides using FA mounting solution (FAMF, VMRD). The cells were then visualized for immunofluorescence under Zeiss Axioplan 2 upright fluorescence microscope at X400 magnification.

5.2.7 Flow cytometry

A549 cells ($2X10^5$/well) in 6-well plates were synchronized for cell cycle phase by serum starvation for which, they were cultured successively in 5%, 1%, 0% FBS-supplemented DMEM for 24 hrs each, and then recovered in 5% FBS-supplemented DMEM for 24 hrs, followed by culture in either control or CucWi-N-supplemented medium for 48 hours. Cells were harvested by trypsinization. Two hundred thousand cells per milliliter counted using an automated cell counter ($TC20^{TM}$, Bio-Rad) were washed twice and re-suspended in 300 µl PBS. Cells were fixed by adding 700 µl ice cold 100% ethanol slowly with mild vortexing. Fixed cell pellets were incubated in -20°C for overnight, centrifuged at 2000 rpm, washed twice with PBS and centrifuged. RNA was degraded by incubation with 100 µg/ml RNAse (EN0531, ThermoFisher) at 37°C for 90 mins. Suspensions were centrifuged at 2000 rpm for 7 mins, and re-suspended in 200 µl Guava Cell Cycle Reagent (4500-0220, Millipore) and incubated at room temperature for 30 mins in dark, diluted in 1-2 mL PBS and taken up for data acquisition and cell cycle analysis on Guava PCA-96 system.

5.2.8 Senescence induction

Control or CucWi-N treated cells were serially passaged by 1:16 split ratio until they attained senescence and stopped dividing. Culture medium supplemented with or without CucWi-N was replaced every 2-3 days. Cells were harvested for protein, mRNA, immunofluorescence analyses at each passage. To induce replicative senescence in A549 cells, cells were subjected to 5 μM doxorubicin (D1515, Sigma-Aldrich) for 1-2 hrs followed by culture in either the control or CucWi-N-supplemented medium under standard incubation conditions.

5.2.9 Mortalin ELISA

Cell lysates (containing 100 μg protein) derived from control or CucWi-N treatment with or without doxorubicin induced senescence were plated into clear flat bottom polystyrene Costar® 96-well plate (3632, Corning) pre-coated with 100 ng/mL antibody to mortalin diluted in coating buffer (421701, BioLegend) and diluent buffer (421203, Biolegend), and incubated for overnight at room temperature. Wells were then washed with washing buffer (0.05% Tween 20 in PBS) thrice for 1 minute each, and reloaded with 100 ng/mL antibody to mortalin diluted in diluent buffer. The plate was incubated for overnight at room temperature, following which it was washed thrice for 1 minute each and incubated with 100 ng/mL horseradish peroxidase-conjugated secondary antibody goat anti-mouse HRP (31430, ThermoScientific) diluted in diluent buffer for 3 hours at room temperature. The plate was washed thrice for 1 minute each and then incubated with TMB substrate (421101, BioLegend) for 30 minutes for color development. Stop solution (423001, BioLegend) was added onto the substrate and mixed, and optical density was measured at 450 nm using Tecan infinite M200® Pro microplate reader (Tecan Group Ltd., Mannedorf, Switzerland). Recombinant mortalin protein diluted in diluent buffer was used as the standard. Mortalin protein concentration

was calculated against the control using the slope equation obtained in the standard curve and the graph was plotted in percentage taking the control as 100%.

5.2.10 Would scratch migration assay

A549 cells ($1.5x10^5$ well) were plated in a 6-well plate and allowed to settle overnight. A linear scratch was made using a sterile pipette tip (200 µl) to simulate an area devoid of cells. The cells were either cultured in control or CucWi-N-supplemented medium. Movement of cells into the scratched area was monitored under Nikon Eclipse TE300 inverted phase contrast microscope at X400 magnification every 6 hrs. Photographs of scratch and migrating cells were captured every 24 hrs.

5.2.11 Invasion assay

Invasion assay was carried out using BioCoat™ Matrigel™ Invasion kit (3-354480, Corning®). A549 cells ($5X10^4$/well) were suspended in 0.5 ml serum free DMEM were plated into the top of invasion inserts and the bottom well of a 24-well plate was filled with 0.75 ml DMEM supplemented 10% FBS. After 48 hours, the inserts were transferred to fresh plates and washed thrice with PBS. Cells suspended in the Matrigel™ basement membrane matrix at the bottom of each insert were fixed in methanol:acetone (1:1) and stained with 0.5% Crystal Violet for overnight followed by washing with ultrapure water to remove the excess stain. The inserts were air-dried and photographed, followed by visualization under Nikon Eclipse TE300 inverted phase contrast microscope at X400 magnification.

5.2.12 Bioinformatics

Molecular docking studies of Cucurbitacin B (PubChem CID 5281316) on mortalin (PBD ID 4KBO) protein and Cucurbitacin B, Withanone (PubChem CID 21679027) and their combination on hnRNP-K (PBD ID 1ZZI) protein were carried out using AutoDock 4.2 suite. Molecular dynamic simulation of the docked complex was studied for 50 ns.

Preparation of protein and ligand structures for docking studies: All the protein structures used for docking studies were retrieved from Protein Data Bank. For human mortalin apo form of ATPase domain with resolution of 2.8 Å was downloaded (PDB ID: 4KBO) [248]. The coordinates of p53 protein were extracted from a p53-DNA complex (PDB ID: 4MZR) [249]. The resolution of the structure was 2.9 Å. The crystal structure of KH3 domain of hnRNP-K with 15-mer ssDNA is available at 1.8 Å resolution (PDB ID: 1ZZI) [250]. The PDB corresponding to only hnRNP-K was used for performing the docking experiments. All the three protein structures were prepared using the protein preparation wizard of Schrodinger to be used for docking. The missing hydrogen atoms were added and the resulting structures were optimized. The other processing steps involved removal of bad contacts, bond length optimization, creation of disulfide bonds, capping of protein terminals, and conversion of selenomethionines to methionine residues. The short stretches of missing amino acids and missing side chains were added using the prime module of Schrodinger.

The 3-D conformers of natural compounds- Withanone and Cucurbitacin B were obtained from PubChem (CID: 21679027 and 5281316 respectively). These molecules were also prepared for docking using the LigPrep module of Schrodinger. This ligand preparation protocol generates different tautomeric, stereochemical and ionization variants of the small molecules followed by energy minimization and flexible filtering.

Docking of protein molecules with natural compounds: The p53 binding site in mortalin (253-282 amino acids), mortalin binding site of p53 (323-337 amino acids), and hnRNP-K residues comprising the KH3 domain were targeted for docking with the small molecules. A grid was generated to cover all the important residues for each of the above-mentioned protein using the Glide module of Schrodinger. The prepared natural compounds- Withanone and Cucurbitacin B were then docked against the three proteins using Glide's extra precision (XP) docking protocol.

The molecular interactions between the protein-ligand complexes were studied using the Ligplus program. H-bonds were taken into consideration when the distance between acceptor-donor atoms was less than 3.3 Å, with maximum hydrogen-acceptor atom distance of 2.7 Å and acceptor-H-donor angle greater than 90°.

Assessing the stability of the docked complexes: To investigate the dynamic stability of the docked complexes, molecular dynamics (MD) simulations were carried out using the Desmond module of Schrodinger. Firstly, the docked complexes were solvated in a triclinic periodic box of TIP3 water and an appropriate number of counter-ions were added to neutralize the system. The distance between the walls of the box and the complex was kept 10 Å to prevent the interaction of ligand bound protein with its own periodic image. The prepared system was then subjected to energy minimization up to a maximum of 3000 steps using a steepest decent method or until a gradient threshold (25 kCal/mol/Å) was not reached. After equilibration, the protein-ligand complexes were simulated for 50 ns in each case. Optimized Potential for Liquid Simulations 3 (OPLS3) force field was used to carry out all the simulation experiments. Temperature of 300 K and a constant pressure of 1 atm was used with a time step of 2 fs for the production MD. Smooth particle Mesh Edwald method was used to calculate long distance electrostatic interactions. For

calculating coloumbic short-range interactions a cutoff radius of 9 Å was used. Frames were captured after every 4.8 ps of the time interval to obtain the simulation trajectory.

A steady RMSD profile of the protein backbone and ligand in reference to the first frame over the entire simulation trajectory was used as a measure to assess the stability of the docked complexes.

5.2.13 Animal studies

Athymic balb/c nude female mice (4 wk old) were purchased from NihonClea, and acclimatized for two weeks under standardized animal house conditions. Animals were orally pre-fed with either vehicle (0.1% carboxymethyl cellulose) or with CucWi-N-supplemented vehicle (Cuc 1 mg/kg + Wi-N 10 mg/kg BW) in 200 µl suspension every alternate day for a week. Animals were injected with healthy A549 cells ($5X10^6$/injection) in 150 µl PBS subcutaneously (for subcutaneous xenograft) over the left and right flank (ventrally), and intravenously (for lung metastases) through tail vein injections. Upon emergence of tumor buds from xenografts, mice were regularly fed with the oral suspensions thrice a week for nearly 8 weeks. Tumors were regularly monitored and sized with Vernier caliper. Tumors volume was calculated using the formula $V=(LxW^2)/2$ with caliper measurements of length (L) and width (W) of the tumors. Mice were sacrificed by cervical dislocation before tumors grew to about 1.5 cm length and were examined for internal tumors and lung metastasis. Dissected tumors were isolated and lysed in lysis buffer for protein analysis. A qualitative hemolytic assay to test safety of CucWi-N from causing erythrocyte lysis was performed. Blood extracted from a healthy mice heart was diluted with diluent buffer (0.85% NaCl containing 10 mM $CaCl_2$) to obtain 2% RBC suspension. 150 µl

suspension was mixed with 75 µl diluent buffer and 75 µl of CucWi-N (Cuc 1 µM + Wi-N 50 µM, in 100% DMSO) by gentle pipetting. The mixture was incubated at room temperature for 1 hr, followed by centrifugation at room temperature for 5 min at 16000 rpm. 200 µl of the supernatant was loaded into a 96-well plate well to read absorbance at 540 nm. Ratio of absorbance corresponded to the degree of hemolysis. 0.2% Triton X-100 in diluent buffer was taken as the positive control. The antioxidant enzyme activities of catalase (CAT) and malondialdehyde (MDA) levels in the plasma were measured as per manufacturer's instructions using Catalase assay kit (707002, Cayman Chemical) and TBARS colorimetric microplate assay kit (FR40, Oxford Biomedical Research), respectively. All animal experiments were performed following the protocols for animal experiments recognized and approved by Institute Animal ethical committee.

5.2.14 Statistical analysis

All the calculations were done using Microsoft® office. Statistical significance was calculated by unpaired t test of GraphPad software® (2017) using mean, SD and N from three independent experiments, and shown as $^{*}p<0.05$, $^{**}p<0.01$, $^{***}p<0.001$.

5.3 Results

We investigated dose-dependent toxicity of Cucurbitacin-B (Cuc) to human cancer (A549) and normal (TIG-3) cells. As shown in Fig. 10, Cuc showed higher cytotoxicity to the normal cells. Withanone (Wi-N), on the other hand, was not toxic to either of the cell types at doses from 2.5 to 10 µM in short term (48 h) cytotoxicity assays. We next tried various combinations of two compounds and found that a Cuc:Wi-N combination in a ratio of 1:500 was more cytotoxic to

cancer than the normal cells (Fig. 11). Low, medium and high doses of CucWi-N resulted into ~15%, ~30% and ~50% loss in A549 cell viability. These doses were nearly non-toxic (>90% cell viability) to the normal cells. We selected these three doses (Fig. 12) to analyze the mechanism(s) of their anticancer activity by biochemical, molecular and imaging assays. In Quantitative Cell Viability (QCV) assay, direct observation of control and treated (low and medium; 48 h) cells under the microscope revealed stressed morphology (spindle shaped flat and large cells) in a dose dependent manner in cancer, but not normal cells (Fig. 13). CucWi-N treated cancer cells showed inhibition of clonogenicity in a dose dependent manner (Fig. 14). Of note, the low dose that resulted in only 20% decrease in viability in short term (48 h) assays caused significant reduction (80%) in colony forming efficiency (10 days). Consistent with this and the above data, the growth analysis revealed that inhibition of cell proliferation over 3 days of continual treatment of low dose of CucWi-N was more pronounced in the cancer cells than the normal cells (Fig. 15).

We next performed molecular analysis of growth and apoptosis signaling in cancer and normal cells subjected to the treatment of high dose of CucWi-N. We found that whereas CucWi-N treated cancer cells showed downregulation of CDK-2, CDK-4, Cyclin D1 and Cyclin E, normal cells showed increase in most of these proteins (Figs. 16 and 17), indicating selective growth arrest in cancer cells by CucWi-N was mediated by downregulation of proteins involved in cell cycle progression. On the other hand, analysis of proteins involved in apoptosis showed no significant difference in control and treated cells. We next performed flow cytometry and cell cycle analysis and found that the CucWi-N indeed caused arrest in the S-phase of cell cycle in the cancer cells (Fig. 18). Cells were next treated with high dose for 4 or 24 h. Microscopic observations of treated cancer cells showed changes in nuclear membrane and flattened irregular morphology as early as 4 h of treatment (Fig. 19). We anticipated that such changes may be mediated by changes in Lamin

A/C. Immunostaining of cells with Lamin A/C specific antibodies showed downregulation of Lamin A/C in cancer, but not in normal cells, and was remarkably apparent in cells treated for 12-24 h (Fig. 19).

Based on the above data on cell cycle arrest and decrease in Lamin A/C, we predicted that CucWi-N may induce replicative senescence in cancer cells. In order to investigate this, cancer cells were treated with low dose of CucWi-N in a continuous culture regime. As shown in Fig. 20, compared to the control cells, treated cells showed slow growth that was clearly apparent in about 18 days followed by gradual decline in proliferation until the cells stopped dividing in about 60 days (Fig. 20). Molecular analyses revealed that gradual arrest in growth was associated with progressive downregulation of proteins (phosphorylated pRB, hnRNP-K and mortalin) critically involved in cell cycle progression and continued proliferation of cancer cells. On the other hand, proteins involved in DNA damage signaling and growth arrest (CARF and p53) were upregulated (Fig. 21). The results were confirmed by several independent experiments and multiple assays including immunocytostaining (data not shown) and ELISA (Fig. 22) that confirmed downregulation of mortalin. Induction of DNA damage signaling and growth arrest was also endorsed by increase in MRN complex (Fig. 23). We next determined if CucWi-N induced selective growth arrest in cancer cells was mediated by this axis by using doxorubicin induced senescence model. Of note, CucWi-N treated cancer cells showed decrease in MRE11, Rad50 and NBS1; their senescent derivatives showed milder decrease in MRE11 and RAD50; NBS1 did not show any change (Fig. 23) suggesting that CucWi-N-induced selective growth arrest in the cancer cells may be mediated by downregulation of one or more members of MRN complex.

Cancer cells often show increase in their migration capacity resulting into their metastasis from the primary to secondary sites in the body. We next examined the migration capacity of

control and treated cells by wound scratch and cell invasion assays. We found dose-dependent inhibition of migration and invasiveness of the cancer cells treated with CucWi-N (Fig. 24 and 25). Since mortalin and hnRNP-K proteins have been shown to be the key regulators of cell migration and cancer metastasis [220, 222, 225], we investigated if CucWi-N induced decrease in these proteins contributing to the observed phenotypes. Expression analyses of these and other (VEGF, Vimentin, MMP2 and Fibronectin) proteins involved in cell migration and invasion indeed showed their downregulation in CucWi-N treated cells. Of note, cells treated with not only the high but also the low dose showed significant downregulation of expression of these proteins (Figs. 26 and 27). Furthermore, staining pattern of mortalin was seen to shift from perinuclear (typical of cancer cells) to pancytoplasmic (typical of normal cells) and signified induction of senescence as reported earlier [29, 251].

In view of earlier reports that Wi-N activates growth arrest signaling in cancer cells by abrogation of mortalin-p53 complexes and reactivation of p53 protein [195], we currently examined if Cuc could function in a similar way. Molecular dynamics analysis showed that it could bind to mortalin (binding energy of -4.212 kCal/mol) at the Thr267 and Gly269 that are involved in interaction of mortalin to p53 (Figs. 28 and 29). Interestingly, MKT-077, that has been shown to bind to mortalin was used as a positive control, showed lower binding energy (-2.042 kCal/mol) suggesting that Cuc may be a better mortalin inhibitor (Fig. 30). We next examined binding of Cuc to p53. Although it showed interactions to p53 residues Thr118 and Lys321, no interactions with mortalin-binding domain of p53 (amino acid residues 323-337) [233] were observed (Fig. 31). These data suggested that enhanced activity of CucWi-N may involve other mechanisms. We next subjected Cuc and Wi-N to molecular docking analysis using hnRNP-K as a target molecule (Fig. 31 and 32). Individual binding of Cuc and Wi-N showed comparable energy (-2.93 kCal/mol and

-2.34 kCal/mol, respectively) (Fig. 30). We then subjected two molecules together (Cuc and Wi-N) to molecular docking analysis. Interestingly, we found that binding efficacy of Cuc to hnRNP-K:Wi-N complex was double (-4.69 kCal/mol) as compared to the binding of Wi-N to hnRNP-K:Cuc complex (binding energy -2.62 kCal/mol) (Fig. 30). During the 50 ns long simulation of the triple docked complex (Cuc:Wi-N:hnRNPK) one hydrogen bond involving Cuc and Lys87 residue of hnRNP-K was stable during the entire process indicating the high stability of the complex (Fig. 33). The molecular docking analysis data suggested that CucWi-N may cause stronger inactivation of cancer cell proliferation and migration signaling by targeting mortalin and hnRNP-K proteins. We next examined subcellular localization and expression level of these proteins in cells treated with either the individual compounds or their combination. As shown in Fig. 34 and 35, cells treated with CucWi-N showed stronger downregulation of mortalin and hnRNP-K than Cuc or Wi-N individually.

We next tested the anticancer therapeutic potential of CucWi-N in nude mice subcutaneous xenograft tumor progression model. Animals orally fed with CucWi-N suspension for 9 weeks demonstrated suppression of subcutaneous tumors (Figs. 36 and 37). They also exhibited reduced intra-pulmonary metastatic lesions (Fig. 38) and total blood MDA levels (Fig. 39), and increased catalase activity (Fig. 39), collectively advocating the anti-carcinogenic, anti-metastatic, and anti-oxidant effects of CucWi-N. CucWi-N was safe to use in the animal model, since it neither cause any significant weight loss or toxicity to the animals, nor it caused hemolysis *in vivo* (Figs. 37 and 39). Furthermore, subcutaneous tumors derived from the treated and vehicle animals were subjected to protein analysis. As shown in Fig. 40, and in line with the *in vitro* data, we observed consistent downregulation of the key proteins responsible for cancer cell migration, invasion, survival and stress signalings (Fig. 40) endorsing the cancer therapeutic potential of CucWi-N.

5.4 Discussion

The process of carcinogenesis involves discrete molecular changes over time resulting in not only the aberrant growth of cells and tissues, but also their invasion to the neighboring and distant sites. Although the last 2 decades has seen remarkable progress in cancer diagnosis and treatment, cancer mortality is increasing exponentially and is expected to double by the next decade. All cancers constitute rapidly dividing cancer cells that lose their differentiated characteristics and are vulnerable to structural changes and damage. Such characteristics are often used as assay system for anti-cancer drug discovery and validation. Conventional treatment for benign tumors is surgical resection or radiotherapy; malignant and metastasis tumors are treated with chemotherapy. Conventional synthetic chemotherapeutic agents are expensive, cause multiple adverse effects and drug resistance, therefore continual development of less toxic and economical anti-cancer drugs is warranted. Fridlender et al. have summarized and appraised the anticancer potential in a number of herbs [252]. They revealed a profound link in cancer prevention and curative therapies using herbs such as allspice, basil, clove, and garlic, etc. Active anticancer ingredients from a large number of herbs have been identified in the recent years [253]; autonomous or collaborative therapy of these bioactive ingredients or herbal extracts are shown to reduce the development and/or progression of a variety of human cancers through various mechanisms [106, 121, 254-256]. We recently showed anticancer potential in the root extract of the plant *Helicteres angustifolia* and its bioactive Cucurbitacin B (Cuc) [29], which has been acknowledged for its anticancer properties in several other studies [40, 82-87, 241]. Unfortunately, it caused acute toxicity *in vivo* [53, 57, 241] and was also toxic to normal cells *in vitro* [29]. In order to recruit the

cytotoxic potential of Cuc for cancer cells selectively, we engineered its cocktail with Withanone (Wi-N), a steroidal lactone bioactive of *Withania somnifera L*., which has been shown to bring about negligible toxicity to normal cells [44 {Priyandoko, 2011 #6320, 47, 176, 255]. It was also shown to offer side benefits (protection against oxidative and chemical stresses, and lifespan extension) autonomously to the normal cells [206, 212, 255]. In combination with Withaferin A, it demonstrated selective toxicity to cancer cells and therapeutic potential for suppression of tumor growth and metastasis i*n vivo* [202]. In line with this, we developed CucWi-N (a 1:500 molar ratio of Cucurbitacin B and Withanone,) and found that it possessed remarkable anticancer activity. It was relatively safe for normal cells. Dose response data showed that CucWi-N at even low doses inhibited the cancer cell clonogenicity and proliferation. The effect was significantly stronger in cancer than in the normal cells (Figs. 10 to 15) and was supported by molecular data including selective downregulation of CDK-2/4 and Cyclin D1/E in cancer cells causing cell cycle arrest in the S-phase (Figs. 16 to 19). Microscopic observation on the control and CucWi-N treated cells showed stressed and flattened morphology in the latter; changes in nuclear membrane were observed as early as 4 h consistent with earlier report [96]. Furthermore, we found that CucWi-N treated normal cells showed recovery from stressed phenotype. It may be attributed to Wi-N as suggested in earlier studies [204, 206, 212].

In view of the changes observed in nuclear membrane, we predicted and validated that CucWi-N treatment caused laminopathy (lamin-dependent nucleus-mediated destruction of the cell morphology) [239, 257] selectively in cancer cells (Figs. 16 to 19). Furthermore, by serial passaging of cancer cells in sub-toxic low doses of CucWi-N, we demonstrated that it caused replicative senescence (Fig. 20 to 23) - an expected outcome of laminopathy [258, 259]. CucWi-N-induced senescence in the cancer cells was supported by molecular changes including, gradual

downregulation of $pRB^{phospho}$, hnRNP-K and mortalin, and activation of CARF and p53. pRB (Retinoblastoma protein, a major tumor suppressor coded by *RB1* tumor suppressor gene) phosphorylation and its release from pRB-E2F complex is essential for cell cycle progression [241, 260]. hnRNP-K, a multifunctional protein enriched in dividing and migrating cells has been implicated in proliferation and migration capacities of cancer cells [220, 223]. Mortalin, a stress chaperone, has been linked to proliferative and anti-apoptotic characteristics of cancer cells. Together, decrease in $pRB^{phospho}$, hnRNP-K and mortalin expression demonstrated decrease in proliferation and cell cycle arrest in CucWi-N treated cancer cells. Furthermore, shift of the staining pattern of mortalin from perinuclear (characteristic of cancer cells) to pancytoplasmic (characteristic of normal cells) endorsed induction of senescence [225, 230, 232]. This was further supported by increase in p53 (tumor suppressor) and CARF proteins, which have been established as stress, senescence and growth arrest regulating intracellular protein markers [261-264] and shown to be upregulated at the onset of replicative senescence [261, 263]. Consistent induction of wild type p53 activity [265] and upregulation of CARF have been shown to cause senescence/growth arrest of cells [266, 267]. Furthermore, CucWi-N treated cancer, but not the normal, cells showed downregulation of MRN complex.

Several studies have reported the crucial role of MRN complex (constituted of MRE11, Rad50 and NBS1 proteins) in genomic stability, DNA repair mechanisms and induction of senescence [240, 268]. It was shown to be tightly associated with DNA-damage mediated repair mechanism and delay of senescence by both telomerase and ALT mechanisms. MRN has been established as sensor of DNA damage and triggers the repair by regulation and expression of several proteins that in turn have been shown to regulate telomere structure, function and replicative senescence [269]. Its inhibition results into unresponsiveness to DNA damage gradually

leading to senescence [270, 271]. MRE11 has been shown to be central to the DNA repair mechanism in telomerase-positive cells [272, 273]. Activated by ATM phosphorylation, it promotes local separation of the double stranded DNA helix at the damage site and recruit the repair machinery [274]. MRE11 depletion was associated with telomere damage and defective nuclease functions [275]. NBS1, on the other hand, was shown to play a crucial role in alternate lengthening of telomere (ALT) mechanism of telomere maintenance and cancer cell immortality [276, 277]. NBS1 knockdown has been shown to result in impaired DNA damage response, accumulation of double stranded DNA breaks and accelerated senescence [278-280]. Of note, while MRE11 has been shown to play a key role in telomerase-based immortality, NBS1 was shown to be central in ALT-mechanism. We found that CucWi-N treatment caused marked inhibition of MRE11 and NBS1 in the cancer cells (Fig. 23) suggesting that it may be effective for both telomerase plus and ALT cells. Furthermore, these changes in doxorubicin-induced senescent cells were not as pronounced as in cancer cells attributing to the selective induction of senescence in the latter.

Lamin A and C are the most studied lamin proteins, which form a network structuring into the nuclear lamina and play a fundamental role in the organization of the nuclear architecture [281-283]. Lamin expression is directly linked to the structural integrity of a cell and is enriched in differentiated cells. It has been shown to mediate nucleo-cytoplasmic trafficking of molecules including hnRNP-K and mortalin [226, 284]. Deficient lamina has been shown to give rise to laminopathies like conductive cardiac dystrophy, skeletal defects and lipodystrophy [285]. Lamins were shown to interact with SUN1, a mammalian inner nuclear envelop mRNA exporter and structurally bridge nuclear membrane to cytoskeleton [282]. Knockdown of SUN1 protein resulted into indirect laminopathy, cellular morphological defects and an overall downregulation of hnRNP-

K. On the other hand, MKT-077 (mortalin inhibitor) was shown to cause extensive caspase-dependent apoptotic cell death, which was mediated by cleavage of PARP and lamin A [283]. Foster et al. showed that depletion of lamin A caused cross-linking and folding of mortalin that favored the formation of dynamic actin filaments over stress fibers [281]. In light of this information, it is suggestive that CucWi-N-mediated decrease in mortalin, hnRNP-K and lamin A/C may be linked events.

Molecular docking analysis of Cuc and Wi-N to 3 target proteins (mortalin, p53 and hnRNP-K) revealed that whereas Cuc has strong affinity for the mortalin protein and formed stable hydrogen bonds within its p53 binding site, no stable bonding within the mortalin binding site of p53 protein was seen (Figs. 28 and 29). Wi-N, on the other hand, has been shown to abrogate mortalin-p53 complexes by binding to both the proteins [175]. Docking of Cuc and Wi-N revealed comparative affinity hnRNP-K protein (Figs. 31 to 33). Of note when Cuc showed high binding affinity when the Wi-N was pre-docked to hnRNP-K (Fig. 30). These data may explain the higher therapeutic potential of the CucWi-N combination. *In vivo* nude mice tumor progression data and the protein analysis of tumors from control and CucWi-N fed mice revealed that CucWi-N has no toxicity to mice and possesses strong tumor suppression and anti-metastasis capability (Figs. 36 to 40). Cancer cell metastasis involves upregulation of EMT proteins such as MMPs and Vimentin [286, 287], hnRNP-K [220, 222] and mortalin [225]. Of note, CucWi-N inhibited migration and invasion capacity of the cancer cells, even at the non-toxic dose, and was supported with the downregulation hnRNP-K, mortalin, VEGF, Vimentin, MMP2 and Fibronectin (Figs. 24 to 27).

Here, we hypothesized and aimed to develop a combination of the bioactives hailing from the Indian and Chinese Ginsengs, which could serve as a natural, affordable, and safe anticancer drug. Cellular phenotype and molecular analyses provided evidence that it was safe for normal

cells and caused replicative senescence in cancer cells. We have demonstrated that CucWi-N targets mortalin and hnRNP-K proteins, cause decrease in Lamin and MRN complex proteins resulting into the induction of senescence and decrease in the migration of the cancer cells. We propose CucWi-N as a potent cancer preventive and therapeutic anticancer cocktail, which warrants clinical evaluation.

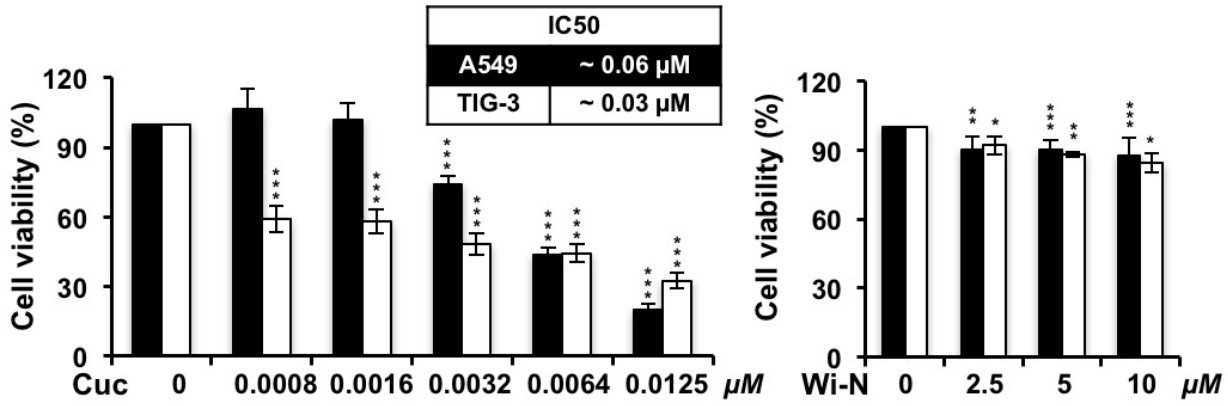

Fig. 10. Effect of CucWi-N on cell survival and multiplication: Dose titration of Cucurbitacin B and Withanone on A549 and TIG-3 cells as independent agents over 48 hrs.

Garg et al. 2018 J Gerontol A Biol Sci Med Sci (Communicated)

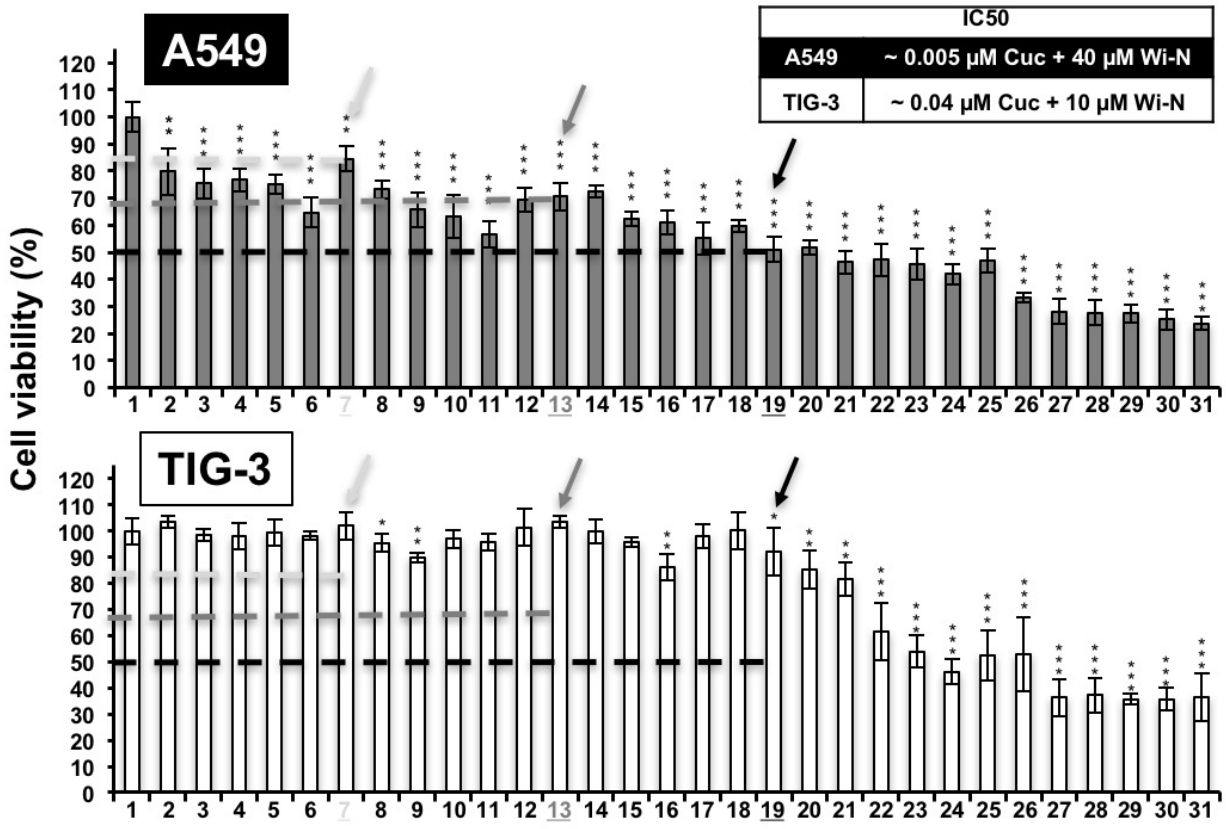

Fig. 11. Effect of CucWi-N on cell survival and multiplication: Dose titration of Cucurbitacin B and Withanone on A549 and TIG-3 cells in combination.

Garg et al. 2018 J Gerontol A Biol Sci Med Sci (Communicated)

	Cuc	Wi-N
1	0	0
2	0.0025 µM	2.5 µM
3		5 µM
4		10 µM
5		20 µM
6		40 µM
7	0.005 µM	2.5 µM
8		5 µM
9		10 µM
10		20 µM
11		40 µM
12	0.01 µM	2.5 µM
13		5 µM
14		10 µM
15		20 µM
16		40 µM
17	0.02 µM	2.5 µM
18		5 µM
19		10 µM
20		20 µM
21		40 µM
22	0.04 µM	2.5 µM
23		5 µM
24		10 µM
25		20 µM
26		40 µM
27	0.08 µM	2.5 µM
28		5 µM
29		10 µM
30		20 µM
31		40 µM

CucWi-N	Cuc	Wi-N
Low	0.005 µM	2.5 µM
Medium	0.01 µM	5 µM
High	0.02 µM	10 µM
w/w ratio	1:420	
Molar ratio	1:500	

Fig. 12. Effect of CucWi-N on cell survival and multiplication: Chart depicting selection of 1:500 molar ratio dose of the combination for further *in vitro* analysis over 48 hrs.

Garg et al. 2018 J Gerontol A Biol Sci Med Sci (Communicated)

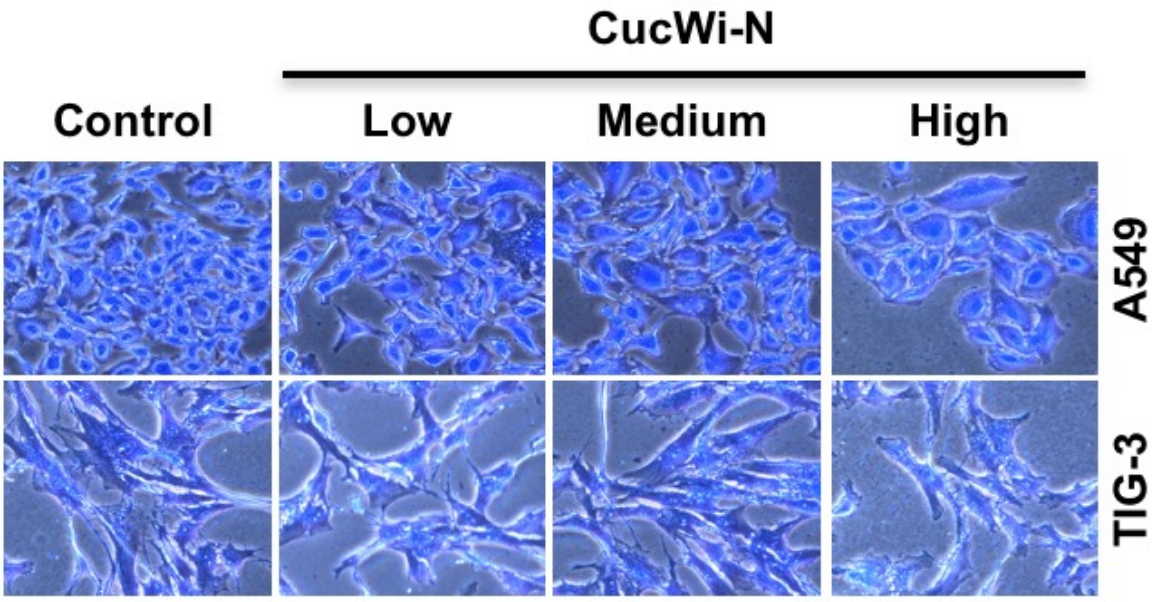

Fig. 13. Effect of CucWi-N on cell survival and multiplication: Crystal violet stained A549 and TIG-3 cells demonstrating the effect of CucWi-N treatment on cell morphology over 48 hrs.

Garg et al. 2018 J Gerontol A Biol Sci Med Sci (Communicated)

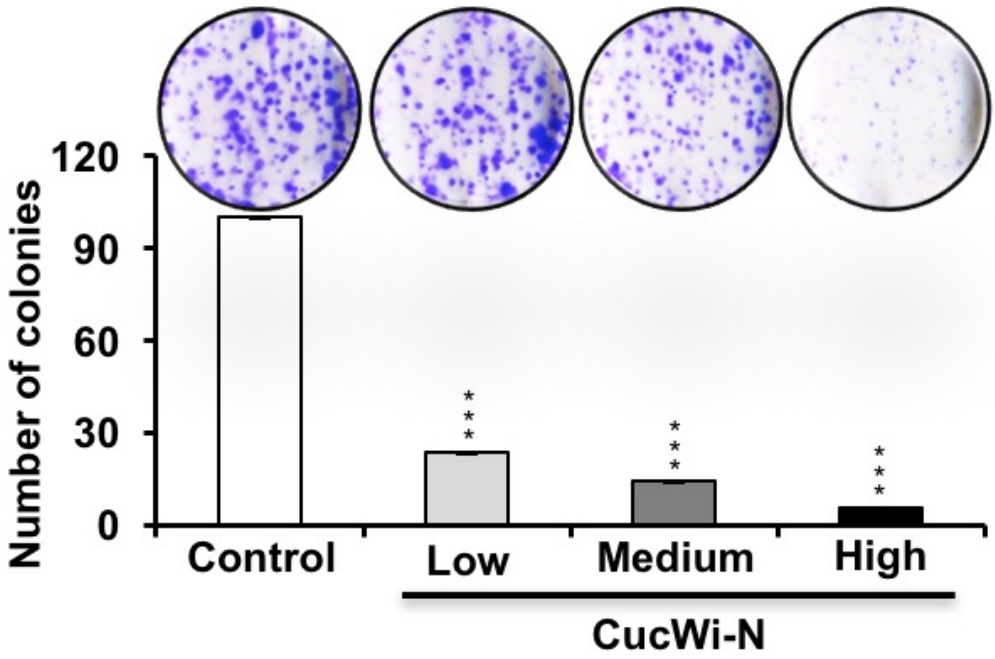

Fig. 14. Effect of CucWi-N on cell survival and multiplication: Clonogenicity assay demonstrating the effect of CucWi-N treatment on A549 cell colony forming capacity.

Garg et al. 2018 J Gerontol A Biol Sci Med Sci (Communicated)

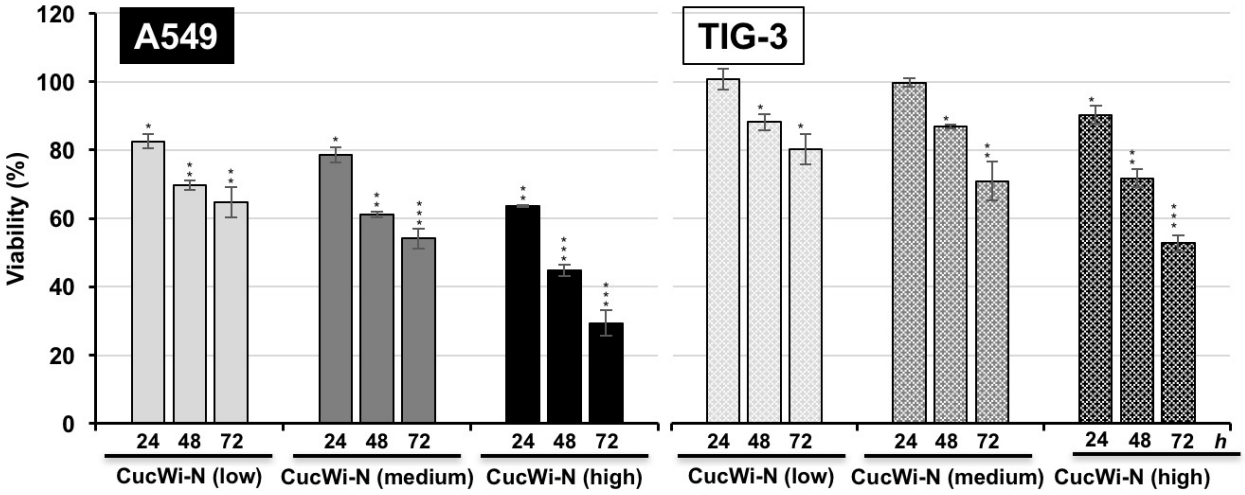

Fig. 15. Effect of CucWi-N on cell survival and multiplication: Cell proliferation assay demonstrating the effect of CucWi-N treatment on A549 and TIG-3 cell multiplication over 72 hrs.

Garg et al. 2018 J Gerontol A Biol Sci Med Sci (Communicated)

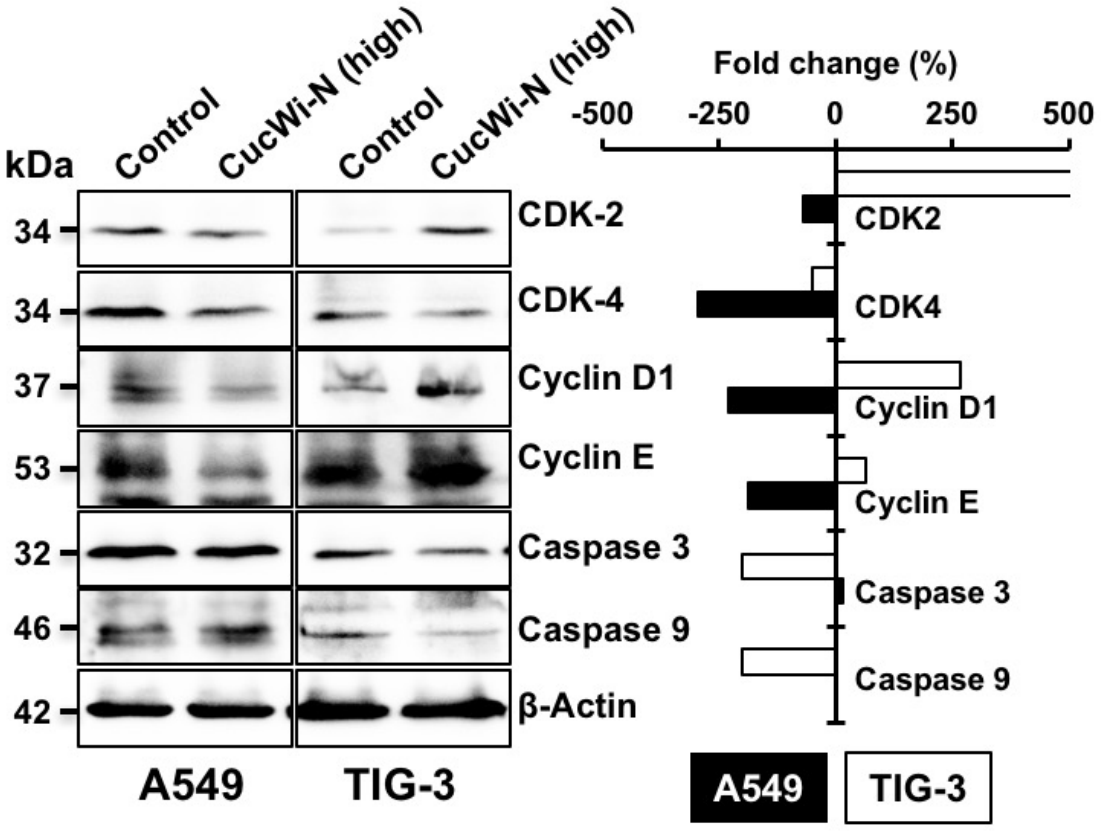

Fig. 16. Effect of CucWi-N on expression of key regulators of cell growth: evidence for selective growth inhibition in cancer cells treated with CucWi-N (high) for 48 hrs.

Garg et al. 2018 J Gerontol A Biol Sci Med Sci (Communicated)

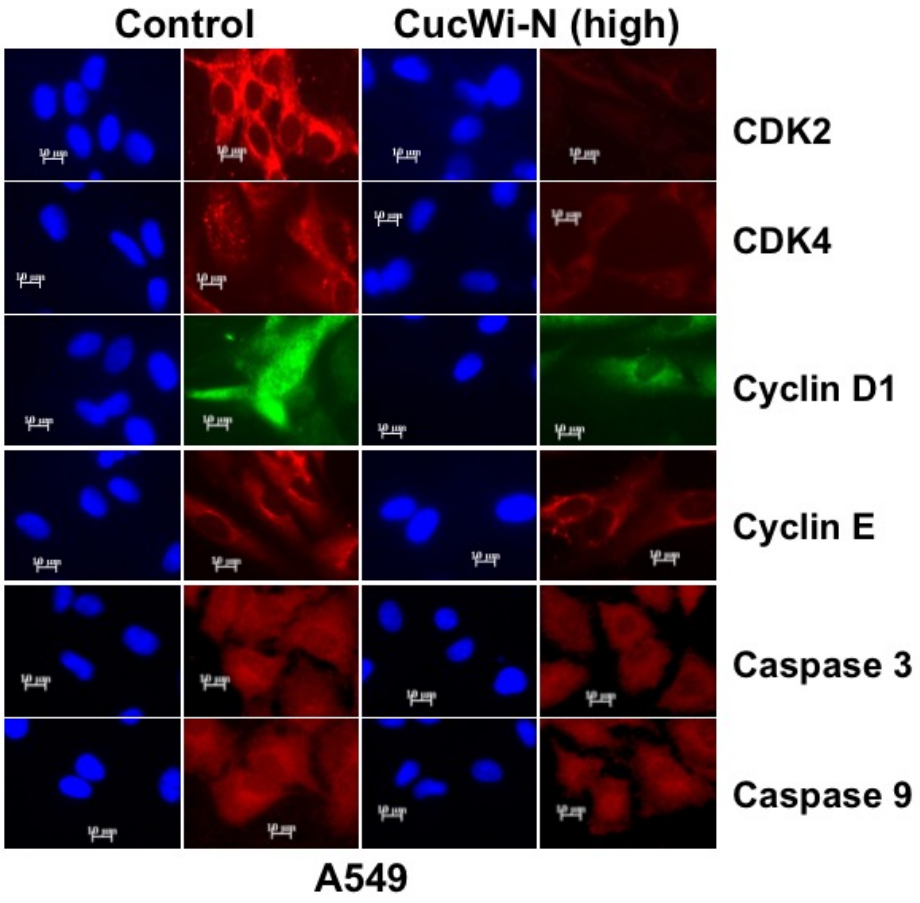

Fig. 17. Molecular expression of selective growth limiting potential of CucWi-N: Immunocytostaining analysis of cell growth and arrest proteins in A549 cells treated with CucWi-N (high) for 48 hrs.

Garg et al. 2018 J Gerontol A Biol Sci Med Sci (Communicated)

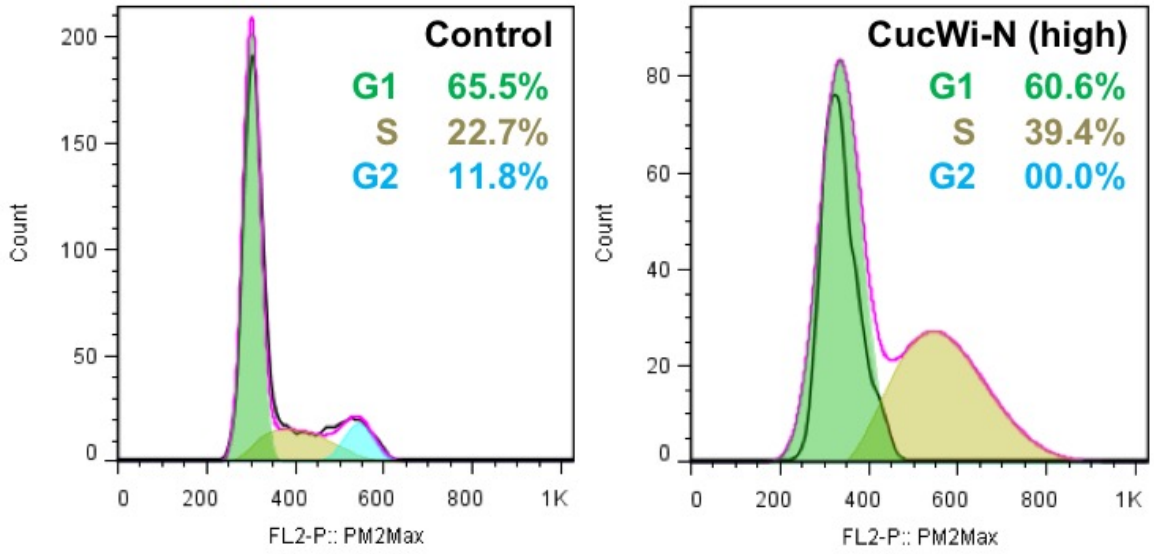

Fig. 18. Molecular evidence for growth limiting potential of CucWi-N: Cell cycle analysis of A549 cells treated with CucWi-N (high) for 48 hrs.

Garg et al. 2018 J Gerontol A Biol Sci Med Sci (Communicated)

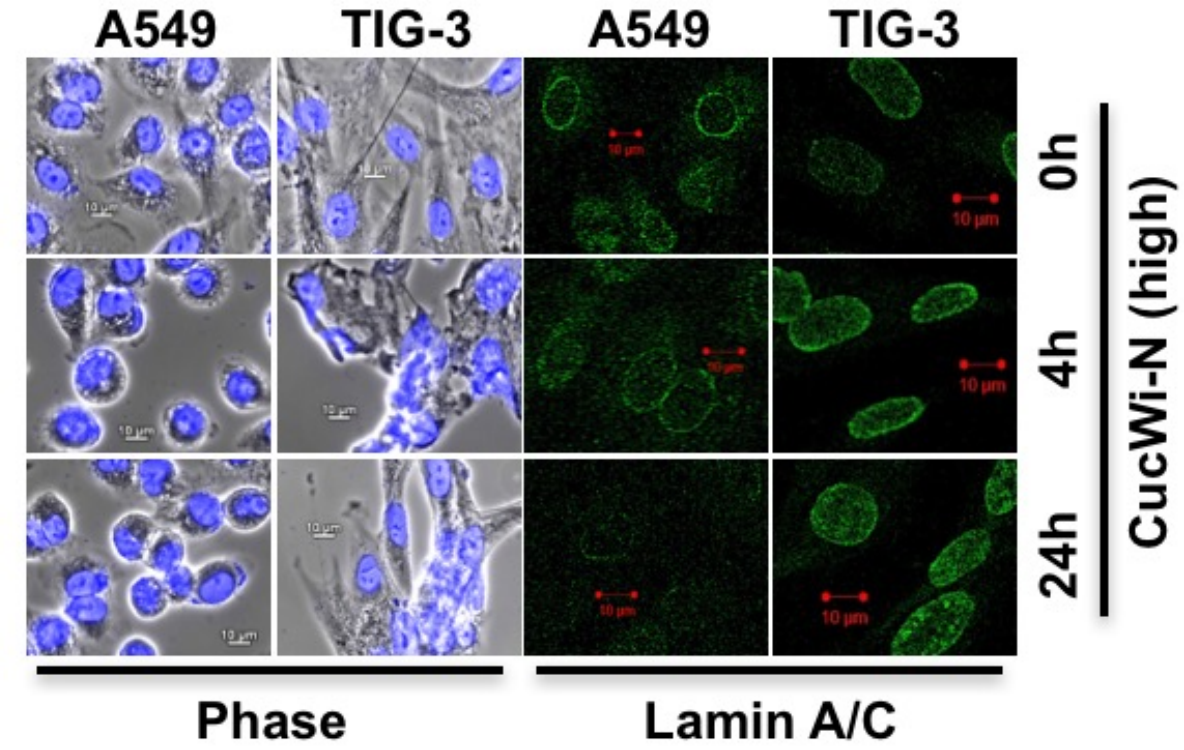

Fig. 19. Molecular evidence of selective growth limiting potential of CucWi-N: Expression analysis for Lamin A/C by immunocytostaining in cells treated with CucWi-N with varying time periods.

Garg et al. 2018 J Gerontol A Biol Sci Med Sci (Communicated)

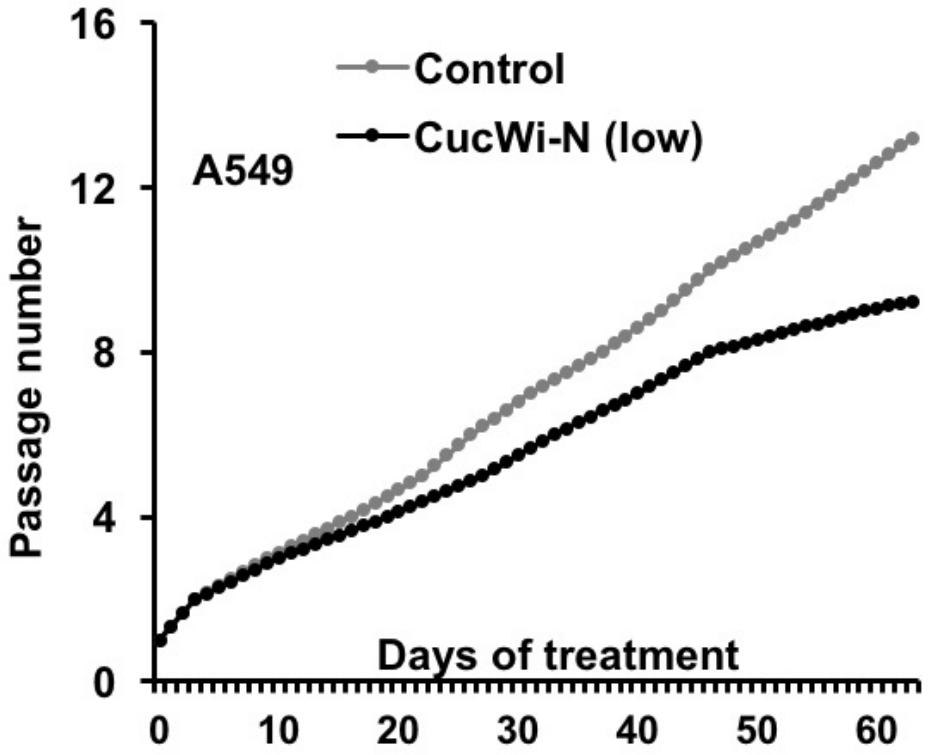

Fig. 20. Induction of senescence and inhibition of expression of migratory proteins by CucWi-N: Serial passaging of A549 cells with CucWi-N (low) led to the induction of replicative senescence and growth arrest in 65 days.

Garg et al. 2018 J Gerontol A Biol Sci Med Sci (Communicated)

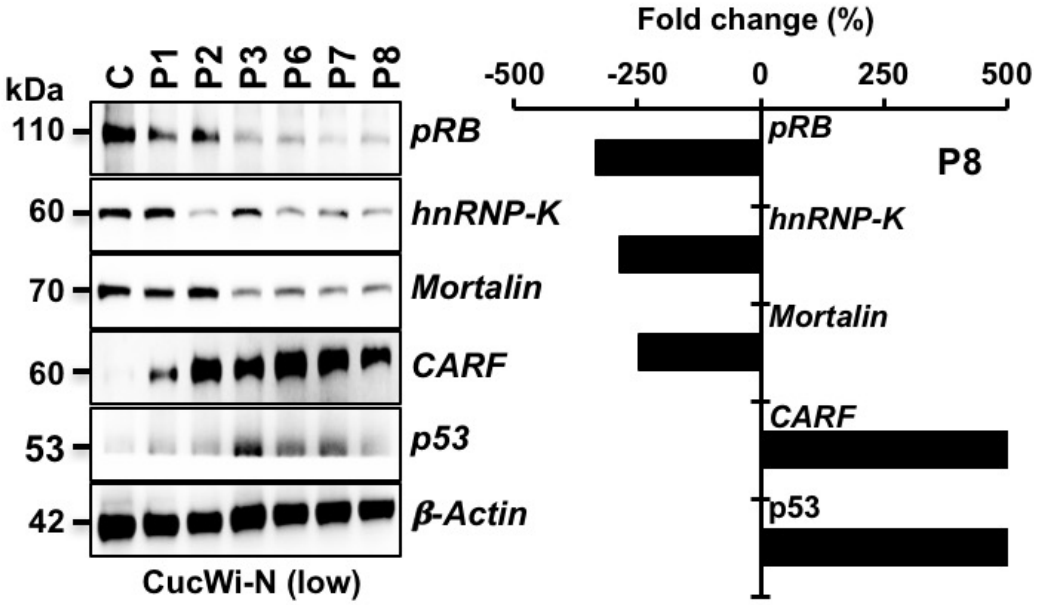

Fig. 21. Induction of senescence and inhibition of expression of migratory proteins by CucWi-N: Immunoblotting analysis (left) and quantification (right) of cell growth and stress proteins in A549 cells serially passaged in CucWi-N.

Garg et al. 2018 J Gerontol A Biol Sci Med Sci (Communicated)

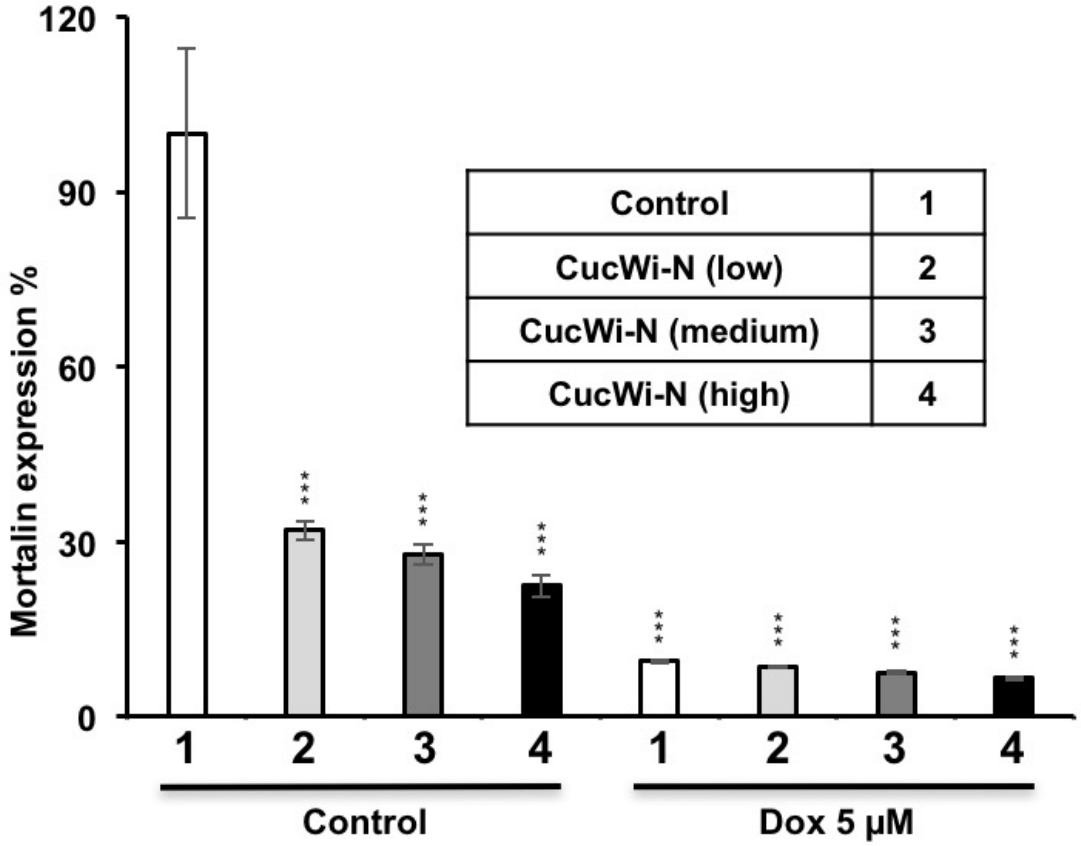

Fig. 22. Induction of senescence and inhibition of expression of migratory proteins by CucWi-N: Mortalin ELISA analysis for mortalin quantification in A549 and doxorubicin-mediated senescent A549 cells treated with or without CucWi-N over 48 hrs.

Garg et al. 2018 J Gerontol A Biol Sci Med Sci (Communicated)

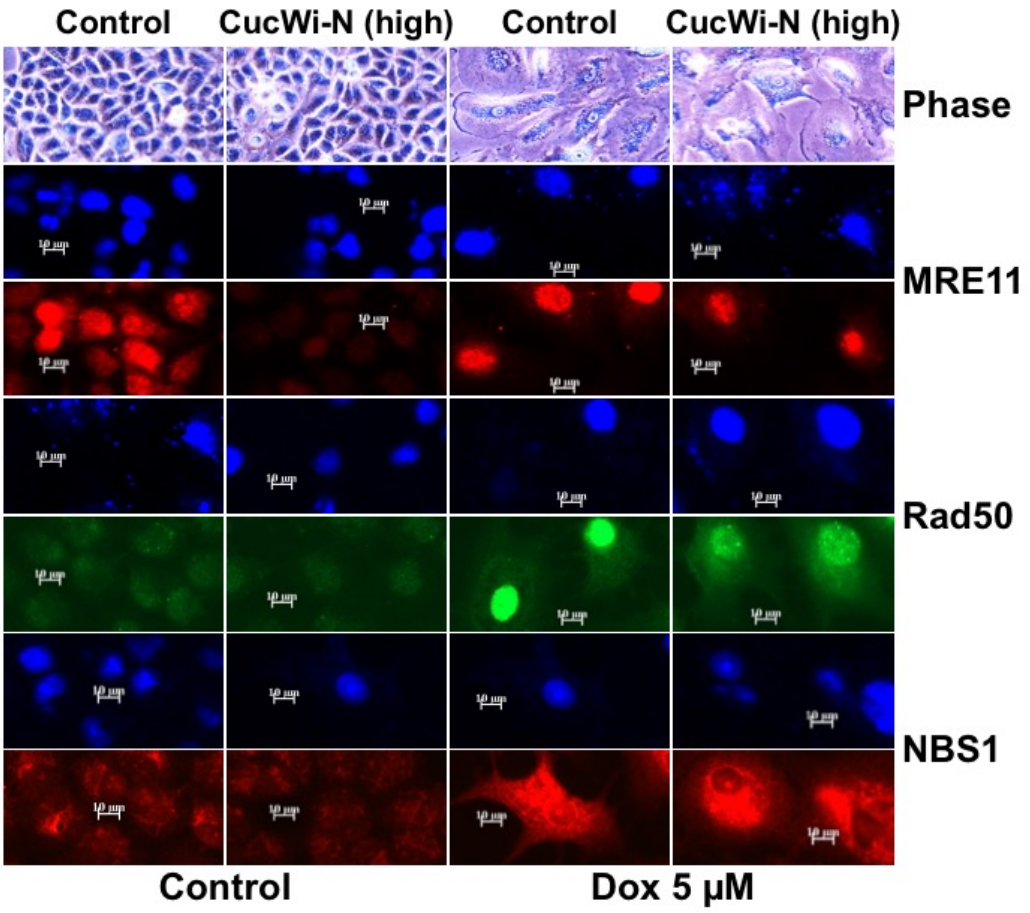

Fig. 23. Induction of senescence and inhibition of expression of migratory proteins by CucWi-N: Immuncytostaining of DNA repair mechanism protein complex in A549 and doxorubicin-mediated senescent A549 cells treated with CucWi-N (high) over 48 hrs.

Garg et al. 2018 J Gerontol A Biol Sci Med Sci (Communicated)

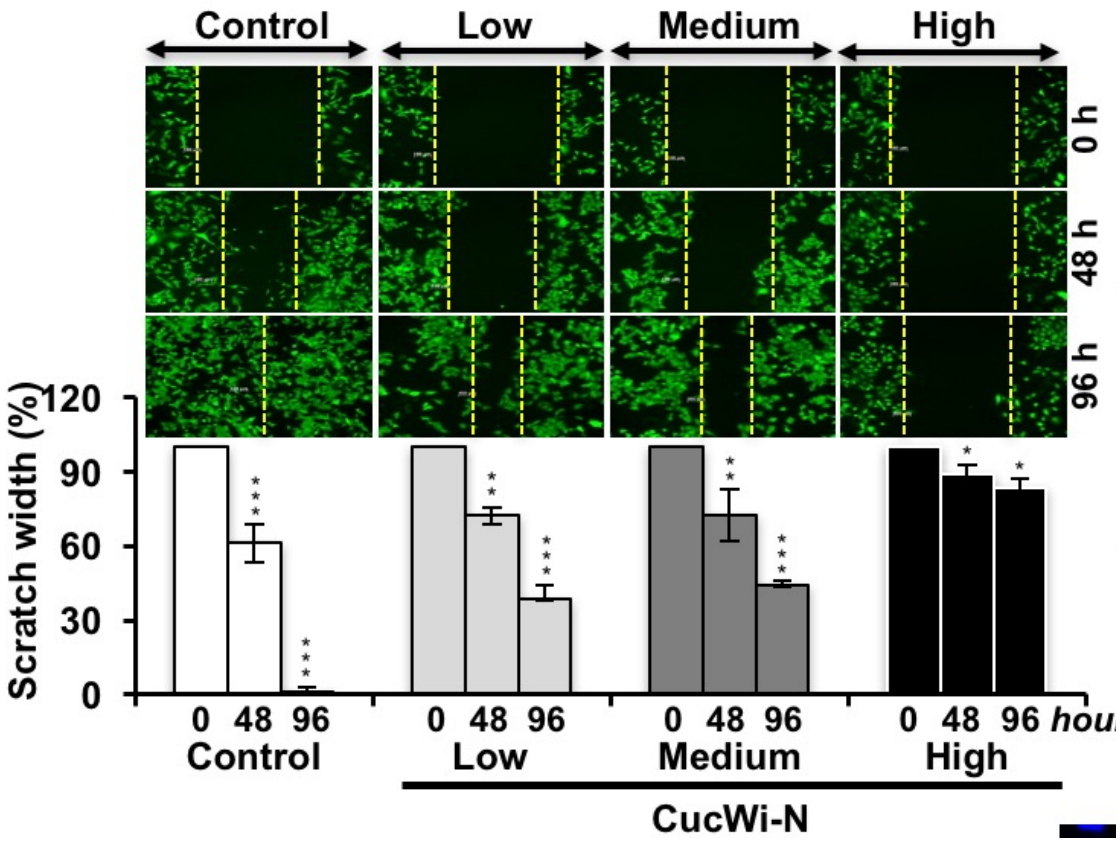

Fig. 24. Inhibition of cell migration potential of the A549 cells by CucWi-N: Wound scratch migration assay and analysis of A549 cells treated with CucWi-N over 96 hrs.

Garg et al. 2018 J Gerontol A Biol Sci Med Sci (Communicated)

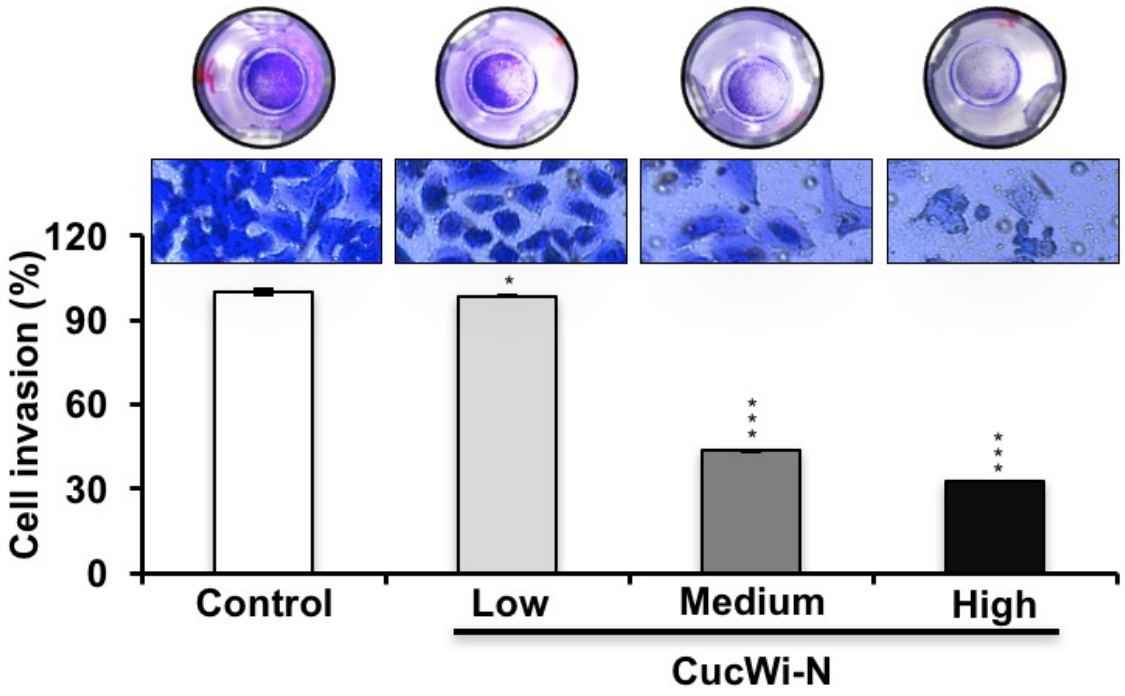

Fig. 25. Inhibition of cell migration potential of the A549 cells by CucWi-N: Corning® BioCoat™ Matrigel™ invasion assay and analysis of A549 cells treated with CucWi-N over 48 hrs.

Garg et al. 2018 J Gerontol A Biol Sci Med Sci (Communicated)

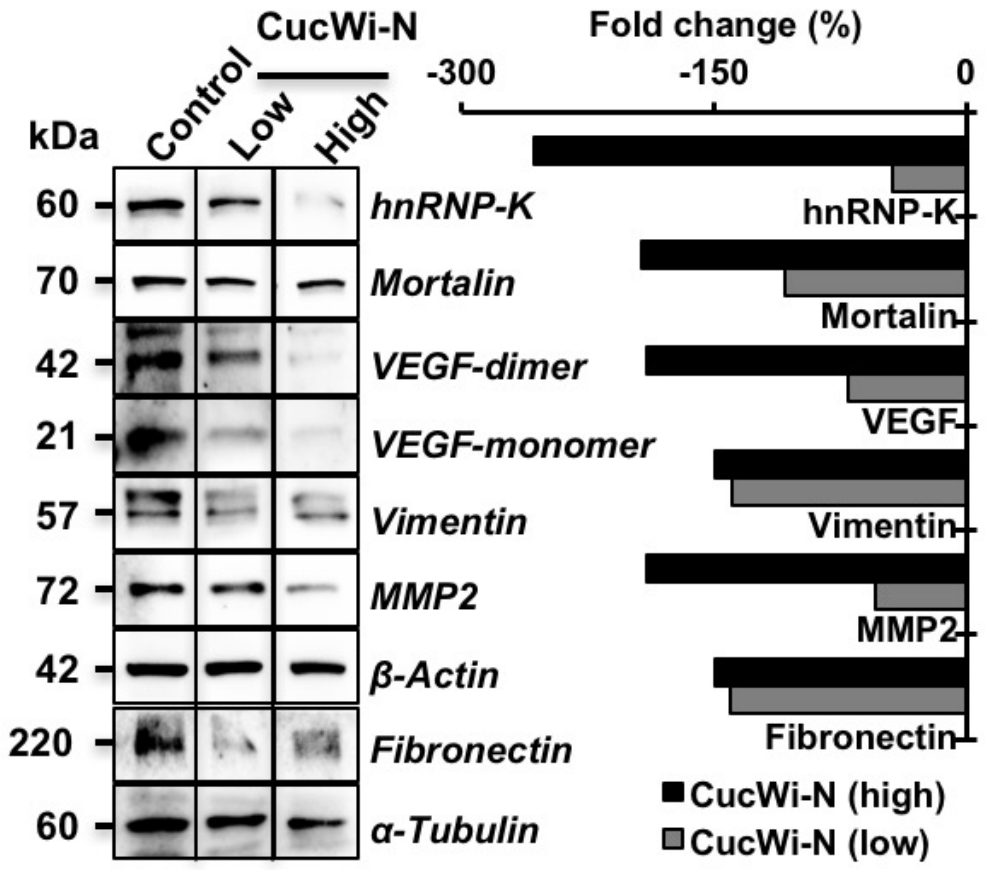

Fig. 26. Inhibition of cell migration potential of the A549 cells by CucWi-N: Immunoblotting analysis (left) and quantification (right) of involved proteins in A549 cells treated with CucWi-N (low/high) for 48 hrs.

Garg et al. 2018 J Gerontol A Biol Sci Med Sci (Communicated)

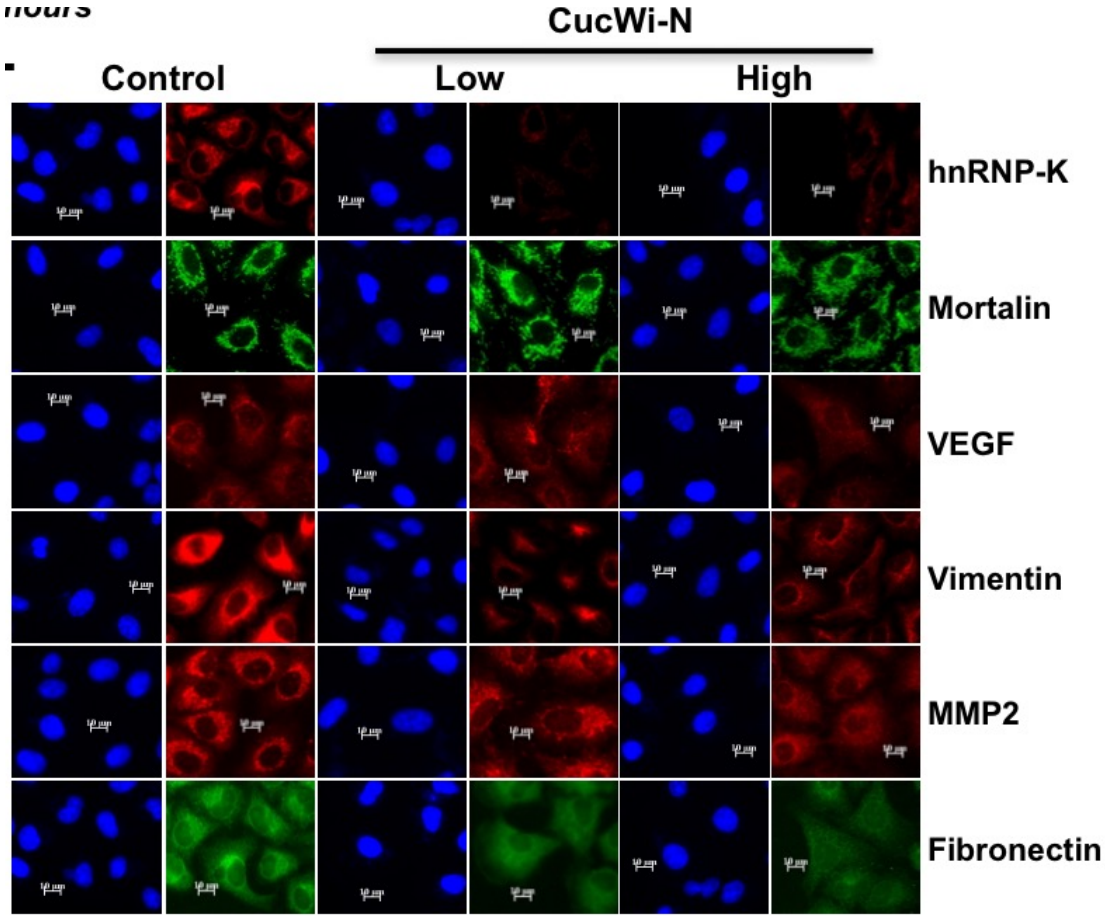

Fig. 27. Inhibition of cell migration potential of the A549 cells by CucWi-N: Immuncytostaining of involved proteins in A549 cells treated with CucWi-N (low/high) for 48 hrs.

Garg et al. 2018 J Gerontol A Biol Sci Med Sci (Communicated)

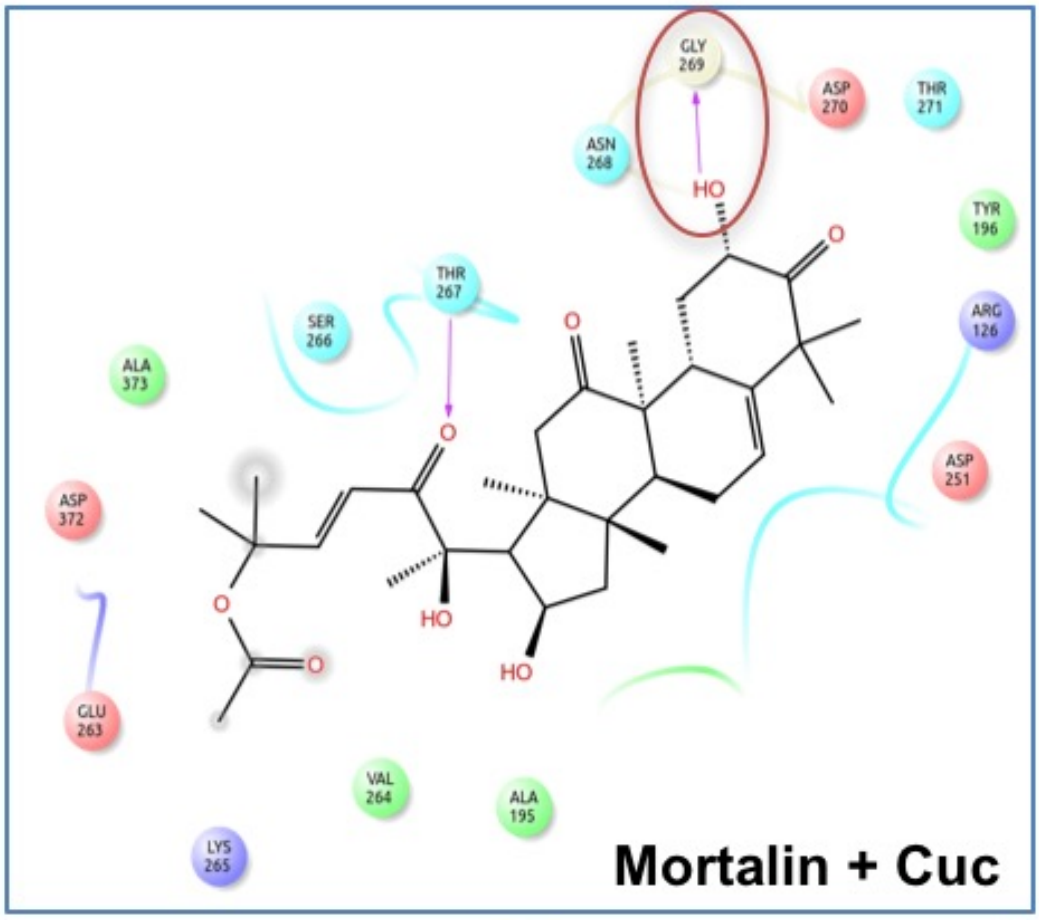

Fig. 28. *In silico* analysis of interactions of Cuc and Wi-N with mortalin protein involved in cell proliferation and migration: Docking simulation diagram of Cucurbitacin B with mortalin showing binding at interacts Thr267 and Gly269 lying within the p53 binding region.

Garg et al. 2018 J Gerontol A Biol Sci Med Sci (Communicated)

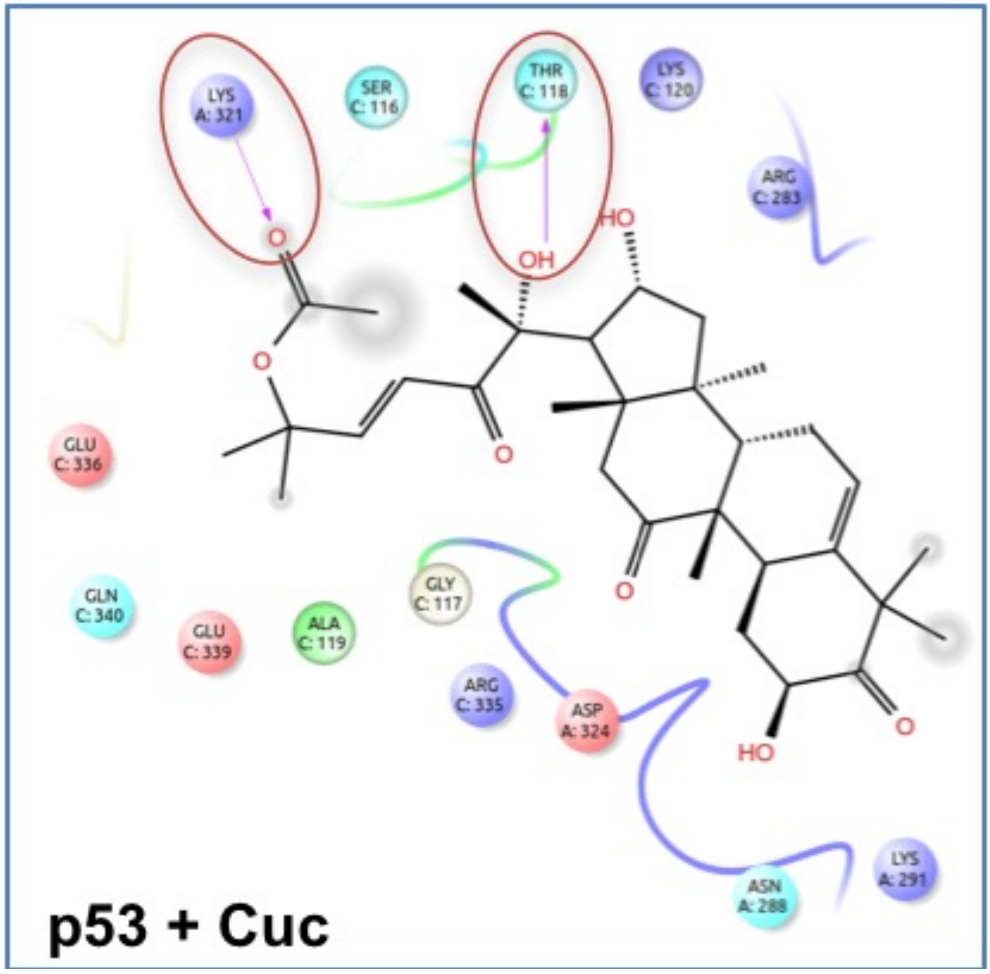

Fig. 29. *In silico* analysis of interactions of CucWi-N with p53 tumor suppressor protein: Docking simulation diagram of Cucurbitacin B with p53 showing binding at interacts Thr118 and Lys321 lying outside the mortalin binding region.

Garg et al. 2018 J Gerontol A Biol Sci Med Sci (Communicated)

Complex	Binding Energy (kCal/mol)
Mortalin + MKT-077	-2.042
Mortalin + Cuc	**-4.212**
p53 + Cuc	-2.640
hnRNPK + Cuc	-2.930
hnRNPK + Wi-N	-2.340
Cuc + hnRNPK:Wi-N	**-4.690**
Wi-N + hnRNPK:Cuc	-2.620

Fig. 30. *In silico* analysis of interactions of CucWi-N with different target proteins: Chart tabulating the specific binding energies Cuc, Wi-N, CucWi-N and controls with various target proteins.

Garg et al. 2018 J Gerontol A Biol Sci Med Sci (Communicated)

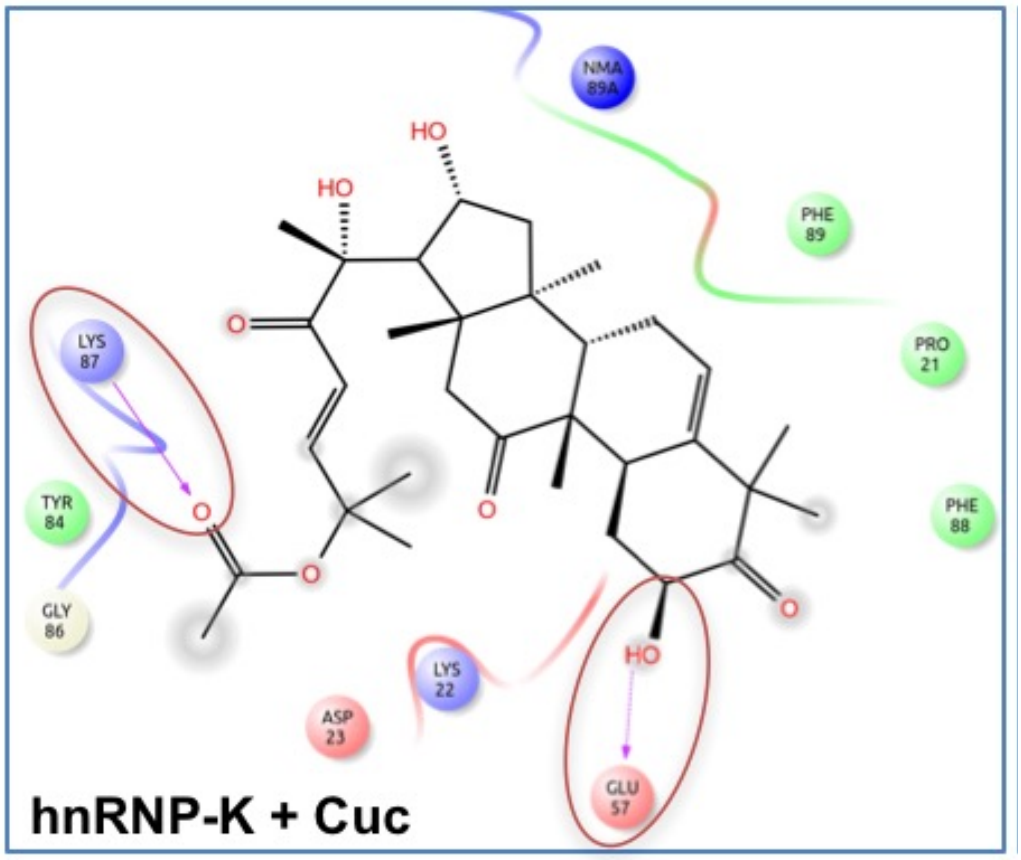

Fig. 31. *In silico* analysis of interactions of CucWi-N with hnRNP-K regulator of cell migration protein: Docking simulation diagram of Cucurbitacin B with hnRNP-K.

Garg et al. 2018 J Gerontol A Biol Sci Med Sci (Communicated)

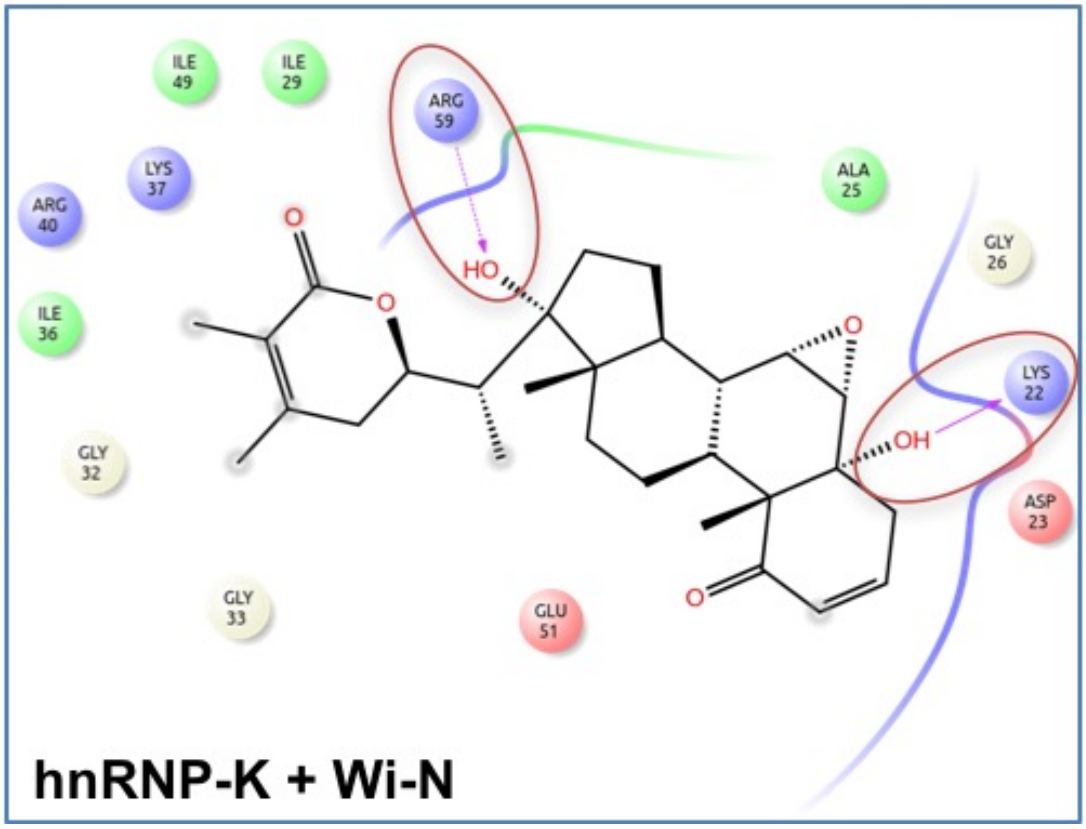

Fig. 32. *In silico* analysis of interactions of CucWi-N with target proteins: Docking simulation diagram of Withanone with hnRNP-K.

Garg et al. 2018 J Gerontol A Biol Sci Med Sci (Communicated)

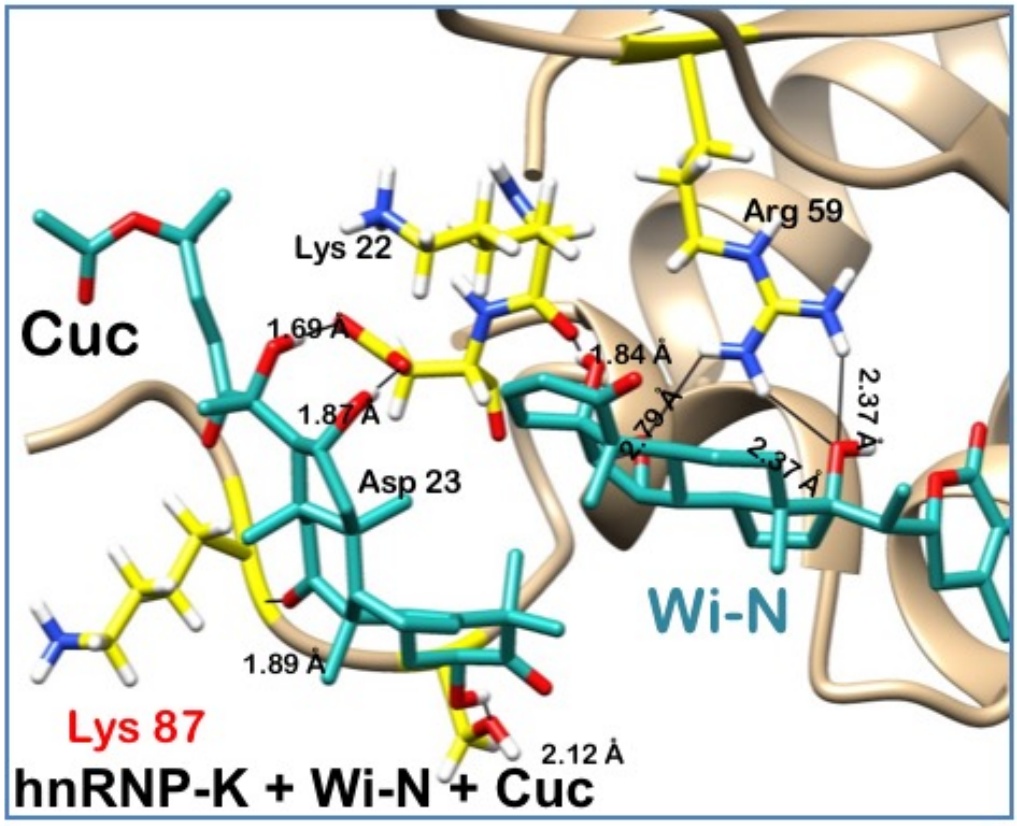

Fig. 33. *In silico* analysis of interactions of CucWi-N with target proteins: Docking simulation diagram of CucWi-N with hnRNP-K showing stable hydrogen bond binding at the interact Lys87.

Garg et al. 2018 J Gerontol A Biol Sci Med Sci (Communicated)

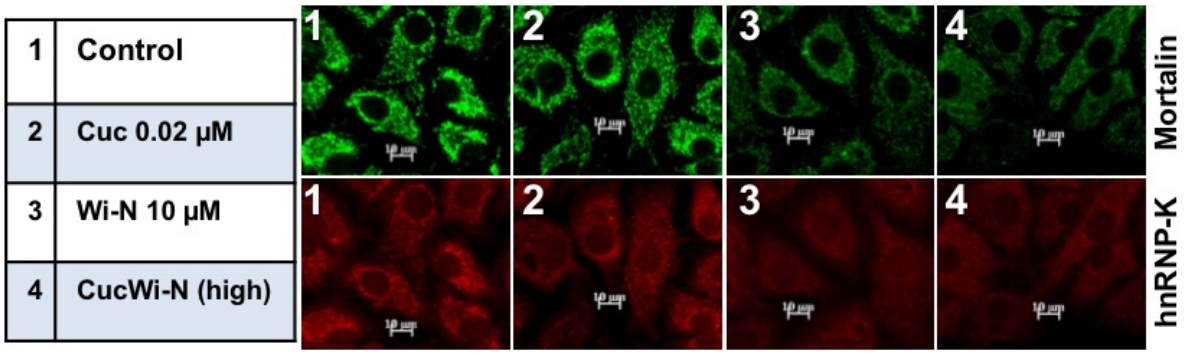

Fig. 34. *In silico* analysis of interactions of CucWi-N with target proteins: Immunocytostaining analysis of Cucurbitacin B, Withanone and CucWi-N (high) with hnRNP-K protein.

Garg et al. 2018 J Gerontol A Biol Sci Med Sci (Communicated)

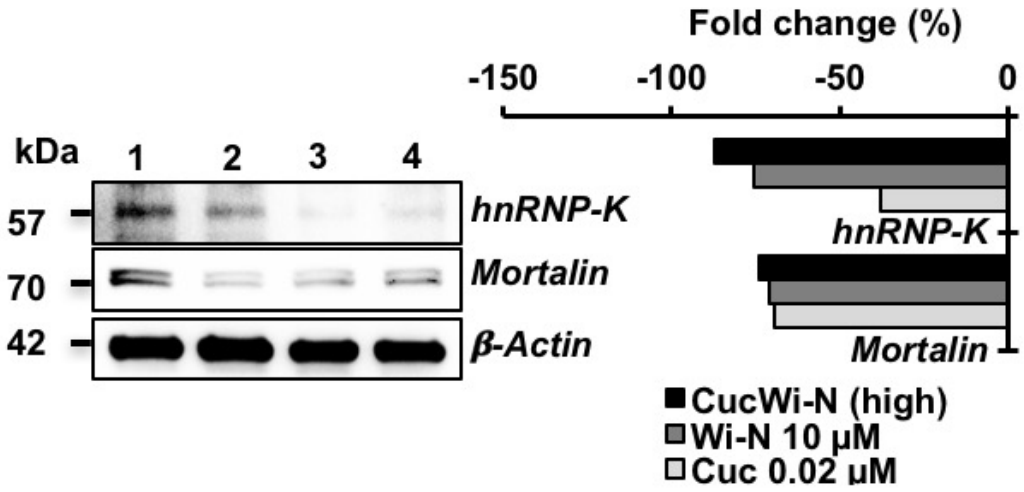

Fig. 35. *In silico* analysis of interactions of CucWi-N with target proteins: Immunoblotting analysis (left) and quantification (right) of Cucurbitacin B, Withanone and CucWi-N (high) with hnRNP-K protein.

Garg et al. 2018 J Gerontol A Biol Sci Med Sci (Communicated)

Fig. 36. *In vivo* validation of anti-tumor activity of CucWi-N (1:10 weight ratio dose) treatment over 65 days: Representation of subcutaneous A549-xenograft suppressing effect of CucWi-N.

Garg et al. 2018 J Gerontol A Biol Sci Med Sci (Communicated)

(Animal experiment approved by AIST Animal Ethical Committee)

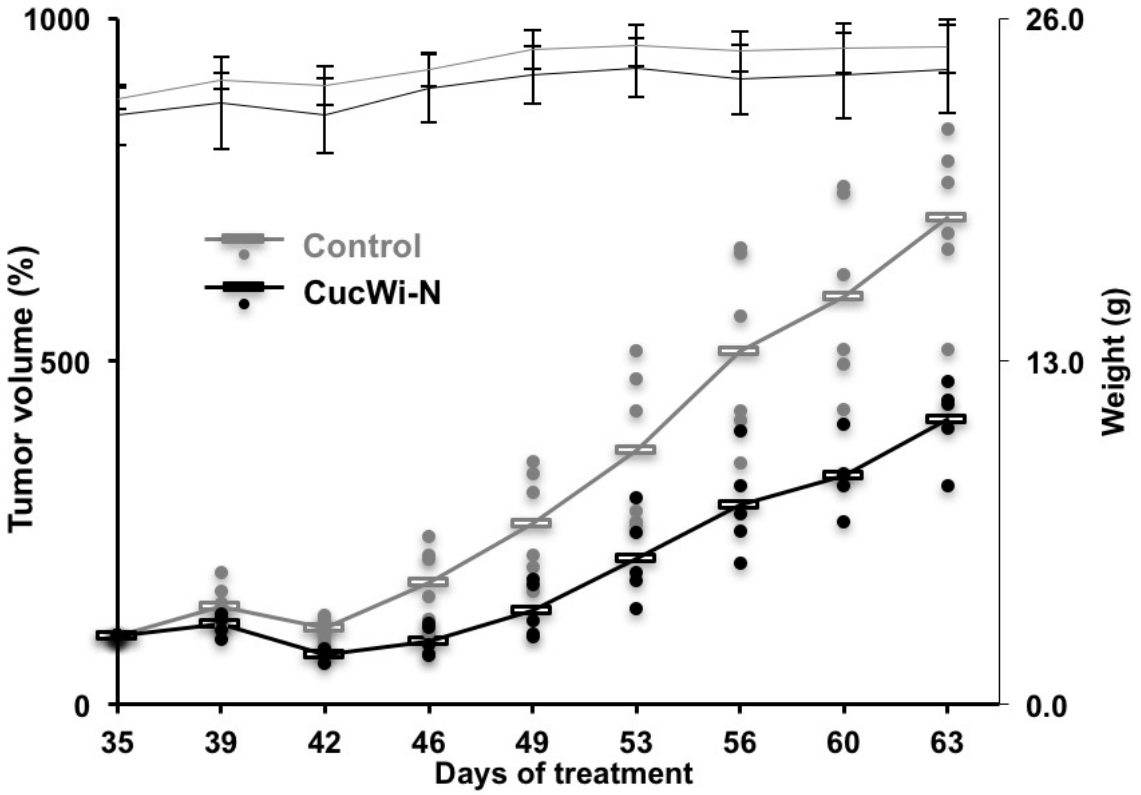

Fig. 37. *In vivo* validation of anti-tumor activity of CucWi-N (1:10 weight ratio dose) treatment over 65 days: Graphical representation of weight and subcutaneous A549-xenograft size changes due to CucWi-N.

Garg et al. 2018 J Gerontol A Biol Sci Med Sci (Communicated)

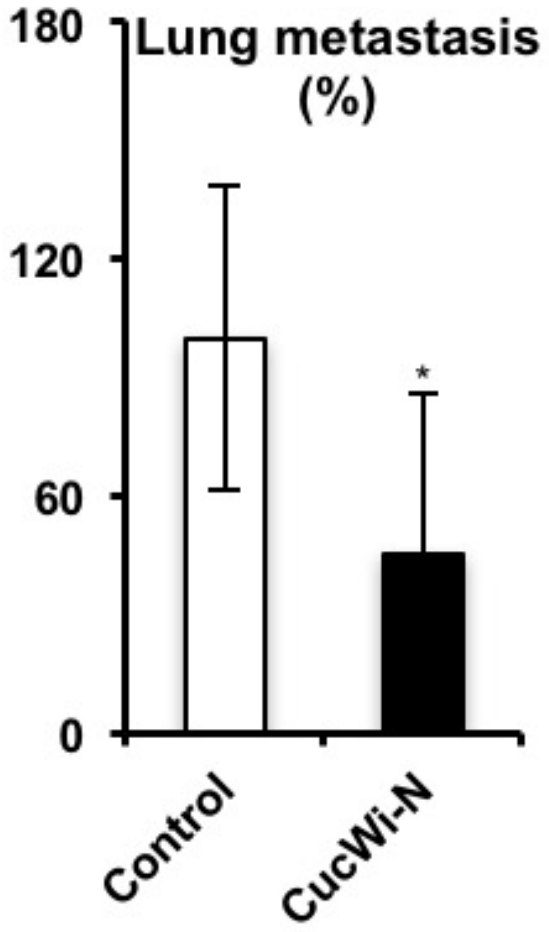

Fig. 38. *In vivo* validation of anti-tumor activity of CucWi-N (1:10 weight ratio dose) treatment over 65 days: Graphical representation of lung metastasis inhibition due to CucWi-N.

Garg et al. 2018 J Gerontol A Biol Sci Med Sci (Communicated)

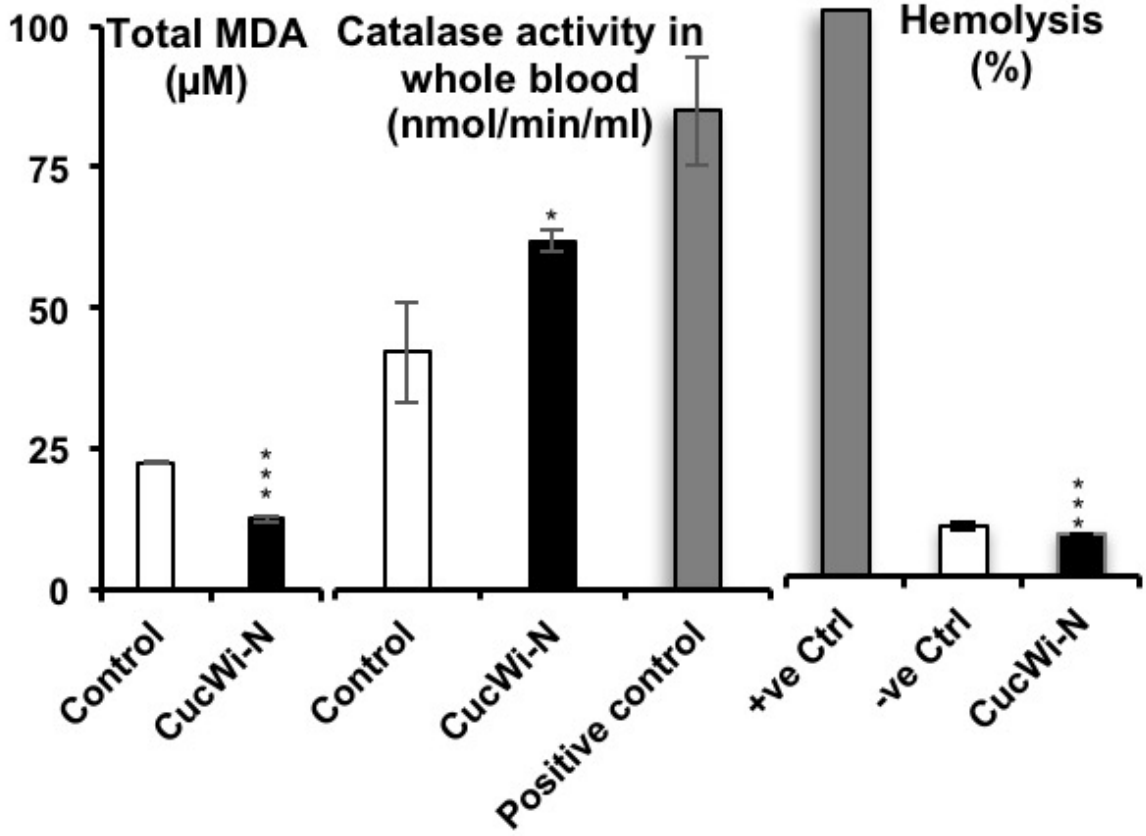

Fig. 39. *In vivo* validation of anti-tumor activity of CucWi-N (1:10 weight ratio dose) treatment over 65 days: Graphical representation of anti-oxidant and hemolytic activity of CucWi-N.

Garg et al. 2018 J Gerontol A Biol Sci Med Sci (Communicated)

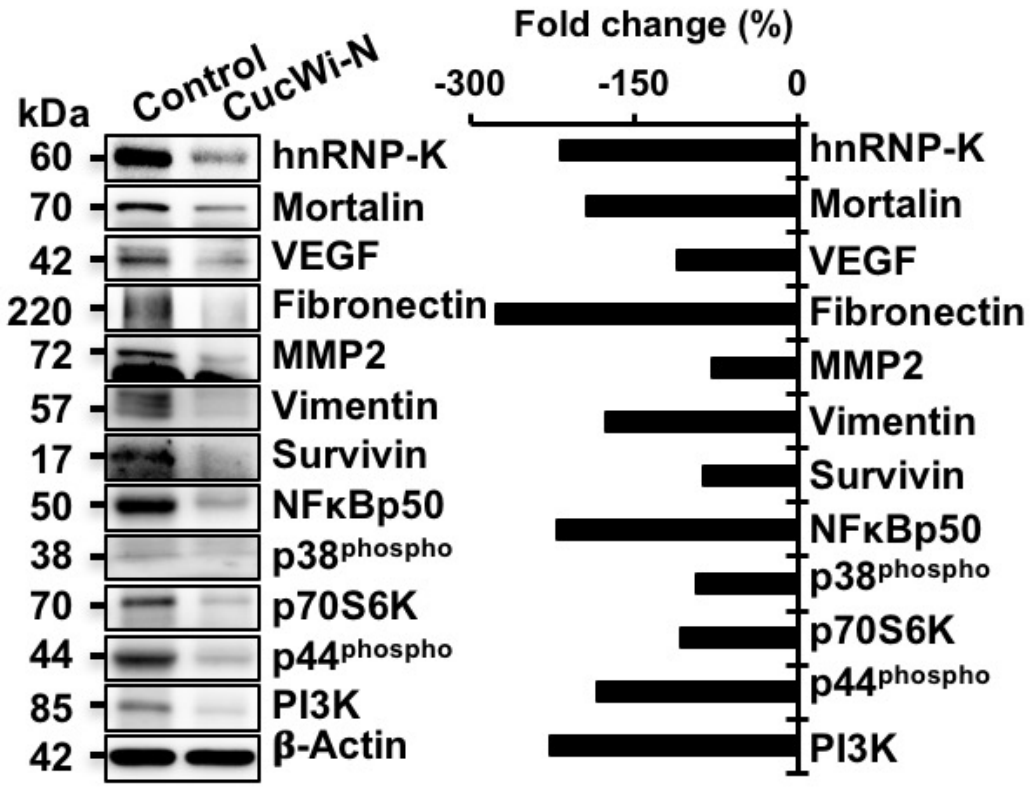

Fig. 40. *In vivo* validation of anti-tumor activity of CucWi-N (1:10 weight ratio dose) treatment over 65 days: Immunoblotting analysis (left) and quantification (right) of tumorigenesis-promoting proteins in tumor lysates derived from animals treated with CucWi-N.

Garg et al. 2018 J Gerontol A Biol Sci Med Sci (Communicated)

Chapter 6

Quantitative and Qualitative Cell Viability Assay

6.1 Introduction

Cancer is, most often, described as a continuous and sequential syndrome of diseases, where a normal cell acquires an immortal and immature state, and continues to divide uncontrollably. It is discretely characterized and differentiated from the normal cells by their potential to immortality, growth in colonies, migrate, evade immune system and trigger angiogenesis [288]. One of the mainstay in cancer treatment is chemotherapy that usually ranges from months to years. Its major objective is to eliminate or counterbalance the growth and function of the cancer cells without harming the normal cells in the body. However most molecular targeted therapies are toxic to normal cells and often result into resistance and relapse [289]. Drug development involves extremely complicated route that initiates with simple viability/cytotoxicity assays performed on cultured cancer and normal cells. Conventionally these assays are performed in short term (few hours to maximum 2-3 days) and rely on mitochondrial activity of viable cells that is linked to reliable quantitative read-outs. These have been proved very informative for extremely toxic drugs that cause sudden death of cells by mechanisms including apoptosis, necrosis or autophagy. However, the drugs with slow, but still useful, action such as induction of growth arrest, senescence or differentiation require long term assessment [289-293].

In *in vivo* conditions, cancer cells grow from a single cell to a densely packed mass, subsequently the effect of anticancer molecule varies accordingly. In order to mimic these conditions in a wet laboratory, it is essential to treat cells grown not only in sparse and dense monolayers, but also in colonies. Furthermore, the effect of drugs may range from induction of stress, senescence, differentiation, or apoptosis that are usually interconnected. An initial stressed state of the living cells might further result into either sensitization and death, or resistance. Therefore, it is extremely important to take into account the morphology along with viability to implicate the effect on cell

proliferation. Various metabolic-activity-based methods involving tetrazolium reduction, resazurin reduction, protease viability markers, ATP measurement, and real-time luciferase luminescence have been developed and described as reliable indicators of living cell viability. However, each one of these is tagged with its own set of advantages and disadvantages and lack ubiquitous application. The most conspicuous factors limiting their use include concerns about specificity, cost, reagent-induced toxicity, operational interference, and reliability [294, 295].

Great investments have been apportioned to identification and development of potential anticancer candidates and to develop their regimens [296]. National Institutes of Health financial chart reported expenditure of about 5589 million US dollars in fiscal year 2016, out of which about 10% was spent on research-related activities [297-299]. These stakes are not justified if they do not sum up into successful clinical trials. Cancer toll is increasing with a speed that the American Cancer Society has already labeled it as the emerging epidemic [300]. This alarming scenario warrants rapid and elaborate investments in cancer drug discovery programs. Instead, the shrinking budget for medicinal research world-wide reflects lack of sophisticated instruments and personnel in small laboratories and offers additional constrains. Under such compelling demand, an upgrade in the research methodology requiring lower cost and yielding more reliable outcomes will be extremely useful. Based on these facts, we integrated the conventional cell viability assays in a way that one can take multiple read-outs from a simpler amalgamated experiment. We demonstrate that our Quantitative and Qualitative Cell Viability (QCV) assay – is a substitute encompassing clonogenecity, cell viability and morphology readout as a single module and bypassing metabolism-based assays, especially applicable for compounds with color and longer mechanism of action – a novel, reliable and reproducible, relatively less expensive and simple technique for drug discovery programs.

6.2 Materials and methods

6.2.1 Cell lines and reagents

Cells purchased from DS Pharma/ JRCB, Japan were cultured either on Roswell Park Memorial Institute culture medium (RPMI, Life Technologies) (C6: rat brain glioma, DLD-1: colorectal adenocarcinoma and MKN45: human gastric carcinoma) or Dulbecco's Modified Eagle's culture medium (DMEM, Wako Chemicals) (A549: human non-small-cell lung carcinoma, DU145: human prostate adenocarcinoma, HeLa: human cervical adenocarcinoma, HT1080: human fibrosarcoma, MCF7: human breast adenocarcioma, MDA MB 231: human breast adenocarcinoma, Panc-1: human pancreatic epithelioid carcinoma, PLC/PRF/5: human hepatoma, SKOV-3: human ovarian adenocarcinoma, U2OS: human osteosarcoma, TIG-3: normal human lung fibroblasts and MRC5: normal human lung fibroblasts) or McCoy's 5A culture medium (Life Technologies) (G361: human malignant melanoma).

6.2.2 Generation of standard curve

As presented in Fig.41, C6 cells (0, 5000, 10000, 20000, 40000, 80000 per well) were plated identically into two 12-well plates and incubated at 37°C and 5% CO_2 for overnight to allow the cells adhere to the surface (Fig. 41). Cells in plate 1 were trypsinized using EDTA-trypsin (50 µL) and suspended in growth medium (70 µL). The cells were counted manually using cell counter (TC20™ Automated Cell Counter, Bio-Rad). Simultaneously the cells in the plate 2 were fixed by incubating with ice cold methanol:acetone (1:1) for 3-5 minutes on ice, followed by washing with PBS and staining with 0.5% Crystal Violet at room temperature for 2-3 hours. Stained cells were washed with PBS and allowed to air dry overnight. To the air-dried colonies, 120 µL de-staining solution was added and mixed by gentle pipetting. 100 µL CV-homogenized solution was then

loaded into a 96-well plate to measure optical density at 570 nm using a spectrophotometer (Tecan Infinite 200® Pro, Tecan Group Ltd., Mannedorf, Switzerland). Finally, a scatter graph was plotted using optical density against cell number to obtain *c* and *m* values for C6 cells (Fig. 42).

6.2.3 MTT-based short-term viable cell microscopy

Correlation between the changes in cell number and morphology as the result of treatment by an agent in a 96-well plate MTT-based cytotoxic assay was checked in C6 or U2OS cells. 1000 cells per well were plated in a 96-well plate and allowed to settle overnight, followed by treatment with DMEM supplemented with or without colored cytotoxic extract labelled CN-04 or HA-05 from our drug library. The control or extract treated cells were incubated at 37°C and 5% CO_2. After 48 hours cell pictures by a high resolution inverted microscope were recorded following which, 10 µL of 3-(4,5-dimethylthiazol-2yl)-2,5-diphenyltetrazolium bromide (MTT; Sigma Chemical Corp, St. Louis, MO) in phosphate buffered saline (PBS; 2 mg/mL) was added to each well and incubated at same conditions for 4 hours. All the media and dissolved MTT from the wells was aspirated and replaced with 100% DMSO, followed by measurement of optical density at 570 nm using Tecan Infinite 200 PRO (Tecan Group Ltd., Mannedorf, Switzerland). Cell viability and standard deviation were calculated using standard office software (Microsoft Office 2016).

6.2.4 MTT-based long-term cell viability assay

Growth efficiency of live cells in a 96-well plate was determined by an MTT-based proliferation assay. 200, 400, 600, 800 and 1000 C6 cells per well were plated in 96-well plates (in 4 sets) and allowed to settle overnight, followed by change in growth medium DMEM every

alternate day. Cells were incubated at 37°C and 5% CO_2. After every 48 hours, cell viability was calculated in one set each by employing the method described in the previous section. At the end cell viability trend, standard deviation, slope equation and R^2 values in all 4 sets were collectively calculated using standard office software (Microsoft Office 2016).

6.2.5 Qualitative and Quantitative Cell Viability (QCV) assay

C6 cells (100 per well) were plated in a 12-well plate and incubated at 37°C and 5% CO_2 for overnight to settle down. Individual cells were then allowed to grow into colonies in favorable conditions over the next 8-10 days (estimated duration for 15-20 population doublings for C6 cells). Culture medium with or without the colored extract CN-04 0.25-0.75% or colorless drug CB-01 0.5% was changed every alternate day, until wide, visible, and viable colonies of cells were formed in the control group. Cells were fixed using methanol:acetone (1:1) and stained with 0.5% crystal violet at room temperature for 2-3 hours, followed by 3 PBS washes and air drying overnight. CV stained cell pictures were recorded by an inverted high resolution phase contrast microscope. Dried assay plate was scanned and the colonies were manually counted. 120 µL de-staining solution was mixed to dissolve the CV stain from the cells, from which 100 µL was loaded into a 96-well plate to measure optical density at 570 nm using a spectrophotometer (Tecan Infinite 200® Pro, Tecan Group Ltd., Mannedorf, Switzerland). Using the equation {*cell number = (OD – c)/m*}, an average of long term cytotoxicity was obtained. All calculations and graphs were obtained using standard office software (Microsoft Office 2016).

6.2.6 Statistics

All the experiments were performed in triplicates, and the data were expressed as mean ± standard deviation. Statistical analysis was performed using GraphPad® software, Inc. (California, USA), based on independent experiments, and depicted as *<0.05, **0.01, and ***<0.001.

6.3 Results

We followed the protocol as indicated in the later section and tested in sixteen cancer cell lines (Fig. 42). The optical densities in triplicates were plotted to obtain standard curves and slope (y-intercept values). R^2-value more than 98% was considered significant (more than 85% of standard deviation explained), keeping in mind that these values will be useful to quantitate optical density into absolute cell number [301, 302].

In our regular cell viability assays using MTT, we observed that drug response is driven by cell density to a large extent. Hence we examined the effect of cell density to growth or drug response in a time dependent manner. As shown in Fig. 43, the experiments initiated with 200 rat brain glioma C6 cells showed the most efficient growth in 8 days followed by cell density/adhesion dependent growth inhibition (Fig. 43). Trend-line slope, y-intercept and R^2 values drawn showed that only the 200-variant could qualify to be significant (criteria to qualify = $R^2 > 98\%$) (Fig. 44). However, 200 cells per well to begin a viability assay in a 96-well plate may be considered incompetent as a result of high probability of experimental errors.

We next used plant extract HA-05 that possessed color. In independent 48-hour MTT-based assays, we found that its color interfered with the optical density (Fig. 45). Whereas low doses of the extract showed cytotoxicity by means of optical density followed by an increment, microscopic evaluation showed a clear dose dependent decrease in the cell density and stressed

morphology in the cells. Such errors in the readouts as a result of plating efficiency, color, or the space in a 6-7 mm diameter well, urge remodeling.

To elucidate the differences in the experimental output between the MTT-based 48-hours assay and QCV assay, we subjected C6 cells to our extract CN-04 that possesses color. MTT-based readouts showed a discrepancy in the readings - they showed an increase in cell viability up to 0.25% concentration dose (Fig. 46) however, the cell observations under the microscope did not support these data. Cells macroscopically looked to be stressed and dying with increasing dose of the extract. In order to confirm the possibility of interference of the color, we placed only extract (without cells) in a 96-well plate and incubated overnight in the same conditions as the living cells, then we took the readouts in the same way after a 4-hour incubation with MTT dye. We found that the optical density from the wells corresponded directly with the dose of the extract (Fig. 47). To eliminate color based discrepancy in the MTT-based cell count, we performed our QCV assay using the same extract. As shown in Fig. 48, cell viability (absolute cell count), morphological condition and the colony forming potential of the cells treated with CN-04 0.25-0.75% showed comprehensible consistency (Fig. 48).

In order to further validate QCV assay for colorless agents, we performed colony formation assay using 0.5% of CB-01 (colorless cytotoxic extract). Besides the decrease in clonogenic potential, we corroborated considerable difference in the morphology of the treated cells against the control group (Fig. 49). Optical density readout after de-staining revealed long-term quantifiable cell viability. Using the slope and y-intercept values given in Fig. 42, we calculated the absolute cell concentrations in control and treated cells (Fig. 49). Moreover, we found that the reduction in clonogenicity and viability as a result of the treatment were not the same. While only approximately 35% colonies (Fig. 49) remained after 8 days of treatment and culture, 65% cells

(Fig. 49) in total survived, indicating plausible presence of individual, scattered and unperceivable cells within the well. Since these results suggest that the colony number and the absolute cell count are two separate entities, they must be noted separately.

6.4 Discussion

Conventional cell viability assays in cultured cells are the standard and essential step of drug discovery protocols. However, these are complicated by drug and/or chromogen characteristics and interactions including crystallization, chemical interference, membrane permeability alteration, toxicity, and formazan fabrication as seen with variation in culture medium condition, serum and glucose concentration and protein content [303-305]. Such hurdles have been implicated for drugs including epirubicin, paclitaxel, docetaxel, cisplatin, sodium azide, imatinib, ursolic acid, chloroquine, rottlerin, curcumin, temozolomide, verampil, resveratrol, kaempferol, luteolin, quercetin, angiotensin, norepinephrine, amyloid β-peptide, interferon-gamma, glutathione S-transferase, nanoparticle-based medicines, and many more [306]. Furthermore, the mechanism of action for many natural anticancer drugs may be slower and hence demand time and dose dependent response over longer period [307]. In order to circumvent these difficulties and accommodate wide range of drugs, we assimilated the standard assays to yield quantitative and reliable readout from a prime experiment. In our QCV assay, it is possible to examine the effect of drugs in short as well as longer span of time that also allows to investigate the effect of drug on clonogenic potential of cells. Such readouts are more relevant to the cancer therapy regimens ranging from months to years [290, 292, 293, 308]. Furthermore, our QCV assay allows observations on cell morphology, an important factor to contemplate drug response characteristics and signalings [309-311]. Evaluation based on fixed cells make the use of methanol-based CV

stain solution more pertinent in this technique, accounting for absolute cell count instead of only the metabolically viable. The multidimensional aspects of our assay depict its economic performance, an important criterion in the scenario of shrinking research budget and increasing need of anti-cancer drug screening and drug development from natural resources. Taken together, QCV provides an easy way to obtain qualitative and quantitative read-outs of drug effect on cell viability in a reliable and reproducible way, with reduced efforts and time constrains.

6.5 Protocol

6.5.1 Equipment and reagents

Cell counter; Spectrophotometer at 570 nm wavelength; Microscope; Incubator at 37°C with 5% CO_2. Prepare a 0.5% w/v crystal violet solution in distilled water with 25% v/v methanol - mix well and store at room temperature. Prepare de-staining solution by mixing 15% v/v methanol and glacial acetic acid each in distilled water - mix well and store at room temperature.

6.5.2 Generation of standard curve

1. Plate 0, 5000, 10000, 20000, 40000, 80000 cells per well identically into two 12-well plates. Incubate at 37°C and 5% CO_2 for cells to settle down (12-48 hours).
2. Confirm the healthy cell condition under the microscope and proceed as follows –
3. Plate 1 – trypsinize the cells using 50 µL EDTA-trypsin, neutralize reaction with 70 µL growth medium and count using cell counter.
4. Plate 2 – Fix the cells by incubating with ice cold methanol:acetone (1:1) fixative for 3-5 minutes on ice. Wash the fixed cells with PBS and stain with 0.5% crystal violet at room temperature for 2-3 hours followed by washing with PBS and air dry. Add 120 µL de-staining

solution and mix well. Take 100 µL solution and load into a 96-well plate. Measure optical density at 570 nm using a spectrophotometer.

5. Plot a scatter graph of the optical density from plate 2 against the cell number from plate 1. Find out the "$y = mx + c$", where 'c' is the y-intercept and 'm' is the slope.

6.5.3 QCV assay protocol

1. Plate 100 cells per well in a 12-well plate. Incubate at 37°C and 5% CO_2 for cells to settle down.
2. Treat the cells in appropriate conditions in plates and incubate for appropriate time.
3. Fix the cells and stain with 0.5% crystal violet at room temperature for 2-3 hours.
4. Wash the plate and let it air dry.
5. Take cell pictures (for Cell morphology observation).
6. Scan the cell plate and manually count the number of colonies (colony formation assay).
7. Add 120 µL de-staining solution and mix well. Take 100 µL solution and load into a 96 well plate. Measure optical density using a spectrophotometer at wavelength 570 nm. Use the equation {*cell number = (OD – c)/m*} to find out the number of cells (= long-term treatment cytotoxicity / cell viability).

6.5.4 General considerations

Calibration of instruments and technique is recommended prior to operation. The incubation time for cell adherence, cytotoxicity and population doubling should be standardized for best outcomes. Troubleshooting guide is tabulated in Fig. 50.

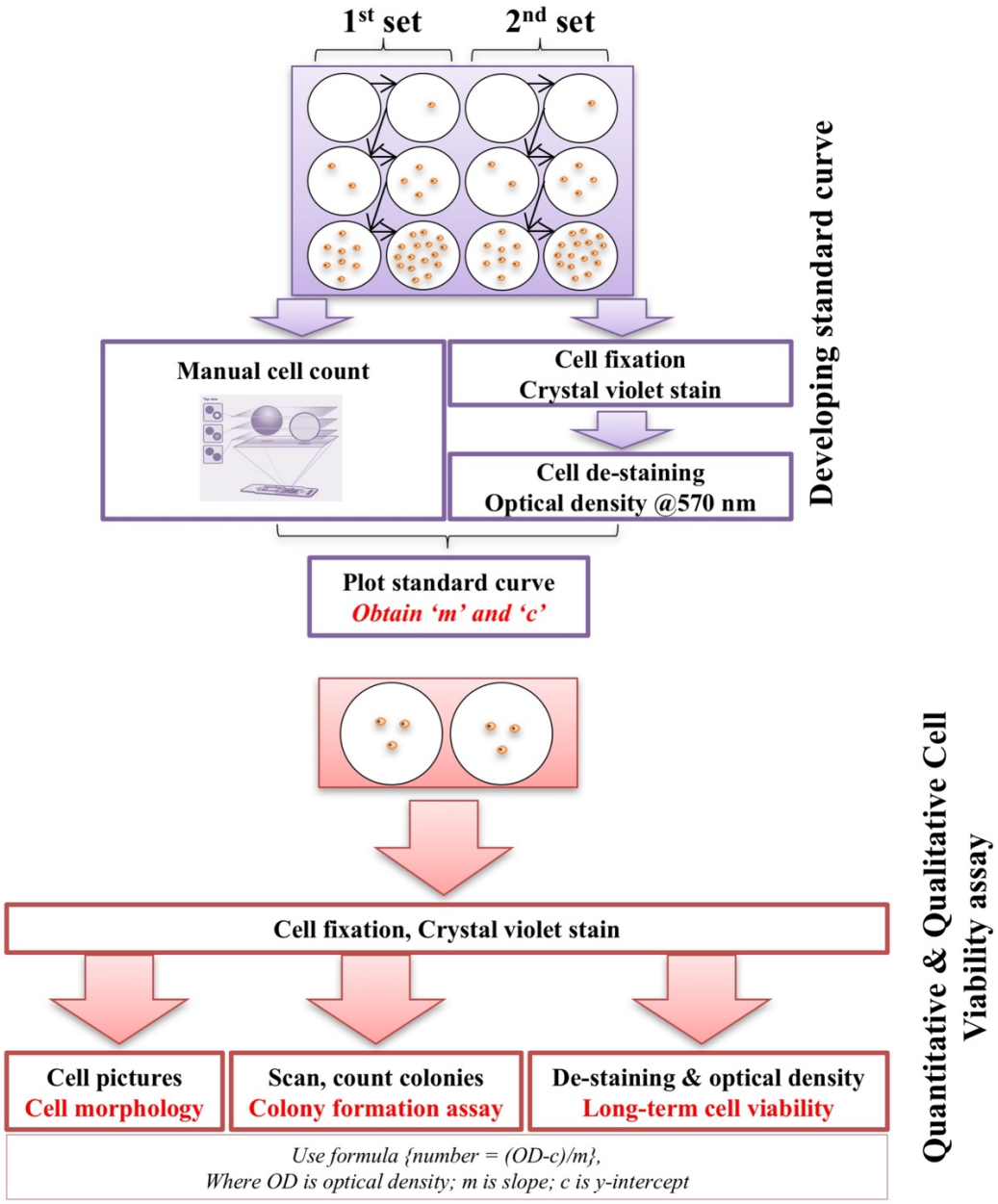

Fig. 41. Schematic presentation of the protocol: Top - Determination of standard curve and slope equation; bottom - QCV assay to determine cell viability, colony forming potential and cell morphology after long-term culture of cells.

Garg et al. 2018 BMC Research Notes 11(1): 403

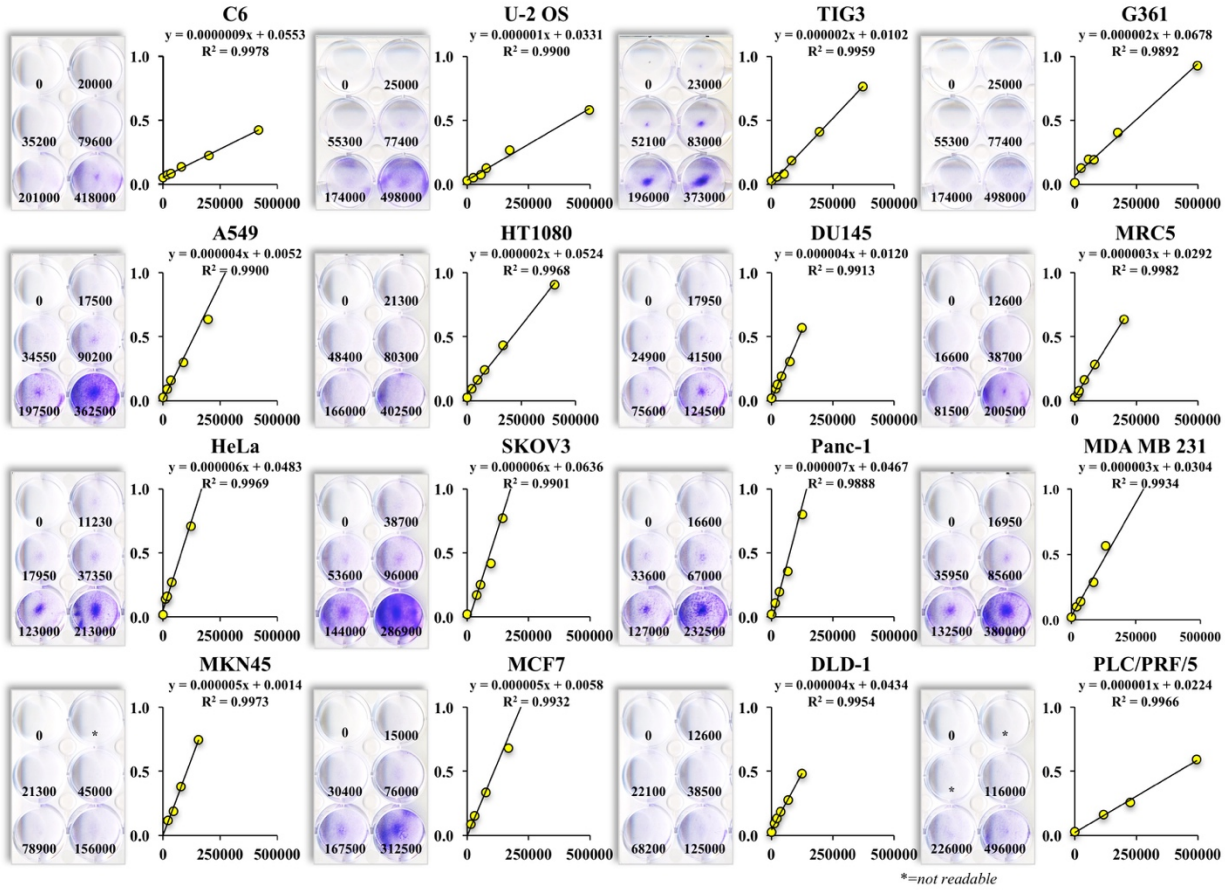

Fig. 42. QCV standardization and determination of slope/y-intercept and R^2 value in 16 cancer cell lines.

Garg et al. 2018 BMC Research Notes 11(1): 403

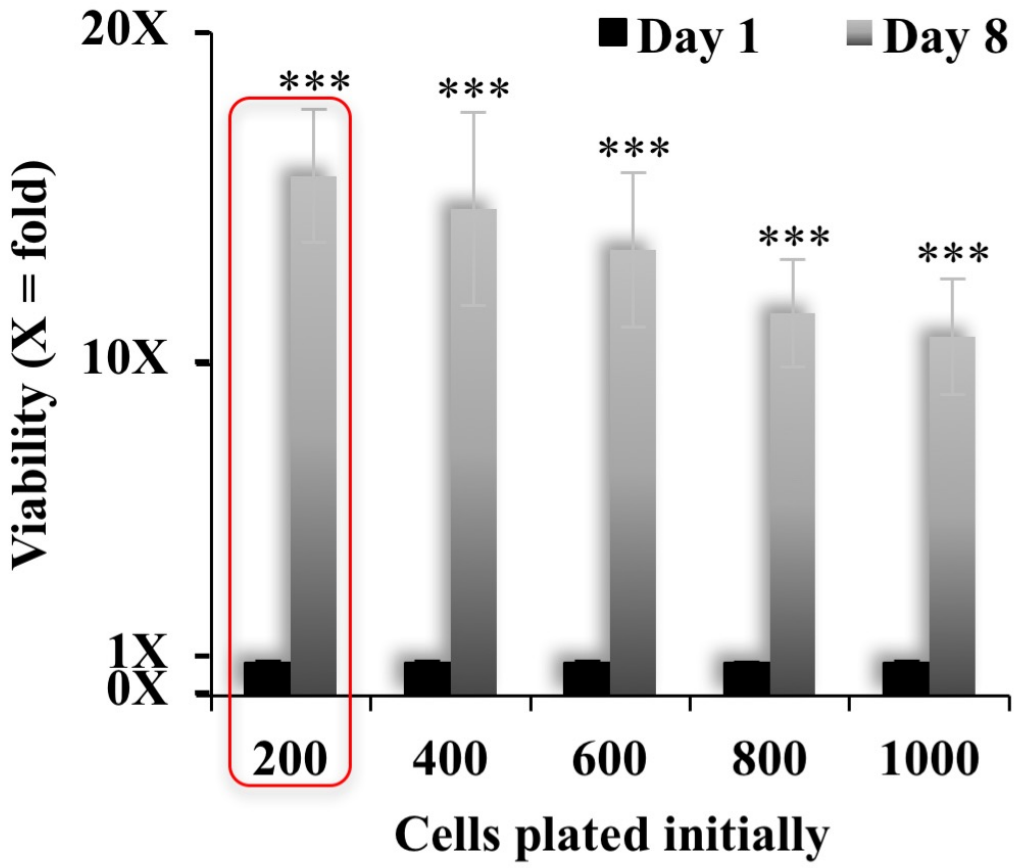

Fig. 43. Interference of cell number and color of the test reagent in the cytotoxicity assays using conventional MTT assay - Cell viability after 8 days of culture in a 96-well plate well.

Garg et al. 2018 BMC Research Notes 11(1): 403

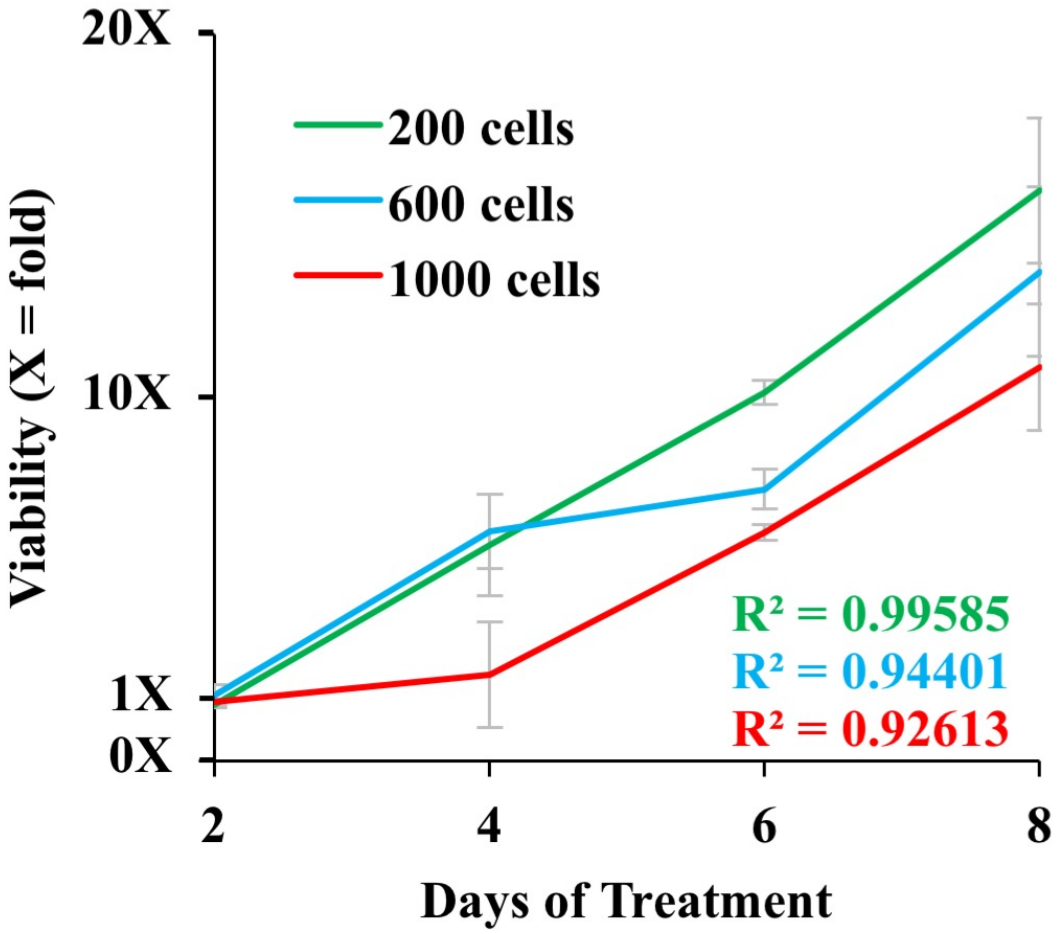

Fig. 44. Interference of cell number and color of the test reagent in the cytotoxicity assays using conventional MTT assay - Cell growth pattern over 8 days in a 96-well plate.

Garg et al. 2018 BMC Research Notes 11(1): 403

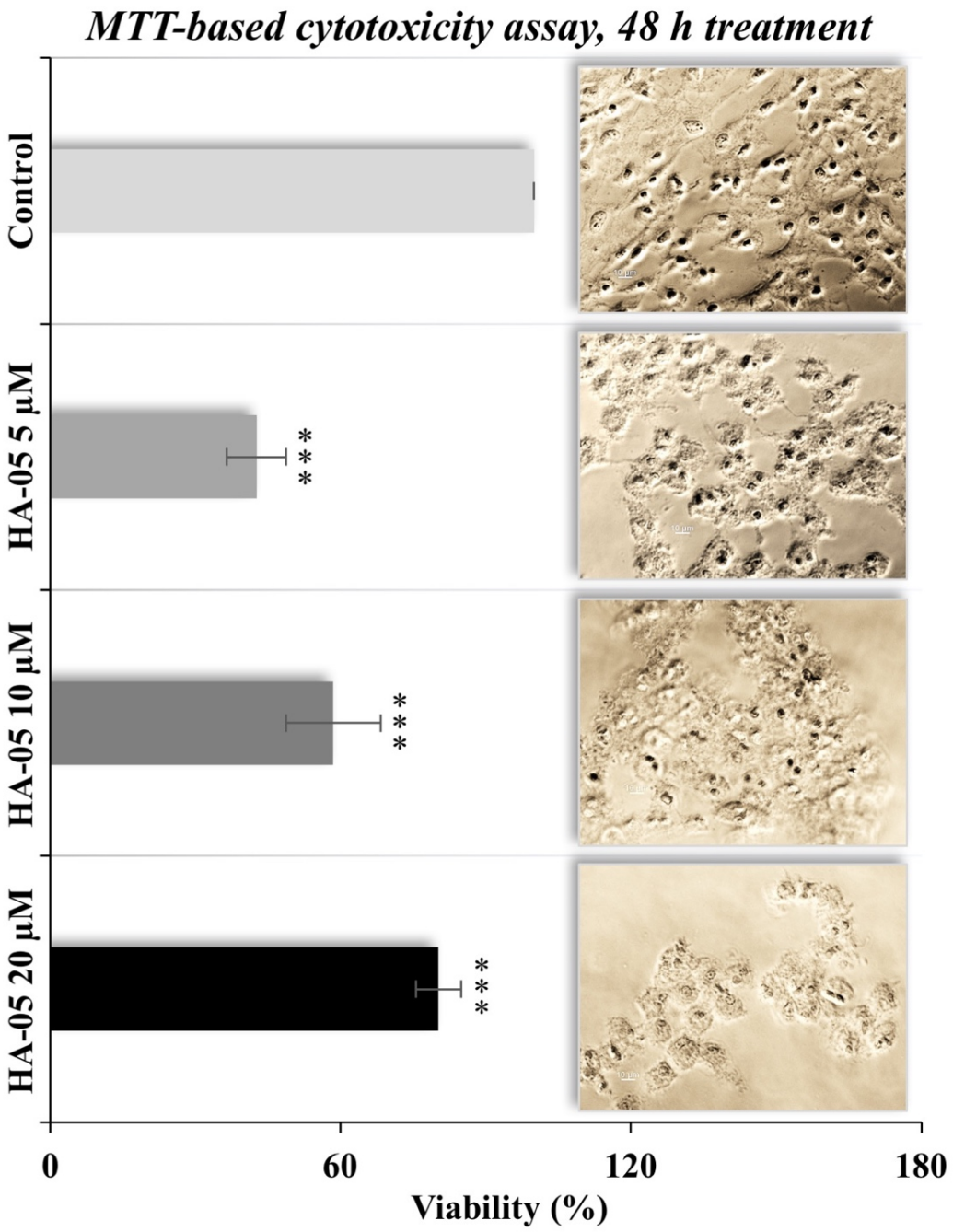

Fig. 45. Interference of cell number and color of the test reagent in the cytotoxicity assays using conventional MTT assay - Cell viability after 48 hours treatment with colored extract HA-05 (left) and cell pictures (right) against control.

Garg et al. 2018 BMC Research Notes 11(1): 403

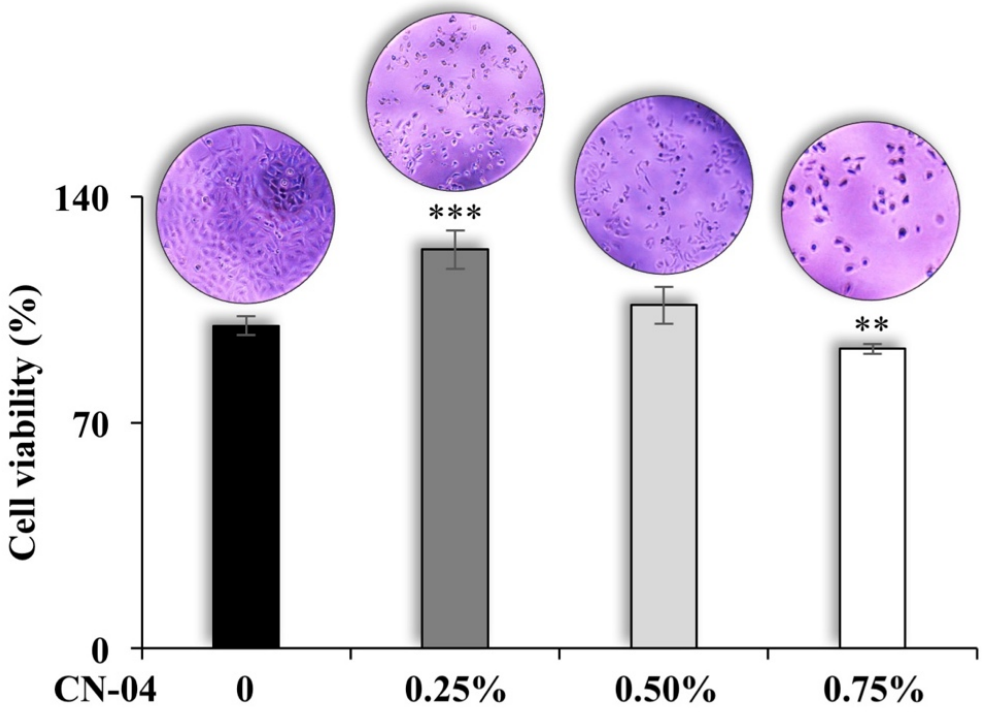

Fig. 46. Determination of cytotoxicity of a colored reagent by conventional MTT assays and institution of QCV assay - Viability of cells treated with the reagent for 48h showed haphazard pattern, while the cell pictures showed dose-dependent cytotoxicity.

Garg et al. 2018 BMC Research Notes 11(1): 403

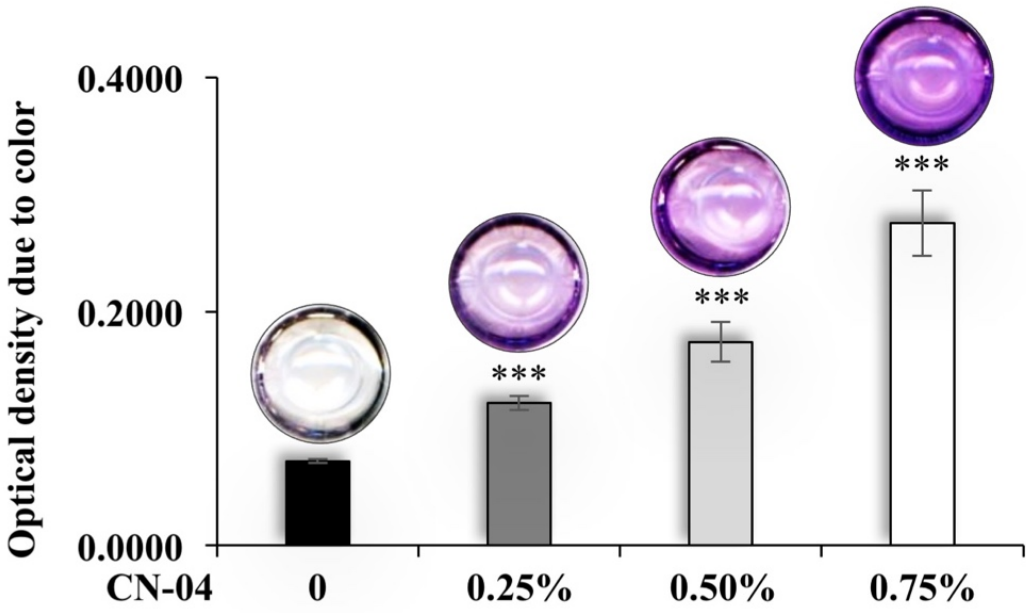

Fig. 47. Determination of cytotoxicity of a colored reagent by conventional MTT assays and institution of QCV assay - Dose-dependent increase in optical density was observed as a result of color of the reagent.

Garg et al. 2018 BMC Research Notes 11(1): 403

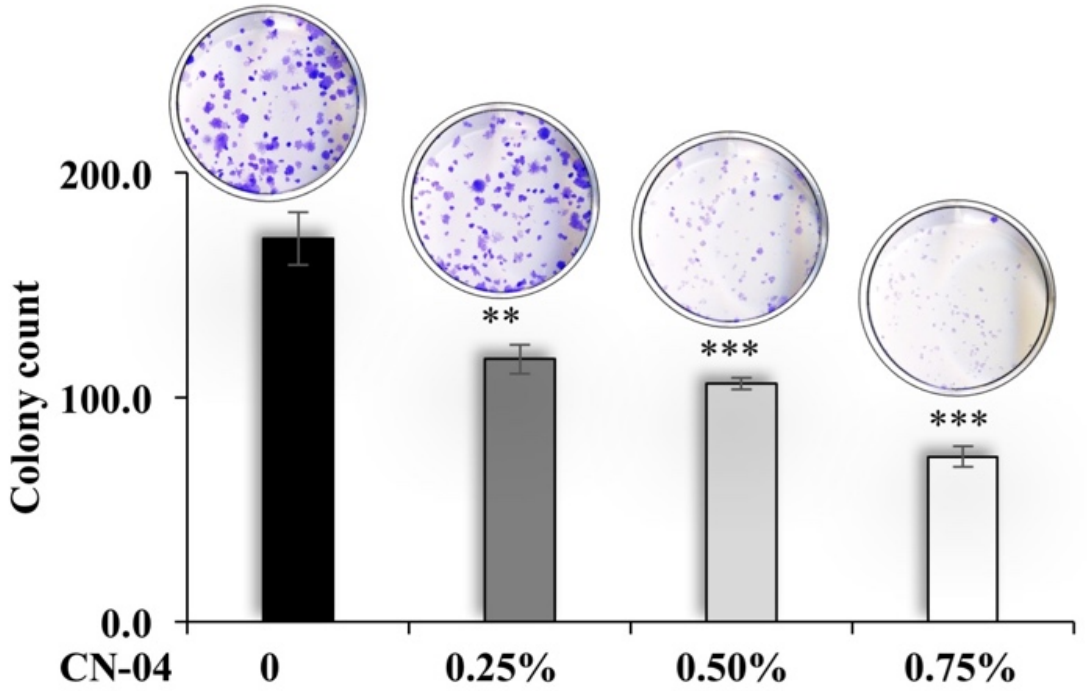

Fig. 48. Determination of cytotoxicity of a colored reagent by conventional MTT assays and institution of QCV assay - Colony number determined by dissolving crystal violet stain, and the morphology of the cells correlated with each other proportionately.

Garg et al. 2018 BMC Research Notes 11(1): 403

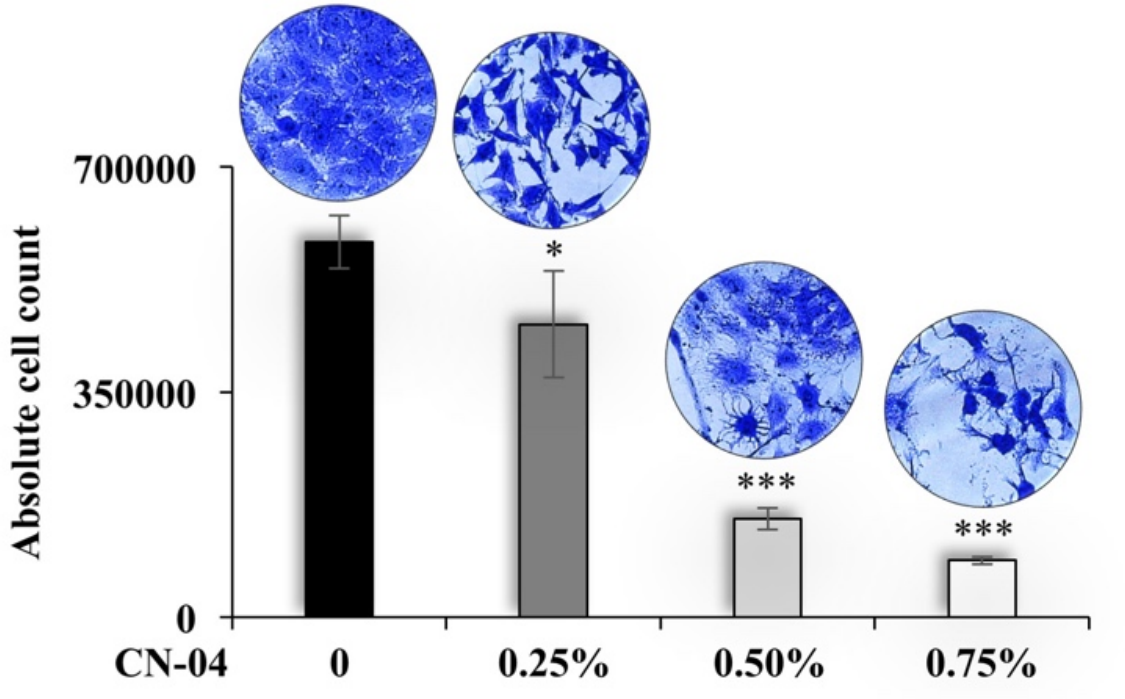

Fig. 49. Determination of cytotoxicity of a colored reagent by conventional MTT assays and institution of QCV assay - Quantitative cell number determined by dissolving crystal violet stain, and the morphology of the cells correlated with each other proportionately.

Garg et al. 2018 BMC Research Notes 11(1): 403

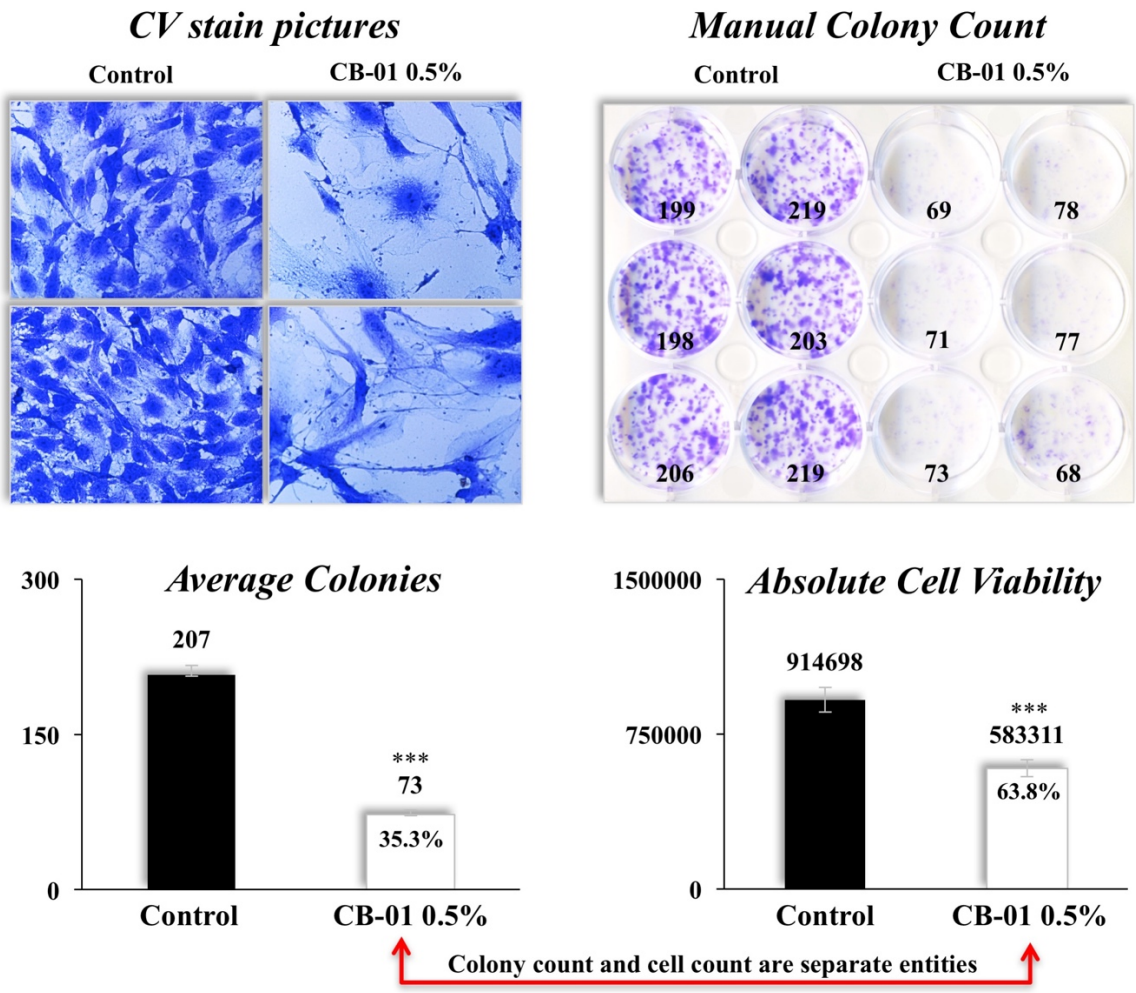

Fig. 50. Validation of QCV Assay: Crystal violet stained cell pictures at the end of 8 days treatment are shown (top left); manually counted cell colonies in six variants of control and treated wells (top right); quantified colony number (bottom left); quantified absolute cell count by dissolving crystal violet in de-staining solution and using slope equation for C6 cells (bottom right).

Garg et al. 2018 BMC Research Notes 11(1): 403

Troubleshooting Guide

Problem	Possible cause	Recommendation
Unexpected cell number in manual count	Cell contamination	Check the cell condition under the microscope before cell detachment. Do only one saline wash before applying the cell detachment reagent. Apply all reagents on to the wall of the wells.
	Inadequate cell detachment	Give adequate time to the cells for detachment. Incubate the cells in the 37˚C and 5% CO_2 incubator while cell detachment.
	Congested cell counting slide	Use a new or a clean cell counting slide.
Undetectable cell number reading in manual count	Too diluted cells for the cell counting chamber	Ensure that the cell count is as high as possible. Concentrate the suspension by adding minimum cell detachment solution and culture media.
Cell colonies uncountable	Cell colonies are too large	Plate less cells. Fix cells before colonies fuse with each other
R^2-value less than 98%	Positive interference in optical density due to plate negative control	Subtract negative control from the optical density.
	CV stain wash-off	Wash cells gently along the walls of the plate
	Pipetting error	Consider more replicates

Fig. 51. Troubleshooting guide for QCV assay.

Garg et al. 2018 BMC Research Notes 11(1): 403

Chapter 7

Conclusions

Stress is a pathological response of living tissue to an external stimulus. These stimuli can range from chemicals, radiations and hormones to genetic conditions. In an attempt to fight the stressors, the living tissue may sometimes undergo a physiological or pathological change, which may develop into a disease. These changes may be acute, chronic, or even permanent. Many stress related phenomena have been identified –early aging, cancer, neuro-degeneration, melanogenesis, inflammation, etc. These warrant continual interventions and updating. Considerable progress has been made in gene-targeted therapeutic approaches in the last few decades. However, undesired toxicity of synthetic drugs, drug resistance, spread of disease and recurrence pose serious hurdle to its treatment and prognosis.

Several studies have indicated that stress is tightly connected to carcinogenesis. Cancer is a complex disease, most consistently defined as uncontrolled and indefinite proliferation of cells. Customary treatments include surgery, radio- and chemo-therapies involving removal or killing of cancer cells, respectively. Cancer represents a highly stressed physiological state in which the cells escape the stress-signaling mediated growth arrest. Natural compounds have recently attracted attention due to their safety and economic aspects. We screened some natural purified compounds for anti-stress and anti-cancer potential. We anticipated that in addition to their value for cancer therapy, these may also possess cancer-preventive potentials. The later constitutes a highly prioritized field of research in the current scenario of (i) increasing levels of stress due to high use of chemicals in our daily living and (ii) increasing old age societies world-wide. We identified candidate compounds that showed enhanced cytotoxicity to the cancer cells, such as the combination of Cucurbitacin B and Withanone and tamarind seed extracts. In the process of initial screening, we encountered the discrepancies and the results, and later found that this was due to the color of the compounds/extracts we used.

In the first route of exploration, we invented, developed, verified and proposed a technique as an upgrade from the conventional chromogen-related methods – quantitative and qualitative cell viability assay (QCV assay). Often the herbal extracts and the purified active components possess color that interferes with such quantitative cytotoxicity estimation. Furthermore, their action is rather slow/gradual and requires long term assays such as effect on clonogenic potential of cells in 1-2 weeks, which cannot be performed in 96-well plate and hence the quantitative assessments are fairly difficult. At the same time, the visual observations of cell morphology hold significant hints to molecular signaling underlining the effect of drugs. Our broad-spectrum QCV assay has the capacity to present the long-term cytotoxicity results along with clonogenicity and morphological assessment of the cells.

In second path, we screened tamarind seed extracts and found their potential as potent anti-melanogenesis medicine (details not shown). We obtained tamarind seed extracts by 95% ethanol and water extraction. In cell based assays, we found that the extracts were safe for both cancer and normal cells (in the range of 0.01-1.0%, for at least 4 weeks). Consistently, molecular studies revealed no effect on the expression/activity of tumor suppressor proteins. We next recruited oxidative stress models; hydrogen peroxide (H_2O_2), ultraviolet radiation (UV) and diacylglycerol 1–oleoyl-2-acetyl-sn-glycerol (OAG) and investigated the anti-stress potential of the extracts and found that whereas the extracts did not offer any protection to stress caused by H_2O_2 or UV, they significantly compromised OAG induced melanogenesis.

Towards our final step, we developed a combination of Cucurbitacin B (from *Helicteres angustifolia, Chinese Ginseng*) and Withanone (from *Withania somnifera, Indian Ginseng*), and analyzed its anticancer potency, mechanism of action with particular focus to non-small-cell lung cancer. We performed cell culture assays including short-term and long-term viability, migration

and invasion assays. Molecular markers defining each of the phenotype were analyzed by Western blotting or immunocytostaining with specific antibodies. We found that 1:500 molar ratio combination (called CucWi-N) of Cucurbitacin B and Withanone possessed potent anticancer activity as compared to each of the compounds. *In silico* analysis revealed that Cucurbitacin B abrogates mortain-p53 interactions resulting in activation of tumor suppressor activity of p53. At sub-toxic dose Cucurbitacin B showed synergistic affinity with Withanone to target hnRNP-K protein (necessary for cancer cell migration). In *in vitro* analysis, we found that whereas Cucurbitacin B alone was more cytotoxic to the normal cells, its combination with Withanone significantly and dose-dependently caused changes at cellular and protein level indicating inhibition of stemness and aggressiveness of the cancer cells and induction of replicative senescence. Due to the selectivity of the drugs, at a dose safe to use for the normal cells, the combination via inhibition of mortalin and hnRNP-K combination caused DNA damage and inhibited lamin A/C. This stimulated DNA repair mechanism with higher expression of lamin-A/C and PARP 1, and resulted into gradual cellular senescence. In the senescent cells, the combination inhibited the repair mechanism by inhibited MRE-Rad50-NBS1 complex. Finally, it also inhibited a number of stem-cell, migratory and invasiveness markers to be called as a potent anti-metastatic cancer formulation. We sincerely believe that the CucWi-N is a potential anticancer drug that warrants further mechanistic and clinical studies, and has been so far a significant contribution to science.

References

1. Massague, J. and A.C. Obenauf, *Metastatic colonization by circulating tumour cells.* Nature, 2016. **529**(7586): p. 298-306.
2. Organization, W.H., *World Cancer Factsheet*, in http://gicr.iarc.fr/public/docs/20120906-WorldCancerFactSheet.pdf, I.A.f.R.o. Cancer, Editor. 2012, Cancer Research UK: UK.
3. Cheung, E.C. and K.H. Vousden, *The role of p53 in glucose metabolism.* Curr Opin Cell Biol, 2010. **22**(2): p. 186-91.
4. Engelmann, D. and B.M. Putzer, *Emerging from the shade of p53 mutants: N-terminally truncated variants of the p53 family in EMT signaling and cancer progression.* Sci Signal, 2014. **7**(345): p. re9.
5. Hengartner, M.O., *The biochemistry of apoptosis.* Nature, 2000. **407**(6805): p. 770-6.
6. Sharpless, N.E. and R.A. DePinho, *p53: good cop/bad cop.* Cell, 2002. **110**(1): p. 9-12.
7. Sherr, C.J. and F. McCormick, *The RB and p53 pathways in cancer.* Cancer Cell, 2002. **2**(2): p. 103-12.
8. Korenjak, M. and A. Brehm, *E2F-Rb complexes regulating transcription of genes important for differentiation and development.* Curr Opin Genet Dev, 2005. **15**(5): p. 520-7.
9. Bates, S., et al., *p14ARF links the tumour suppressors RB and p53.* Nature, 1998. **395**(6698): p. 124-5.
10. Dakeng, S., et al., *Inhibition of Wnt signaling by cucurbitacin B in breast cancer cells: reduction of Wnt-associated proteins and reduced translocation of galectin-3-mediated beta-catenin to the nucleus.* J Cell Biochem, 2012. **113**(1): p. 49-60.

11. Borg, A.J., et al., *Decreased STAT3 in human idiopathic fetal growth restriction contributes to trophoblast dysfunction.* Reproduction, 2015. **149**(5): p. 523-32.

12. Hossain, D.M., et al., *TLR9-Targeted STAT3 Silencing Abrogates Immunosuppressive Activity of Myeloid-Derived Suppressor Cells from Prostate Cancer Patients.* Clin Cancer Res, 2015. **21**(16): p. 3771-82.

13. Liu, F., et al., *B7H3 promotes cell migration and invasion through the Jak2/Stat3/MMP9 signaling pathway in colorectal cancer.* Mol Med Rep, 2015. **12**(4): p. 5455-60.

14. Nefedova, Y. and D.I. Gabrilovich, *Targeting of Jak/STAT pathway in antigen presenting cells in cancer.* Curr Cancer Drug Targets, 2007. **7**(1): p. 71-7.

15. Peyser, N.D., et al., *Loss-of-Function PTPRD Mutations Lead to Increased STAT3 Activation and Sensitivity to STAT3 Inhibition in Head and Neck Cancer.* PLoS One, 2015. **10**(8): p. e0135750.

16. Thomas, S.J., et al., *The role of JAK/STAT signalling in the pathogenesis, prognosis and treatment of solid tumours.* Br J Cancer, 2015. **113**(3): p. 365-71.

17. Wen, W., et al., *Synergistic anti-tumor effect of combined inhibition of EGFR and JAK/STAT3 pathways in human ovarian cancer.* Mol Cancer, 2015. **14**: p. 100.

18. Yao, X., et al., *Cell Surface GRP78 Accelerated Breast Cancer Cell Proliferation and Migration by Activating STAT3.* PLoS One, 2015. **10**(5): p. e0125634.

19. Royds, J.A., et al., *Response of tumour cells to hypoxia: role of p53 and NFkB.* Mol Pathol, 1998. **51**(2): p. 55-61.

20. Xu, S., et al., *Differential regulation of mitogen-activated protein/ERK kinase (MEK)1 and MEK2 and activation by a Ras-independent mechanism.* Mol Endocrinol, 1997. **11**(11): p. 1618-25.

21. Pal, I. and M. Mandal, *PI3K and Akt as molecular targets for cancer therapy: current clinical outcomes.* Acta Pharmacol Sin, 2012. **33**(12): p. 1441-58.

22. Harley, C.B., *Aging of cultured human skin fibroblasts.* Methods Mol Biol, 1990. **5**: p. 25-32.

23. Hayflick, L., *The Limited in Vitro Lifetime of Human Diploid Cell Strains.* Exp Cell Res, 1965. **37**: p. 614-36.

24. Kimmelman, A.C. and E. White, *Autophagy and Tumor Metabolism.* Cell Metab, 2017. **25**(5): p. 1037-1043.

25. Kaefer, C.M. and J.A. Milner, *The role of herbs and spices in cancer prevention.* J Nutr Biochem, 2008. **19**(6): p. 347-61.

26. Chen, H.Y., et al., *Identifying chinese herbal medicine network for eczema: implications from a nationwide prescription database.* Evid Based Complement Alternat Med, 2015. **2015**: p. 347164.

27. Hu, X., D. Cheng, and Z. Zhang, *Antidiabetic activity of Helicteres angustifolia root.* Pharm Biol, 2016. **54**(6): p. 938-44.

28. Hung, Y.C., et al., *Adjuvant Chinese Herbal Products for Preventing Ischemic Stroke in Patients with Atrial Fibrillation.* PLoS One, 2016. **11**(7): p. e0159333.

29. Li, K., et al., *Functional Characterisation of Anticancer Activity in the Aqueous Extract of Helicteres angustifolia L. Roots.* PLoS One, 2016. **11**(3): p. e0152017.

30. Teschke, R., et al., *Herbal traditional Chinese medicine and its evidence base in gastrointestinal disorders.* World J Gastroenterol, 2015. **21**(15): p. 4466-90.

31. Chen, Z.T., S.W. Lee, and C.M. Chen, *Cucurbitacin B 2-sulfate and cucurbitacin glucosides from the root bark of Helicteres angustifolia.* Chem Pharm Bull (Tokyo), 2006. **54**(11): p. 1605-7.

32. Pan, M.H., et al., *Cytotoxic triterpenoids from the root bark of Helicteres angustifolia.* Chem Biodivers, 2008. **5**(4): p. 565-74.

33. Chen, W., et al., *Pregnane, coumarin and lupane derivatives and cytotoxic constituents from Helicteres angustifolia.* Phytochemistry, 2006. **67**(10): p. 1041-7.

34. Wang, G.C., et al., *Two pregnane derivatives and a quinolone alkaloid from Helicteres angustifolia.* Fitoterapia, 2012. **83**(8): p. 1643-7.

35. Sun, Y., et al., *Synergistic effect of cucurbitacin B in combination with curcumin via enhancing apoptosis induction and reversing multidrug resistance in human hepatoma cells.* Eur J Pharmacol, 2015. **768**: p. 28-40.

36. Tannin-Spitz, T., et al., *Growth inhibitory activity of cucurbitacin glucosides isolated from Citrullus colocynthis on human breast cancer cells.* Biochem Pharmacol, 2007. **73**(1): p. 56-67.

37. Liu, T., et al., *Inhibitory effects of cucurbitacin B on laryngeal squamous cell carcinoma.* Eur Arch Otorhinolaryngol, 2008. **265**(10): p. 1225-32.

38. Touihri-Barakati, I., et al., *Cucurbitacin B purified from Ecballium elaterium (L.) A. Rich from Tunisia inhibits alpha5beta1 integrin-mediated adhesion, migration, proliferation of human glioblastoma cell line and angiogenesis.* Eur J Pharmacol, 2017. **797**: p. 153-161.

39. Lee, D.H., et al., *Synergistic effect of low-dose cucurbitacin B and low-dose methotrexate for treatment of human osteosarcoma.* Cancer Lett, 2011. **306**(2): p. 161-170.

40. Kausar, H., et al., *Cucurbitacin B potently suppresses non-small-cell lung cancer growth: identification of intracellular thiols as critical targets.* Cancer Lett, 2013. **332**(1): p. 35-45.

41. Schwartz, G.K. and M.A. Shah, *Targeting the cell cycle: a new approach to cancer therapy.* J Clin Oncol, 2005. **23**(36): p. 9408-21.

42. Sreelatha, S., A. Jeyachitra, and P.R. Padma, *Antiproliferation and induction of apoptosis by Moringa oleifera leaf extract on human cancer cells.* Food Chem Toxicol, 2011. **49**(6): p. 1270-5.

43. Widodo, N., et al., *Selective killing of cancer cells by leaf extract of Ashwagandha: identification of a tumor-inhibitory factor and the first molecular insights to its effect.* Clin Cancer Res, 2007. **13**(7): p. 2298-306.

44. Widodo, N., et al., *Selective killing of cancer cells by leaf extract of Ashwagandha: components, activity and pathway analyses.* Cancer Lett, 2008. **262**(1): p. 37-47.

45. Ding, H., et al., *Selective induction of apoptosis of human oral cancer cell lines by avocado extracts via a ROS-mediated mechanism.* Nutr Cancer, 2009. **61**(3): p. 348-56.

46. Piccirillo, S., et al., *Redox mechanisms involved in the selective activation of Nrf2-mediated resistance versus p53-dependent apoptosis in adenocarcinoma cells.* J Biol Chem, 2009. **284**(40): p. 27721-33.

47. Widodo, N., et al., *Selective killing of cancer cells by Ashwagandha leaf extract and its component Withanone involves ROS signaling.* PLoS One, 2010. **5**(10): p. e13536.

48. Duangmano, S., et al., *Cucurbitacin B inhibits human breast cancer cell proliferation through disruption of microtubule polymerization and nucleophosmin/B23 translocation.* BMC Complement Altern Med, 2012. **12**: p. 185.

49. Duangmano, S., et al., *Cucurbitacin B Causes Increased Radiation Sensitivity of Human Breast Cancer Cells via G2/M Cell Cycle Arrest.* J Oncol, 2012. **2012**: p. 601682.

50. Kaushik, U., V. Aeri, and S.R. Mir, *Cucurbitacins - An insight into medicinal leads from nature.* Pharmacogn Rev, 2015. **9**(17): p. 12-8.

51. Sharpless, N.E., et al., *p16(INK4a) and p53 deficiency cooperate in tumorigenesis.* Cancer Res, 2002. **62**(10): p. 2761-5.

52. Alghasham, A.A., *Cucurbitacins - a promising target for cancer therapy.* Int J Health Sci (Qassim), 2013. **7**(1): p. 77-89.

53. Clericuzio, M., et al., *Cucurbitane triterpenoids from Leucopaxillus gentianeus.* J Nat Prod, 2004. **67**(11): p. 1823-8.

54. Chen, J.C., et al., *Cucurbitacins and cucurbitane glycosides: structures and biological activities.* Nat Prod Rep, 2005. **22**(3): p. 386-99.

55. Clericuzio, M., et al., *Cucurbitane triterpenes from the fruiting bodies and cultivated mycelia of Leucopaxillus gentianeus.* J Nat Prod, 2006. **69**(12): p. 1796-9.

56. Wiart, C., *The definition and significance of Cucurbitacin B a STAT3 inhibitors.* Cancer Lett, 2013. **328**(1): p. 188.

57. Dantas, I.N., et al., *Studies on the cytotoxicity of cucurbitacins isolated from Cayaponia racemosa (Cucurbitaceae).* Z Naturforsch C, 2006. **61**(9-10): p. 643-6.

58. Hatam, N.A.R.W., D. A.; Yousif, N. J., *Lipids and Sterols of Citrullus colocynthis.* International Journal of Crude Drug Research, 1990. **28**(3): p. 2.

59. Abou-Khalil, R., et al., *Interaction of cucurbitacins with human serum albumin: Thermodynamic characteristics and influence on the binding of site specific ligands.* J Photochem Photobiol B, 2009. **95**(3): p. 189-95.

60. Oberlies, N.H., et al., *Bioactive constituents of the roots of Licania intrapetiolaris.* J Nat Prod, 2001. **64**(4): p. 497-501.

61. Beutler, J.A., et al., *Novel cytotoxic diterpenes from Casearia arborea.* J Nat Prod, 2000. **63**(5): p. 657-61.

62. Ayyad, S.E., et al., *Cucurbitacins-type triterpene with potent activity on mouse embryonic fibroblast from Cucumis prophetarum, cucurbitaceae.* Pharmacognosy Res, 2011. **3**(3): p. 189-93.

63. Chen, C., et al., *Cucurbitane-type triterpenoids from the stems of Cucumis melo.* J Nat Prod, 2009. **72**(5): p. 824-9.

64. Dat, N.T., et al., *An isoaurone and other constituents from Trichosanthes kirilowii seeds inhibit hypoxia-inducible factor-1 and nuclear factor-kappaB.* J Nat Prod, 2010. **73**(6): p. 1167-9.

65. Wu, K.J., et al., *Direct activation of TERT transcription by c-MYC.* Nat Genet, 1999. **21**(2): p. 220-4.

66. Yesilada, E., et al., *Isolation of an anti-inflammatory principle from the fruit juice of Ecballium elaterium.* J Nat Prod, 1988. **51**(3): p. 504-8.

67. Rawat, I.S., D.; Goel, H. C., *Antioxidant and anti-inflammatory potential of some dietary cucurbits.* Oxid Antioxid Med Sci, 2014. **3**(1): p. 8.

68. Schabort, J.C. and D.J. Potgieter, *A thin-layer and an improved paper-chromatographic method for the separation of cucurbitacin B. and 23, 24-dihydrocucurbitacin B.* J Chromatogr, 1967. **31**(1): p. 235-7.

69. Wakimoto, N., et al., *Cucurbitacin B has a potent antiproliferative effect on breast cancer cells in vitro and in vivo.* Cancer Sci, 2008. **99**(9): p. 1793-7.

70. Duangmano, S., et al., *Antiproliferative effects of cucurbitacin B in breast cancer cells: down-regulation of the c-Myc/hTERT/telomerase pathway and obstruction of the cell cycle.* Int J Mol Sci, 2010. **11**(12): p. 5323-38.

71. Wu, P.L., et al., *Cytotoxic and anti-HIV principles from the rhizomes of Begonia nantoensis.* Chem Pharm Bull (Tokyo), 2004. **52**(3): p. 345-9.

72. Promkan, M., et al., *The effectiveness of cucurbitacin B in BRCA1 defective breast cancer cells.* PLoS One, 2013. **8**(2): p. e55732.

73. Boone, J.J., et al., *Involvement of the HER2 pathway in repair of DNA damage produced by chemotherapeutic agents.* Mol Cancer Ther, 2009. **8**(11): p. 3015-23.

74. Friedrichs, K., et al., *High expression level of alpha 6 integrin in human breast carcinoma is correlated with reduced survival.* Cancer Res, 1995. **55**(4): p. 901-6.

75. Jones, J.L., et al., *Modulation of myoepithelial-associated alpha6beta4 integrin in a breast cancer cell line alters invasive potential.* Exp Cell Res, 1997. **235**(2): p. 325-33.

76. Desgrosellier, J.S. and D.A. Cheresh, *Integrins in cancer: biological implications and therapeutic opportunities.* Nat Rev Cancer, 2010. **10**(1): p. 9-22.

77. Gupta, P. and S.K. Srivastava, *HER2 mediated de novo production of TGFbeta leads to SNAIL driven epithelial-to-mesenchymal transition and metastasis of breast cancer.* Mol Oncol, 2014. **8**(8): p. 1532-47.

78. Gupta, P. and S.K. Srivastava, *Inhibition of Integrin-HER2 signaling by Cucurbitacin B leads to in vitro and in vivo breast tumor growth suppression.* Oncotarget, 2014. **5**(7): p. 1812-28.

79. de Herreros, A.G., et al., *Snail family regulation and epithelial mesenchymal transitions in breast cancer progression.* J Mammary Gland Biol Neoplasia, 2010. **15**(2): p. 135-47.

80. Ren, G., et al., *Cucurbitacin B induces DNA damage and autophagy mediated by reactive oxygen species (ROS) in MCF-7 breast cancer cells.* J Nat Med, 2015. **69**(4): p. 522-30.

81. Sinha, S., et al., *Cucurbitacin B inhibits breast cancer metastasis and angiogenesis through VEGF-mediated suppression of FAK/MMP-9 signaling axis.* Int J Biochem Cell Biol, 2016. **77**(Pt A): p. 41-56.

82. Lang, K.L., et al., *Synthesis and cytotoxic activity evaluation of dihydrocucurbitacin B and cucurbitacin B derivatives.* Bioorg Med Chem, 2012. **20**(9): p. 3016-30.

83. Guo, J., et al., *Cucurbitacin B induced ATM-mediated DNA damage causes G2/M cell cycle arrest in a ROS-dependent manner.* PLoS One, 2014. **9**(2): p. e88140.

84. Zhang, M., et al., *Cucurbitacin B inhibits proliferation and induces apoptosis via STAT3 pathway inhibition in A549 lung cancer cells.* Mol Med Rep, 2014. **10**(6): p. 2905-11.

85. Shukla, S., et al., *Cucurbitacin B Alters the Expression of Tumor-Related Genes by Epigenetic Modifications in NSCLC and Inhibits NNK-Induced Lung Tumorigenesis.* Cancer Prev Res (Phila), 2015. **8**(6): p. 552-62.

86. Silva, I.T., et al., *Cytotoxic effects of natural and semisynthetic cucurbitacins on lung cancer cell line A549.* Invest New Drugs, 2016. **34**(2): p. 139-48.

87. Shukla, S., et al., *Cucurbitacin B inhibits the stemness and metastatic abilities of NSCLC via downregulation of canonical Wnt/beta-catenin signaling axis.* Sci Rep, 2016. **6**: p. 21860.

88. Zhang, Y., et al., *Cucurbitacin B induces rapid depletion of the G-actin pool through reactive oxygen species-dependent actin aggregation in melanoma cells.* Acta Biochim Biophys Sin (Shanghai), 2011. **43**(7): p. 556-67.

89. Bamburg, J.R. and B.W. Bernstein, *Roles of ADF/cofilin in actin polymerization and beyond.* F1000 Biol Rep, 2010. **2**: p. 62.

90. Wang, W., R. Eddy, and J. Condeelis, *The cofilin pathway in breast cancer invasion and metastasis.* Nat Rev Cancer, 2007. **7**(6): p. 429-40.

91. Van Troys, M., et al., *Ins and outs of ADF/cofilin activity and regulation.* Eur J Cell Biol, 2008. **87**(8-9): p. 649-67.

92. Bamburg, J.R., et al., *ADF/Cofilin-actin rods in neurodegenerative diseases.* Curr Alzheimer Res, 2010. **7**(3): p. 241-50.

93. Zhang, Y.T., et al., *Formation of cofilin-actin rods following cucurbitacin-B-induced actin aggregation depends on Slingshot homolog 1-mediated cofilin hyperactivation.* J Cell Biochem, 2013. **114**(10): p. 2415-29.

94. Trichet, L., C. Sykes, and J. Plastino, *Relaxing the actin cytoskeleton for adhesion and movement with Ena/VASP.* J Cell Biol, 2008. **181**(1): p. 19-25.

95. Zhang, Y.T., et al., *VASP activation via the Galpha13/RhoA/PKA pathway mediates cucurbitacin-B-induced actin aggregation and cofilin-actin rod formation.* PLoS One, 2014. **9**(4): p. e93547.

96. Yin, D., et al., *Cucurbitacin B markedly inhibits growth and rapidly affects the cytoskeleton in glioblastoma multiforme.* Int J Cancer, 2008. **123**(6): p. 1364-75.

97. Zheng, Q., et al., *Cucurbitacin B inhibits growth and induces apoptosis through the JAK2/STAT3 and MAPK pathways in SHSY5Y human neuroblastoma cells.* Mol Med Rep, 2014. **10**(1): p. 89-94.

98. Shang, Y., et al., *Cucurbitacin-B inhibits neuroblastoma cell proliferation through up-regulation of PTEN.* Eur Rev Med Pharmacol Sci, 2014. **18**(21): p. 3297-303.

99. Chan, K.T., et al., *Cucurbitacin B induces apoptosis and S phase cell cycle arrest in BEL-7402 human hepatocellular carcinoma cells and is effective via oral administration.* Cancer Lett, 2010. **294**(1): p. 118-24.

100. Niu, Y., et al., *PTEN Activation by DNA Damage Induces Protective Autophagy in Response to Cucurbitacin B in Hepatocellular Carcinoma Cells.* Oxid Med Cell Longev, 2016. **2016**: p. 4313204.

101. Zhu, J.S., Ouyang, D. Y., Shi, Z. J., Xu, L. H., Zhang, Y. T., He, X. H., *Cucurbitacin B induced cell cycle arrest, apoptosis and autophagy associated with G actin reduction and persistent activation of cofilin in Jurkat cells.* Pharmacology, 2012. **89**: p. 348-356.

102. Chan, K.T., et al., *Cucurbitacin B inhibits STAT3 and the Raf/MEK/ERK pathway in leukemia cell line K562.* Cancer Lett, 2010. **289**(1): p. 46-52.

103. Gao, Y., et al., *Inactivation of ATP citrate lyase by Cucurbitacin B: A bioactive compound from cucumber, inhibits prostate cancer growth.* Cancer Lett, 2014. **349**(1): p. 15-25.

104. Zaidi, N., J.V. Swinnen, and K. Smans, *ATP-citrate lyase: a key player in cancer metabolism.* Cancer Res, 2012. **72**(15): p. 3709-14.

105. Zaytseva, Y.Y., et al., *Inhibition of fatty acid synthase attenuates CD44-associated signaling and reduces metastasis in colorectal cancer.* Cancer Res, 2012. **72**(6): p. 1504-17.

106. Liu, T., et al., *Cucurbitacin B, a small molecule inhibitor of the Stat3 signaling pathway, enhances the chemosensitivity of laryngeal squamous cell carcinoma cells to cisplatin.* Eur J Pharmacol, 2010. **641**(1): p. 15-22.

107. Liu, T., et al., *Combined antitumor activity of cucurbitacin B and docetaxel in laryngeal cancer.* Eur J Pharmacol, 2008. **587**(1-3): p. 78-84.

108. Xie, Y.L., et al., *Anticancer effect of cucurbitacin B on MKN-45 cells via inhibition of the JAK2/STAT3 signaling pathway.* Exp Ther Med, 2016. **12**(4): p. 2709-2715.

109. Liu, X., et al., *Cucurbitacin B induces autophagy and apoptosis by suppressing CIP2A/PP2A/mTORC1 signaling axis in human cisplatin resistant gastric cancer cells.* Oncol Rep, 2017. **38**(1): p. 271-278.

110. Zhang, Z.R., M.X. Gao, and K. Yang, *Cucurbitacin B inhibits cell proliferation and induces apoptosis in human osteosarcoma cells via modulation of the JAK2/STAT3 and MAPK pathways.* Exp Ther Med, 2017. **14**(1): p. 805-812.

111. Qu, Y., et al., *Inhibition of paclitaxel resistance and apoptosis induction by cucurbitacin B in ovarian carcinoma cells.* Oncol Lett, 2017. **14**(1): p. 145-152.

112. Ma, J., et al., *Cucurbitacin B inhibits the translational expression of hypoxia-inducible factor-1alpha.* Eur J Pharmacol, 2014. **723**: p. 46-54.

113. Wang, X., et al., *Cucurbitacins: elucidation of their interactions with the cytoskeleton.* PeerJ, 2017. **5**: p. e3357.

114. Zhang, T., et al., *Cucurbitacin induces autophagy through mitochondrial ROS production which counteracts to limit caspase-dependent apoptosis.* Autophagy, 2012. **8**(4): p. 559-76.

115. Marostica, L.L., et al., *Synergistic Antiproliferative Effects of a New Cucurbitacin B Derivative and Chemotherapy Drugs on Lung Cancer Cell Line A549.* Chem Res Toxicol, 2015. **28**(10): p. 1949-60.

116. Silva, I.T., et al., *In vitro and in vivo antitumor activity of a novel semisynthetic derivative of cucurbitacin B.* PLoS One, 2015. **10**(2): p. e0117794.

117. Chen, W., et al., *Cucurbitacin B inhibits growth, arrests the cell cycle, and potentiates antiproliferative efficacy of cisplatin in cutaneous squamous cell carcinoma cell lines.* Int J Oncol, 2010. **37**(3): p. 737-43.

118. Marostica, L.L., et al., *Antitumor effectiveness of a combined therapy with a new cucurbitacin B derivative and paclitaxel on a human lung cancer xenograft model.* Toxicol Appl Pharmacol, 2017. **329**: p. 272-281.

119. Aribi, A., et al., *The triterpenoid cucurbitacin B augments the antiproliferative activity of chemotherapy in human breast cancer.* Int J Cancer, 2013. **132**(12): p. 2730-7.

120. Thoennissen, N.H., et al., *Cucurbitacin B induces apoptosis by inhibition of the JAK/STAT pathway and potentiates antiproliferative effects of gemcitabine on pancreatic cancer cells.* Cancer Res, 2009. **69**(14): p. 5876-84.

121. Iwanski, G.B., et al., *Cucurbitacin B, a novel in vivo potentiator of gemcitabine with low toxicity in the treatment of pancreatic cancer.* Br J Pharmacol, 2010. **160**(4): p. 998-1007.

122. Yar Saglam, A.S., et al., *Treatment with cucurbitacin B alone and in combination with gefitinib induces cell cycle inhibition and apoptosis via EGFR and JAK/STAT pathway in human colorectal cancer cell lines.* Hum Exp Toxicol, 2016. **35**(5): p. 526-43.

123. Tacar, O., P. Sriamornsak, and C.R. Dass, *Doxorubicin: an update on anticancer molecular action, toxicity and novel drug delivery systems.* J Pharm Pharmacol, 2013. **65**(2): p. 157-70.

124. Zhang, Z., et al., *The survivin suppressant YM155 reverses doxorubicin resistance in osteosarcoma.* Int J Clin Exp Med, 2015. **8**(10): p. 18032-40.

125. Kim, S.H., et al., *Doxorubicin has a synergistic cytotoxicity with cucurbitacin B in anaplastic thyroid carcinoma cells.* Tumour Biol, 2017. **39**(2): p. 1010428317692252.

126. Yang, T., et al., *Cucurbitacin B exerts anti-cancer activities in human multiple myeloma cells in vitro and in vivo by modulating multiple cellular pathways.* Oncotarget, 2017. **8**(4): p. 5800-5813.

127. Di Gennaro, E., et al., *Modulation of thymidilate synthase and p53 expression by HDAC inhibitor vorinostat resulted in synergistic antitumor effect in combination with 5FU or raltitrexed.* Cancer Biol Ther, 2009. **8**(9): p. 782-91.

128. Ouyang, D., et al., *Histone deacetylase inhibitor valproic acid sensitizes B16F10 melanoma cells to cucurbitacin B treatment.* Acta Biochim Biophys Sin (Shanghai), 2011. **43**(6): p. 487-95.

129. Cerny, D., et al., *Hepatoprotective effect of curcumin in lipopolysaccharide/-galactosamine model of liver injury in rats: relationship to HO-1/CO antioxidant system.* Fitoterapia, 2011. **82**(5): p. 786-91.

130. Garcia-Nino, W.R. and J. Pedraza-Chaverri, *Protective effect of curcumin against heavy metals-induced liver damage.* Food Chem Toxicol, 2014. **69**: p. 182-201.

131. Lee, H.I., et al., *Low doses of curcumin protect alcohol-induced liver damage by modulation of the alcohol metabolic pathway, CYP2E1 and AMPK.* Life Sci, 2013. **93**(18-19): p. 693-9.

132. Aggarwal, B.B., A. Kumar, and A.C. Bharti, *Anticancer potential of curcumin: preclinical and clinical studies.* Anticancer Res, 2003. **23**(1A): p. 363-98.

133. Tannin-Spitz, T., M. Bergman, and S. Grossman, *Cucurbitacin glucosides: antioxidant and free-radical scavenging activities.* Biochem Biophys Res Commun, 2007. **364**(1): p. 181-6.

134. Smit, H.F., *Picrorhiza scrophulariiflora, from traditional use to immunomodulatory activity*, in *Faculty of Pharmacy*. 2000, University of Utrecht: Utrecht.

135. Jayaprakasam, B., N.P. Seeram, and M.G. Nair, *Anticancer and antiinflammatory activities of cucurbitacins from Cucurbita andreana.* Cancer Lett, 2003. **189**(1): p. 11-6.

136. Miro, M., *Cucurbitacins and their pharmacological effects.* Phytother Res, 1995. **9**: p. 159-168.

137. Xiao, Y., et al., *Cucurbitacin B Protects Against Pressure Overload Induced Cardiac Hypertrophy.* J Cell Biochem, 2017. **118**(11): p. 3899-3910.

138. Hua, S., et al., *Protective Effects of Cucurbitacin B on Acute Lung Injury Induced by Sepsis in Rats.* Med Sci Monit, 2017. **23**: p. 1355-1362.

139. El Naggar el, M.B., et al., *Hepatoprotective and proapoptotic effect of Ecballium elaterium on CCl4-induced hepatotoxicity in rats.* Asian Pac J Trop Med, 2015. **8**(7): p. 526-31.

140. Li, Z.J., et al., *Inhibitory effect of cucurbitacin B on imiquimod-induced skin inflammation.* Biochem Biophys Res Commun, 2015. **459**(4): p. 673-8.

141. Park, S.Y., Y.H. Kim, and G. Park, *Cucurbitacins attenuate microglial activation and protect from neuroinflammatory injury through Nrf2/ARE activation and STAT/NF-kappaB inhibition.* Neurosci Lett, 2015. **609**: p. 129-36.

142. Peters, R.R., M.R. Farias, and R.M. Ribeiro-do-Valle, *Anti-inflammatory and analgesic effects of cucurbitacins from Wilbrandia ebracteata.* Planta Med, 1997. **63**(6): p. 525-8.

143. Seo, C.R., et al., *Cucurbitacin B and cucurbitacin I suppress adipocyte differentiation through inhibition of STAT3 signaling.* Food Chem Toxicol, 2014. **64**: p. 217-24.

144. Hassan, S.T.S., Berchova-Bimova, K., Petras, J., Hassan, K. T. S., *Cucurbitacin B interacts synergistically with antibiotics against Staphylococcus aureus clinical isolates and exhibits antiviral activity against HSV-1.* S Afr J Bot, 2017. **108**: p. 90-94.

145. Duportets, L., et al., *Steroid hormone signaling is involved in the age-dependent behavioral response to sex pheromone in the adult male moth Agrotis ipsilon.* Gen Comp Endocrinol, 2013. **186**: p. 58-66.

146. Mezher, M., *The essential list of regulatory authorities in Asia. Regulatory Affairs Professional Society*. 2015.

147. David, A., Vallance, D. K., *Bitter principles of Cucurbitaceae.* J Pharm Pharmacol 1955. **7**: p. 295-296.

148. Organization, W.H., *WHO monograph on selected medicinal plants*. 2009, World Health Organization. p. 266.

149. Ferguson, J.E., D.C. Fischer, and R.L. Metcalf, *A report of Cucurbitacin poisonings in humans.* Cucurbit Genet Coop Rep, 1983. **6**: p. 73-74.

150. Association, T.G., *Health Safety Regulation – Substances that may be used in listed medicines in Australia*. 2011, Government of Australia. p. 86.

151. Le Men, J., Buffard, G., Provost, J., Tiberghien, R., Forgacs, P., Lagrange, E., Albert, O., Aurousseau, M., *Relations entre la structure de quelques cucurbitacines, leur toxicité et leur activité laxative.* Chimie Thérapeutique, 1969. **4**: p. 459-465.

152. Enslin, P.R., *Bitter principles of the Cucurbitaceae. I. - observations on the chemistry of Cucurbitacin A.* J Sci Food Agric 1954. **5**: p. 410-416.

153. Gry, J., Soborg, I., Anderson, H. C., *Identity, physical and chemical properties, analytical methods*. Cucurbitacins in plant food. 2006, Denmark: Ekspressen Tyrk & Kopicenter. 1.

154. Sezik, E., *Research on the Turkish medicinal plant Ecballium elaterium.* Chem Nat Comp, 1997. **33**: p. 541-542.

155. Steyn, D.G., *The toxicity of bitter-tasting cucurbitaceous vegetables (vegetable marrow, watermelons, etc.) for man.* S Afr Med J, 1950. **24**: p. 713-715.

156. Stoewsand, G.S., Jaworski, A., Shannon, S., Robinson, R. W., *Toxicologic response in mice fed Cucurbita fruit.* J Food Prot, 1985. **48**: p. 50-51.

157. Barri, M.E., et al., *Toxicity of five Sudanese plants to young ruminants.* J Comp Pathol, 1983. **93**(4): p. 559-75.

158. Bakhiet, A.O. and S.E. Adam, *An estimation of Citrullus colocynthis toxicity for chicks.* Vet Hum Toxicol, 1995. **37**(4): p. 356-8.

159. Pilegaard, K., Søborg, I., *Squash med bitter smag.* Nyt fra Levnedsmiddelstyrelsen, 1995: p. 1.

160. Rymal, K.S., Chambliss, O. L., Bond, M. D., Smith, D. A., *Squash containing toxic Cucurbitacin compounds occurring in California and Alabama.* J Food Prot, 1984. **47**: p. 270-271.

161. Raikhlin-Eisenkraft, B., Bentur, Y., *Ecballium elaterium (Squirting Cucumber) – remedy or poison?* Clin Toxicol, 2000. **38**: p. 305-308.

162. Jung, M.E. and R.M. Lui, *Studies toward the total syntheses of cucurbitacins B and D.* J Org Chem, 2010. **75**(21): p. 7146-58.

163. Razavilar, N. and P. Choi, *Molecular dynamics study of the diffusivity of a hydrophobic drug Cucurbitacin B in pseudo-poly(ethylene oxide-b-caprolactone) micelle environments.* Langmuir, 2014. **30**(26): p. 7798-803.

164. Toker, G., et al., *Callus formation and cucurbitacin B accumulation in Ecballium elaterium callus cultures.* Fitoterapia, 2003. **74**(7-8): p. 618-23.

165. Mei, J., et al., *A biotransformation process for the production of cucurbitacin B from its glycoside using a selected Streptomyces sp.* Bioprocess Biosyst Eng, 2016.

166. Lv, Q., et al., *Mucoadhesive buccal films containing phospholipid-bile salts-mixed micelles as an effective carrier for Cucurbitacin B delivery.* Drug Deliv, 2015. **22**(3): p. 351-8.

167. Molavi, O., et al., *Polymeric micelles for the solubilization and delivery of STAT3 inhibitor cucurbitacins in solid tumors.* Int J Pharm, 2008. **347**(1-2): p. 118-27.

168. Patel, S.K., A. Lavasanifar, and P. Choi, *Roles of nonpolar and polar intermolecular interactions in the improvement of the drug loading capacity of PEO-b-PCL with increasing PCL content for two hydrophobic Cucurbitacin drugs.* Biomacromolecules, 2009. **10**(9): p. 2584-91.

169. Cheng, L., et al., *Improve bile duct-targeted drug delivery and therapeutic efficacy for cholangiocarcinoma by cucurbitacin B loaded phospholipid complex modified with berberine hydrochloride.* Int J Pharm, 2015. **489**(1-2): p. 148-57.

170. Wang, W., et al., *Galactosylated solid lipid nanoparticles with cucurbitacin B improves the liver targetability.* Drug Deliv, 2010. **17**(3): p. 114-22.

171. You, L., et al., *The role of STAT3 in autophagy.* Autophagy, 2015. **11**(5): p. 729-39.

172. El-Senduny, F.F., et al., *Approach for chemosensitization of cisplatin-resistant ovarian cancer by cucurbitacin B.* Tumour Biol, 2016. **37**(1): p. 685-98.

173. Khajuria, R.K., et al., *Separation, identification, and quantification of selected withanolides in plant extracts of Withania somnifera by HPLC-UV(DAD)--positive ion electrospray ionisation-mass spectrometry.* J Sep Sci, 2004. **27**(7-8): p. 541-6.

174. PubChem, *Withanone*. 2017, National Center for Biotechnology Information.

175. Vaishnavi, K., et al., *Differential activities of the two closely related withanolides, Withaferin A and Withanone: bioinformatics and experimental evidences.* PLoS One, 2012. **7**(9): p. e44419.

176. Joshi, P., et al., *Epoxide group relationship with cytotoxicity in withanolide derivatives from Withania somnifera.* Steroids, 2014. **79**: p. 19-27.

177. Srivastava, S., et al., *Light and auxin responsive cytochrome P450s from Withania somnifera Dunal: cloning, expression and molecular modelling of two pairs of homologue genes with differential regulation.* Protoplasma, 2015. **252**(6): p. 1421-37.

178. Devkar, S.T., et al., *Evaluation of the bioavailability of major withanolides of Withania somnifera using an in vitro absorption model system.* J Adv Pharm Technol Res, 2015. **6**(4): p. 159-64.

179. Ahlawat, S., et al., *Comparative study of withanolide production and the related transcriptional responses of biosynthetic genes in fungi elicited cell suspension culture of Withania somnifera in shake flask and bioreactor.* Plant Physiol Biochem, 2017. **114**: p. 19-28.

180. Singh, V., et al., *Leaf spot disease adversely affects human health-promoting constituents and withanolide biosynthesis in Withania somnifera (L.) Dunal.* J Appl Microbiol, 2017. **122**(1): p. 153-165.

181. Saema, S., et al., *Ectopic overexpression of WsSGTL1, a sterol glucosyltransferase gene in Withania somnifera, promotes growth, enhances glycowithanolide and provides tolerance to abiotic and biotic stresses.* Plant Cell Rep, 2016. **35**(1): p. 195-211.

182. Sivanandhan, G., et al., *Optimization of elicitation conditions with methyl jasmonate and salicylic acid to improve the productivity of withanolides in the adventitious root culture of Withania somnifera (L.) Dunal.* Appl Biochem Biotechnol, 2012. **168**(3): p. 681-96.

183. Grover, A., et al., *Enhanced withanolide production by overexpression of squalene synthase in Withania somnifera.* J Biosci Bioeng, 2013. **115**(6): p. 680-5.

184. Sivanandhan, G., et al., *Sonication, Vacuum Infiltration and Thiol Compounds Enhance the Agrobacterium-Mediated Transformation Frequency of Withania somnifera (L.) Dunal.* PLoS One, 2015. **10**(4): p. e0124693.

185. Chaurasiya, N.D., et al., *Metabolic clustering of a core collection of Indian ginseng Withania somnifera Dunal through DNA, isoenzyme, polypeptide and withanolide profile diversity.* Fitoterapia, 2009. **80**(8): p. 496-505.

186. Bharti, S.K., et al., *Application of HR-MAS NMR spectroscopy for studying chemotype variations of Withania somnifera (L.) Dunal.* Magn Reson Chem, 2011. **49**(10): p. 659-67.

187. Chaurasiya, N.D., et al., *Analysis of withanolides in root and leaf of Withania somnifera by HPLC with photodiode array and evaporative light scattering detection.* Phytochem Anal, 2008. **19**(2): p. 148-54.

188. Dhar, N., et al., *Dynamics of withanolide biosynthesis in relation to temporal expression pattern of metabolic genes in Withania somnifera (L.) Dunal: a comparative study in two morpho-chemovariants.* Mol Biol Rep, 2013. **40**(12): p. 7007-16.

189. Sivanandhan, G., et al., *Effect of carbon and nitrogen sources on in vitro flower and fruit formation and withanolides production in Withania somnifera (L.) Dunal.* Indian J Exp Biol, 2015. **53**(3): p. 177-83.

190. Sabir, F., et al., *Qualitative and quantitative variations in withanolides and expression of some pathway genes during different stages of morphogenesis in Withania somnifera Dunal.* Protoplasma, 2013. **250**(2): p. 539-49.

191. Tong, X., H. Zhang, and B.N. Timmermann, *Chlorinated Withanolides from Withania somnifera.* Phytochem Lett, 2011. **4**(4): p. 411-414.

192. Sivanandhan, G., et al., *A promising approach on biomass accumulation and withanolides production in cell suspension culture of Withania somnifera (L.) Dunal.* Protoplasma, 2013. **250**(4): p. 885-98.

193. Sivanandhan, G., et al., *Enhanced biosynthesis of withanolides by elicitation and precursor feeding in cell suspension culture of Withania somnifera (L.) Dunal in shake-flask culture and bioreactor.* PLoS One, 2014. **9**(8): p. e104005.

194. Kaul, S.C., et al., *Novel Methods to Generate Active Ingredients-Enriched Ashwagandha Leaves and Extracts.* PLoS One, 2016. **11**(12): p. e0166945.

195. Grover, A., et al., *Withanone binds to mortalin and abrogates mortalin-p53 complex: computational and experimental evidence.* Int J Biochem Cell Biol, 2012. **44**(3): p. 496-504.

196. Grover, A., et al., *Ashwagandha derived withanone targets TPX2-Aurora A complex: computational and experimental evidence to its anticancer activity.* PLoS One, 2012. **7**(1): p. e30890.

197. Wadegaonkar, V.P. and P.A. Wadegaonkar, *Withanone as an inhibitor of survivin: a potential drug candidate for cancer therapy.* J Biotechnol, 2013. **168**(2): p. 229-33.

198. Lee, J., A. Sehrawat, and S.V. Singh, *Withaferin A causes activation of Notch2 and Notch4 in human breast cancer cells.* Breast Cancer Res Treat, 2012. **136**(1): p. 45-56.

199. Antony, M.L., et al., *Growth arrest by the antitumor steroidal lactone withaferin A in human breast cancer cells is associated with down-regulation and covalent binding at cysteine 303 of beta-tubulin.* J Biol Chem, 2014. **289**(3): p. 1852-65.

200. Szarc vel Szic, K., et al., *Pharmacological levels of Withaferin A (Withania somnifera) trigger clinically relevant anticancer effects specific to triple negative breast cancer cells.* PLoS One, 2014. **9**(2): p. e87850.

201. Lee, J., et al., *Withaferin A inhibits experimental epithelial-mesenchymal transition in MCF-10A cells and suppresses vimentin protein level in vivo in breast tumors.* Mol Carcinog, 2015. **54**(6): p. 417-29.

202. Gao, R., et al., *Withanone-rich combination of Ashwagandha withanolides restricts metastasis and angiogenesis through hnRNP-K.* Mol Cancer Ther, 2014. **13**(12): p. 2930-40.

203. Shah, N., et al., *Effect of the alcoholic extract of Ashwagandha leaves and its components on proliferation, migration, and differentiation of glioblastoma cells: combinational approach for enhanced differentiation.* Cancer Sci, 2009. **100**(9): p. 1740-7.

204. Shah, N., et al., *Combinations of Ashwagandha leaf extracts protect brain-derived cells against oxidative stress and induce differentiation.* PLoS One, 2015. **10**(3): p. e0120554.

205. Kataria, H., et al., *Withania somnifera aqueous extract facilitates the expression and release of GnRH: In vitro and in vivo study.* Neurochem Int, 2015. **89**: p. 111-9.

206. Widodo, N., et al., *Deceleration of senescence in normal human fibroblasts by withanone extracted from ashwagandha leaves.* J Gerontol A Biol Sci Med Sci, 2009. **64**(10): p. 1031-8.

207. Khan, S., et al., *Molecular insight into the immune up-regulatory properties of the leaf extract of Ashwagandha and identification of Th1 immunostimulatory chemical entity.* Vaccine, 2009. **27**(43): p. 6080-7.

208. Organization, W.H., *Leishmaniasis*. 2017, World Health Organization.

209. Grover, A., et al., *Blocking protein kinase C signaling pathway: mechanistic insights into the anti-leishmanial activity of prospective herbal drugs from Withania somnifera.* BMC Genomics, 2012. **13 Suppl 7**: p. S20.

210. Wube, A.A., et al., *Constituents of the stem bark of Discopodium penninervium and their LTB4 and COX-1 and -2 inhibitory activities.* Phytochemistry, 2008. **69**(4): p. 982-7.

211. Konar, A., et al., *Protective role of Ashwagandha leaf extract and its component withanone on scopolamine-induced changes in the brain and brain-derived cells.* PLoS One, 2011. **6**(11): p. e27265.

212. Priyandoko, D., et al., *Ashwagandha leaf derived withanone protects normal human cells against the toxicity of methoxyacetic acid, a major industrial metabolite.* PLoS One, 2011. **6**(5): p. e19552.

213. Dar, N.J., et al., *Withanone, an Active Constituent from Withania somnifera, Affords Protection Against NMDA-Induced Excitotoxicity in Neuron-Like Cells.* Mol Neurobiol, 2017. **54**(7): p. 5061-5073.

214. Gupta, M. and G. Kaur, *Aqueous extract from the Withania somnifera leaves as a potential anti-neuroinflammatory agent: a mechanistic study.* J Neuroinflammation, 2016. **13**(1): p. 193.

215. Purushotham, P.M., et al., *Withanolides against TLR4-Activated Innate Inflammatory Signalling Pathways: A Comparative Computational and Experimental Study.* Phytother Res, 2017. **31**(1): p. 152-163.

216. Pandey, A., et al., *Multifunctional neuroprotective effect of Withanone, a compound from Withania somnifera roots in alleviating cognitive dysfunction.* Cytokine, 2017.

217. Dyson, N.J., *RB1: a prototype tumor suppressor and an enigma.* Genes Dev, 2016. **30**(13): p. 1492-502.

218. Green, D.R. and G. Kroemer, *Cytoplasmic functions of the tumour suppressor p53.* Nature, 2009. **458**(7242): p. 1127-30.

219. Levine, A.J., *p53, the cellular gatekeeper for growth and division.* Cell, 1997. **88**(3): p. 323-31.

220. Gao, R., et al., *Heterogeneous nuclear ribonucleoprotein K (hnRNP-K) promotes tumor metastasis by induction of genes involved in extracellular matrix, cell movement, and angiogenesis.* J Biol Chem, 2013. **288**(21): p. 15046-56.

221. Satelli, A. and S. Li, *Vimentin in cancer and its potential as a molecular target for cancer therapy.* Cell Mol Life Sci, 2011. **68**(18): p. 3033-46.

222. Gallardo, M., et al., *hnRNP K Is a Haploinsufficient Tumor Suppressor that Regulates Proliferation and Differentiation Programs in Hematologic Malignancies.* Cancer Cell, 2015. **28**(4): p. 486-499.

223. Inoue, A., et al., *Loss-of-function screening by randomized intracellular antibodies: identification of hnRNP-K as a potential target for metastasis.* Proc Natl Acad Sci U S A, 2007. **104**(21): p. 8983-8.

224. Deocaris, C.C., S.C. Kaul, and R. Wadhwa, *From proliferative to neurological role of an hsp70 stress chaperone, mortalin.* Biogerontology, 2008. **9**(6): p. 391-403.

225. Na, Y., et al., *Stress chaperone mortalin contributes to epithelial-mesenchymal transition and cancer metastasis.* Cancer Res, 2016.

226. Ryu, J., et al., *Identification and functional characterization of nuclear mortalin in human carcinogenesis.* J Biol Chem, 2014. **289**(36): p. 24832-44.

227. Wadhwa, R., et al., *Upregulation of mortalin/mthsp70/Grp75 contributes to human carcinogenesis.* Int J Cancer, 2006. **118**(12): p. 2973-80.

228. Wadhwa, R., et al., *Identification of a novel member of mouse hsp70 family. Its association with cellular mortal phenotype.* J Biol Chem, 1993. **268**(9): p. 6615-21.

229. Lu, W.J., et al., *Induction of mutant p53-dependent apoptosis in human hepatocellular carcinoma by targeting stress protein mortalin.* Int J Cancer, 2011. **129**(8): p. 1806-14.

230. Wadhwa, R., et al., *Differential subcellular distribution of mortalin in mortal and immortal mouse and human fibroblasts.* Exp Cell Res, 1993. **207**(2): p. 442-8.

231. Walker, C., S. Bottger, and B. Low, *Mortalin-based cytoplasmic sequestration of p53 in a nonmammalian cancer model.* Am J Pathol, 2006. **168**(5): p. 1526-30.

232. Kaul, S.C., C.C. Deocaris, and R. Wadhwa, *Three faces of mortalin: a housekeeper, guardian and killer.* Exp Gerontol, 2007. **42**(4): p. 263-74.

233. Kaul, S.C., et al., *Activation of wild type p53 function by its mortalin-binding, cytoplasmically localizing carboxyl terminus peptides.* J Biol Chem, 2005. **280**(47): p. 39373-9.

234. Lu, W.J., et al., *Circulating mortalin autoantibody--a new serological marker of liver cirrhosis.* Cell Stress Chaperones, 2015. **20**(4): p. 715-9.

235. Nigam, N., et al., *Targeting Mortalin by Embelin Causes Activation of Tumor Suppressor p53 and Deactivation of Metastatic Signaling in Human Breast Cancer Cells.* PLoS One, 2015. **10**(9): p. e0138192.

236. Wadhwa, R., et al., *Molecular Characterization and Enhancement of Anticancer Activity of Caffeic Acid Phenethyl Ester by gamma Cyclodextrin.* J Cancer, 2016. **7**(13): p. 1755-1771.

237. Campisi, J., *The biology of replicative senescence.* Eur J Cancer, 1997. **33**(5): p. 703-9.

238. Lleonart, M.E., A. Artero-Castro, and H. Kondoh, *Senescence induction; a possible cancer therapy.* Mol Cancer, 2009. **8**: p. 3.

239. Lammerding, J., et al., *Lamins A and C but not lamin B1 regulate nuclear mechanics.* J Biol Chem, 2006. **281**(35): p. 25768-80.

240. Stracker, T.H. and J.H. Petrini, *The MRE11 complex: starting from the ends.* Nat Rev Mol Cell Biol, 2011. **12**(2): p. 90-103.

241. Garg, S., S.C. Kaul, and R. Wadhwa, *Cucurbitacin B and cancer intervention: Chemistry, biology and mechanisms (Review).* Int J Oncol, 2018. **52**(1): p. 19-37.

242. Kataria, H., et al., *Water extract from the leaves of Withania somnifera protect RA differentiated C6 and IMR-32 cells against glutamate-induced excitotoxicity.* PLoS One, 2012. **7**(5): p. e37080.

243. Kataria, H., et al., *Withania somnifera water extract as a potential candidate for differentiation based therapy of human neuroblastomas.* PLoS One, 2013. **8**(1): p. e55316.

244. Gautam, A., R. Wadhwa, and M.K. Thakur, *Involvement of hippocampal Arc in amnesia and its recovery by alcoholic extract of Ashwagandha leaves.* Neurobiol Learn Mem, 2013. **106**: p. 177-84.

245. Gautam, A., R. Wadhwa, and M.K. Thakur, *Assessment of Cholinergic Properties of Ashwagandha Leaf-Extract in the Amnesic Mouse Brain.* Ann Neurosci, 2016. **23**(2): p. 68-75.

246. Hasan, M.K., et al., *CARF is a novel protein that cooperates with mouse p19ARF (human p14ARF) in activating p53.* J Biol Chem, 2002. **277**(40): p. 37765-70.

247. Wadhwa, R., et al., *Functional significance of point mutations in stress chaperone mortalin and their relevance to Parkinson disease.* J Biol Chem, 2015. **290**(13): p. 8447-56.

248. Amick, J., et al., *Crystal structure of the nucleotide-binding domain of mortalin, the mitochondrial Hsp70 chaperone.* Protein Sci, 2014. **23**(6): p. 833-42.

249. Emamzadah, S., et al., *Reversal of the DNA-binding-induced loop L1 conformational switch in an engineered human p53 protein.* J Mol Biol, 2014. **426**(4): p. 936-44.

250. Backe, P.H., et al., *X-ray crystallographic and NMR studies of the third KH domain of hnRNP K in complex with single-stranded nucleic acids.* Structure, 2005. **13**(7): p. 1055-67.

251. Kaul, Z., et al., *Quantum dot-based mortalin staining as a visual assay for detection of induced senescence in cancer cells.* Ann N Y Acad Sci, 2007. **1100**: p. 368-72.

252. Fridlender, M., Y. Kapulnik, and H. Koltai, *Plant derived substances with anti-cancer activity: from folklore to practice.* Front Plant Sci, 2015. **6**: p. 799.

253. Yin, S.Y., et al., *Therapeutic applications of herbal medicines for cancer patients.* Evid Based Complement Alternat Med, 2013. **2013**: p. 302426.

254. Bakar, F., *Cucurbitacin B Enhances the Anticancer Effect of Imatinib Mesylate Through Inhibition of MMP-2 Expression in MCF-7 and SW480 Tumor Cell Lines.* Anticancer Agents Med Chem, 2016. **16**(6): p. 747-54.

255. Wadhwa, R., R.S. Kalra, and S.C. Kaul, *CARF is a multi-module regulator of cell proliferation and a molecular bridge between cellular senescence and carcinogenesis.* Mech Ageing Dev, 2017. **166**: p. 64-68.

256. Wang, H., et al., *Plants vs. cancer: a review on natural phytochemicals in preventing and treating cancers and their druggability.* Anticancer Agents Med Chem, 2012. **12**(10): p. 1281-305.

257. Schreiber, K.H. and B.K. Kennedy, *When lamins go bad: nuclear structure and disease.* Cell, 2013. **152**(6): p. 1365-75.

258. Kar, B., et al., *Quantitative nucleolar proteomics reveals nuclear re-organization during stress- induced senescence in mouse fibroblast.* BMC Cell Biol, 2011. **12**: p. 33.

259. Wang, A.S., et al., *Loss of lamin B1 is a biomarker to quantify cellular senescence in photoaged skin.* Sci Rep, 2017. **7**(1): p. 15678.

260. Kasten, M.M. and A. Giordano, *pRb and the cdks in apoptosis and the cell cycle.* Cell Death Differ, 1998. **5**(2): p. 132-40.

261. Cheung, C.T., et al., *CARF: an emerging regulator of p53 tumor suppressor and senescence pathway.* Mech Ageing Dev, 2009. **130**(1-2): p. 18-23.

262. Cheung, C.T., et al., *Collaborator of ARF (CARF) regulates proliferative fate of human cells by dose-dependent regulation of DNA damage signaling.* J Biol Chem, 2014. **289**(26): p. 18258-69.

263. Hasan, K., et al., *CARF Is a vital dual regulator of cellular senescence and apoptosis.* J Biol Chem, 2009. **284**(3): p. 1664-72.

264. Singh, R., et al., *Molecular characterization of collaborator of ARF (CARF) as a DNA damage response and cell cycle checkpoint regulatory protein.* Exp Cell Res, 2014. **322**(2): p. 324-34.

265. Sugrue, M.M., et al., *Wild-type p53 triggers a rapid senescence program in human tumor cells lacking functional p53.* Proc Natl Acad Sci U S A, 1997. **94**(18): p. 9648-53.

266. Hasan, M.K., et al., *Alternative reading frame protein (ARF)-independent function of CARF (collaborator of ARF) involves its interactions with p53: evidence for a novel p53-activation pathway and its negative feedback control.* Biochem J, 2004. **380**(Pt 3): p. 605-10.

267. Kalra, R.S., et al., *CARF (Collaborator of ARF) overexpression in p53-deficient cells promotes carcinogenesis.* Mol Oncol, 2015. **9**(9): p. 1877-89.

268. Kim, J.H., et al., *The Mre11-Nbs1 Interface Is Essential for Viability and Tumor Suppression.* Cell Rep, 2017. **18**(2): p. 496-507.

269. Chai, W., et al., *The involvement of the Mre11/Rad50/Nbs1 complex in the generation of G-overhangs at human telomeres.* EMBO Rep, 2006. **7**(2): p. 225-30.

270. Ju, Y.J., et al., *Decreased expression of DNA repair proteins Ku70 and Mre11 is associated with aging and may contribute to the cellular senescence.* Exp Mol Med, 2006. **38**(6): p. 686-93.

271. Spehalski, E., et al., *MRE11 Promotes Tumorigenesis by Facilitating Resistance to Oncogene-Induced Replication Stress.* Cancer Res, 2017. **77**(19): p. 5327-5338.

272. Joseph, I.S., et al., *An mre11 mutation that promotes telomere recombination and an efficient bypass of senescence.* Genetics, 2010. **185**(3): p. 761-70.

273. Tankimanova, M., et al., *Mre11 modulates the fidelity of fusion between short telomeres in human cells.* Nucleic Acids Res, 2012. **40**(6): p. 2518-26.

274. Cannon, B., et al., *Visualization of local DNA unwinding by Mre11/Rad50/Nbs1 using single-molecule FRET.* Proc Natl Acad Sci U S A, 2013. **110**(47): p. 18868-73.

275. Li, Y., et al., *Deficient Activity of the Nuclease MRE11A Induces T Cell Aging and Promotes Arthritogenic Effector Functions in Patients with Rheumatoid Arthritis.* Immunity, 2016. **45**(4): p. 903-916.

276. Jiang, W.Q., et al., *Suppression of alternative lengthening of telomeres by Sp100-mediated sequestration of the MRE11/RAD50/NBS1 complex.* Mol Cell Biol, 2005. **25**(7): p. 2708-21.

277. Zhong, Z.H., et al., *Disruption of telomere maintenance by depletion of the MRE11/RAD50/NBS1 complex in cells that use alternative lengthening of telomeres.* J Biol Chem, 2007. **282**(40): p. 29314-22.

278. Alster, O., et al., *The role of nibrin in doxorubicin-induced apoptosis and cell senescence in Nijmegen Breakage Syndrome patients lymphocytes.* PLoS One, 2014. **9**(8): p. e104964.

279. Colonna, M., *DNA damage response impacts macrophage functions.* Blood, 2015. **126**(22): p. 2440-2.

280. Kang, J., R.T. Bronson, and Y. Xu, *Targeted disruption of NBS1 reveals its roles in mouse development and DNA repair.* EMBO J, 2002. **21**(6): p. 1447-55.

281. Foster, C.R., et al., *The role of Lamin A in cytoskeleton organization in colorectal cancer cells: a proteomic investigation.* Nucleus, 2011. **2**(5): p. 434-43.

282. Li, P. and A.A. Noegel, *Inner nuclear envelope protein SUN1 plays a prominent role in mammalian mRNA export.* Nucleic Acids Res, 2015. **43**(20): p. 9874-88.

283. Starenki, D., et al., *Mortalin (GRP75/HSPA9) upregulation promotes survival and proliferation of medullary thyroid carcinoma cells.* Oncogene, 2015. **34**(35): p. 4624-34.

284. Shin, J.W., et al., *Lamins regulate cell trafficking and lineage maturation of adult human hematopoietic cells.* Proc Natl Acad Sci U S A, 2013. **110**(47): p. 18892-7.

285. Worman, H.J. and G. Bonne, *"Laminopathies": a wide spectrum of human diseases.* Exp Cell Res, 2007. **313**(10): p. 2121-33.

286. Gurzu, S., et al., *Epithelial-mesenchymal, mesenchymal-epithelial, and endothelial-mesenchymal transitions in malignant tumors: An update.* World J Clin Cases, 2015. **3**(5): p. 393-404.

287. Lamouille, S., J. Xu, and R. Derynck, *Molecular mechanisms of epithelial-mesenchymal transition.* Nat Rev Mol Cell Biol, 2014. **15**(3): p. 178-96.

288. Hanahan, D. and R.A. Weinberg, *The hallmarks of cancer.* Cell, 2000. **100**(1): p. 57-70.

289. Midgley, R.S., Y. Yanagisawa, and D.J. Kerr, *Evolution of nonsurgical therapy for colorectal cancer.* Nat Clin Pract Gastroenterol Hepatol, 2009. **6**(2): p. 108-20.

290. Gillet, J.P., S. Varma, and M.M. Gottesman, *The clinical relevance of cancer cell lines.* J Natl Cancer Inst, 2013. **105**(7): p. 452-8.

291. Harris, L.A., et al., *An unbiased metric of antiproliferative drug effect in vitro.* Nat Methods, 2016. **13**(6): p. 497-500.

292. Hsieh, C.H., et al., *The effect of primary cancer cell culture models on the results of drug chemosensitivity assays: the application of perfusion microbioreactor system as cell culture vessel.* Biomed Res Int, 2015. **2015**: p. 470283.

293. Johnson, J.I., et al., *Relationships between drug activity in NCI preclinical in vitro and in vivo models and early clinical trials.* Br J Cancer, 2001. **84**(10): p. 1424-31.

294. Riss, T.L., Moravec, R. A., Niles, A. L., Duellman, S., Benink, H. A., Worzella, T. J., Minor, L., *Cell Viability Assays*, G.S. Sittampalam, Coussens, N. P., Brimacombe, K., Grossman, A., Arkin, M., Auld, D., Austin, C., Baell, J., Bejcek, B., Chung, T. D. Y., Dahlin, J. L., Devanaryan, V., Foley, T. L., Glicksman, M., Hall, M. D., Hass, J. V., Inglese, J., Iversen, P. W., Kahl, S. D., Kales, S. C., Lal-Nag, M., Li, Z., McGee, J., McManus, O., Riss, T., Trask, O. J. Jr., Weidner, J. R., Xia, M. and Xu, X., Editor. 2016, Eli Lilly & Company and the National Center for Advancing Translational Sciences: Bethesda. p. 355-386.

295. Ulukaya, E., M. Colakogullari, and E.J. Wood, *Interference by anti-cancer chemotherapeutic agents in the MTT-tumor chemosensitivity assay.* Chemotherapy, 2004. **50**(1): p. 43-50.

296. Howard, D.H., et al., *Pricing in the Market for Anticancer Drugs.* J Econ Perspect, 2015. **29**(1): p. 139-62.

297. Eckhouse, S., G. Lewison, and R. Sullivan, *Trends in the global funding and activity of cancer research.* Mol Oncol, 2008. **2**(1): p. 20-32.

298. Health, N.I.o., *NIH Management Fund, SSF, and GSA Rent FY 2016*. 2017.

299. Health, N.I.o., *Estimates of Funding for Various Research, Condition, and Disease Categories (RCDC)*. 2017.

300. Society, A.C., *Rising Global Cancer Epidemic*, in *Infographics*. 2016, American Cancer Society.

301. Jelliffe, R.W., et al., *Describing Assay Precision-Reciprocal of Variance Is Correct, Not CV Percent: Its Use Should Significantly Improve Laboratory Performance.* Ther Drug Monit, 2015. **37**(3): p. 389-94.

302. Natarajan, S. and D.G. Remick, *The ELISA Standard Save: calculation of sample concentrations in assays with a failed standard curve.* J Immunol Methods, 2008. **336**(2): p. 242-5.

303. Bernas, T. and J. Dobrucki, *Mitochondrial and nonmitochondrial reduction of MTT: interaction of MTT with TMRE, JC-1, and NAO mitochondrial fluorescent probes.* Cytometry, 2002. **47**(4): p. 236-42.

304. Berridge, M.V. and A.S. Tan, *Characterization of the cellular reduction of 3-(4,5-dimethylthiazol-2-yl)-2,5-diphenyltetrazolium bromide (MTT): subcellular localization, substrate dependence, and involvement of mitochondrial electron transport in MTT reduction.* Arch Biochem Biophys, 1993. **303**(2): p. 474-82.

305. Chakrabarti, R., et al., *Vitamin A as an enzyme that catalyzes the reduction of MTT to formazan by vitamin C.* J Cell Biochem, 2000. **80**(1): p. 133-8.

306. Stepanenko, A.A. and V.V. Dmitrenko, *Pitfalls of the MTT assay: Direct and off-target effects of inhibitors can result in over/underestimation of cell viability.* Gene, 2015. **574**(2): p. 193-203.

307. Baker, D.D., et al., *The value of natural products to future pharmaceutical discovery.* Nat Prod Rep, 2007. **24**(6): p. 1225-44.

308. Bodai, B.I. and P. Tuso, *Breast cancer survivorship: a comprehensive review of long-term medical issues and lifestyle recommendations.* Perm J, 2015. **19**(2): p. 48-79.

309. Baba, A.I., Catoi, C. , *Tumor cell morphology*. 2007, Bucharest: The Publishing House of the Romanian Academy.

310. D'Anselmi, F., et al., *Metabolism and cell shape in cancer: a fractal analysis.* Int J Biochem Cell Biol, 2011. **43**(7): p. 1052-8.

311. Fritz, E., H. Ludwig, and M. Kundi, *Prognostic relevance of cellular morphology in multiple myeloma.* Blood, 1984. **63**(5): p. 1072-9.